Pornprapa Bol

Investigation of drop dispersions in batch settling processes

DISSERTATION

zur Erlangung des akademischen Grades

Doktor der technischen Wissenschaften

eingereicht an der

Technischen Universität Graz

Betreuer

Univ.-Prof. Dipl.-Ing. Dr. techn. Matthäus Siebenhofer

Institut für Chemische Verfahrenstechnik und Umwelttechnik

Graz, Jänner 2014

EIDESSTATTLICHE ERKLÄRUNG

Ich erkläre an Eides statt, dass ich die vorliegende Arbeit selbstständig verfasst, andere als die angegebenen Quellen/Hilfsmittel nicht benutzt, und die den benutzten Quellen wörtlich und inhaltlich entnommenen Stellen als solche kenntlich gemacht habe. Das in TUGRAZonline hochgeladene Textdokument ist mit der vorliegenden Dissertation identisch.

28.01.2015

Datum

Unterschrift

Kurzfassung

In dieser Arbeit wurde die Trennung von Zweiphasensytemen mit Hilfe von Batch-Settling-Prozessen im Labormaßstab untersucht. Die dadurch gewonnenen Informationen werden helfen die Auslegung von industriellen Abscheidern zu verbessern. Der Einfluss der Viskosität und Salzen, sowie Einbauten im Abscheider auf den Trennprozess wurde analysiert. Zur Untersuchung von trüben Stoffsystemen, welche mit den bisherigen optischen Methoden nicht evaluiert werden konnten, wurde ein Ultraschallscan-Verfahren eingeführt. Mit Hilfe dieser Technologie konnten Änderungen des Hold-Up in der dichtgepackten Schicht und sekundäre Sedimentationsprozesse beobachtet werden, die mit den etablierten Verfahren nicht detektierbar sind. Es wurde ein neues Modell zur Beschreibung des Trennverhaltens von polydispersen Tropfenschwärmen entwickelt, dass auf der Geschwindigkeit von Einzeltropfen relativ zum umgebenden Fluid, sowie der Tropfengröße basiert. Des Weiteren wurden aus der kinetischen Analyse des Sedimentationsvorganges und des Koaleszenzvorganges sigmoidale Funktionen für die analytische Beschreibung von Sedimentations- und Koaleszenzkurven als Funktion der Zeit hergeleitet.

Abstract

In this work the separation of two phase systems in batch settling processes was investigated in order to gain information for improved design of industrial settlers. The influence of viscosity, electrolytes and inclined plates on the settling process was investigated. The novel ultrasonic scanning technology is used to characterize systems where the established optical investigation was not applicable. The hold-up change in the dense-packed zone as a function of height and time was investigated. This information is only accessible via ultrasonic scanning and can be used in the future to model the coalescence of droplet in the dense-packed zone. A new model was developed to describe the settling behavior of polydisperse swarm drops based on the velocity of each droplet relative to the surrounding fluid depending on the droplet size. Deduced from a kinetical approach a sigmoidal three-parameter models can be used to describe analytically the settling curves as a function of height and time.

Preface

This PhD Thesis had been supervised by Prof. Dr.-Ing. Andreas Pfennig from April 2011 until November 2014. It did start at TVT-AVT, RWTH Aachen, Germany. During his period in Graz from October 2011 to November 2014 a major part of the experimental work was done. In November 2014 he left Graz University for Liège to the Department of applied Chemistry, leaving me with without a proper strategy and plan how to finish my PhD Thesis on time.

On my appeal the head of the Doctoral School “Chemical Process Engineering” and the Institute of Chemical Engineering and Environmental Technology of Graz University of Technology agreed willingness to supervise the final part of my PhD Thesis. I appreciate the intensive discussion with my final supervisor Prof. Matthäus Siebenhofer and the hard job of finishing my PhD Thesis within the time frame.

Throughout my PhD time, I supervised several students. I would like to thank my students Kanokkan Anusarn, Supinya Manodumrongthum, Albert Cano Castro, Itsaranuwat Aunyindee, James Andrew Peart Findlay, Nuttakul Mungma, Chong Ee Pin, Chanita Tantichumnan, Pruchyamas Punsang, Bianca Höller for their input and experimental work. Especially, I would like to thank for the assistance of the secretaries Eveline Schemitsch and Gabi Staerk and the technical staff Peter Letonja and Markus Lückge.

Finally, I would like to thank my colleague and later husband Jan Bernd, who always supported me and gave me the spirit to go on.

I publish my PhD Thesis with pleasure and gladness, and I hope that it will contribute to progress in modelling of sedimentation and coalescence in liquid-liquid extraction.

Contents

1 Introduction

In the chemical industry many processes are based on crude oil products. It can be foreseen that in the future there will be a considerable increase in processes based on biomass due to the increasing price of crude oil and the fact that biomass is the only sustainable carbon source for chemical processes. Since the molecular structure of biomass contains more oxygen as compared to fossil resources, biomass derived intermediates and products will have a higher viscosity and a lower volatility than current fossil-based systems, due to the stronger intermolecular interactions like polar forces and hydrogen bonding. In addition, solids content from the solids structure of the biomass might increase stemming. The established separation method distillation will be too expensive for separation and isolation of such substances due to the lower volatility of the systems. Thus technical systems will become increasingly difficult to deal with. It can be anticipated that in the future liquid phase-based processes like extraction will increase in application. This requires also an improved knowledge in the field of phase separation of dispersions.

Gravity settlers are used for phase separation widely in industry because of their reliability and operation flexibility. In our research group, a method has been developed that allows the design of settlers for clear systems (Henschke, 1994, Henschke et al., 2002). It is based on simple batch settling experiments on laboratory scale requiring roughly one liter of the technical two-phase system. The settling experiment is recorded on video and evaluated with a model that explicitly accounts for the interactions between the droplets, especially their coalescence (Henschke, 1994, Henschke et al., 2002). Based on this model a design of a technical settler for arbitrary throughput is then possible.

This project aims at closing the gap between the requirements we foresee for reliable settler design in the future and our best design methods today available. The gravity settling models which are available today allow it to describe the sedimentation and coalescence profiles using data from simple settling experiments (Jeelani and Hartland, 1985, Henschke, 1994, Henschke et al., 2002). Due to the limitation of optical evaluation, this model has mostly been validated for simple systems. The real technical systems encountered in industry often not only possess higher viscosity, but

may also be opaque. Therefore, it is more challenging to perform settling experiments with real systems, since the optical evaluation cannot be realized in any case.

A novel approach is the utilization of an ultrasonic scanning technology. In an ultrasonic scanner, a system can be investigated by sound wave. The different properties of the phases lead to different sound velocity and attenuation. Therefore, the height of the sedimenting and coalescing interfaces with time can be measured by changing velocity of sound. Moreover, the local hold-up profile in dense-packed zone can be determined. In addition the drop size distribution of the dispersed phase can be measured and taken into account. One aim of this research work is the development of a model for gravity settling in liquid-liquid dispersions for real technical systems based on the detailed description of batch-settling experiments. Suitable systems that can be analyzed within the ultrasonic scanner have to be found as well.

Another problem occurring with real systems is high viscosity. High viscosity can occur with one phase or both phases. For these systems it has not been completely tested, if the existing settler program can be used to describe coalescence and sedimentation. Therefore high viscosity systems will be investigated in optical cells and the ultrasonic scanner. Moreover, the droplet size in real system is polydisperse. Another possibility to study sedimentation of drop size distributions in high-viscosity systems is to add solid particles of known size and density to either aqueous or organic phase.

While academic test systems are usually clean, a lot of impurities can arise in real industrial systems. These are on the one side solid particles (Ruckes, 2011) and on the other side electrolytes. While the influence of electrolytes has already been studied for low-viscosity systems, the combination of electrolytes and high-viscosity has not yet been discussed. Therefore, the study on high-viscosity systems will be complemented by experiments with additional electrolytes.

2 State of the art

Liquid-liquid extraction is a major separation process in chemical industries besides distillation. The extraction process is often carried out in mixer-settlers. A mixer-settler consists of two sections, a mixing section and a settling section. In the mixing section the two phases are brought into contact and stirred to enable good mass transfer. Due to mixing small droplets are formed which increase the interfacial area and therefore, improve the mass transfer. The generated dispersion is then separated in the settling section. The principle of the separation has been studied by many researchers such as Jeelani and Hartland (1985), Nadiv and Semiat (1995), Henschke et al. (2002), Al-Zuhair (2004), Frising et al. (2006).

2.1 Principle of settling

The phase separation process can be best observed visually in a transparent cylinder as shown schematically in Fig. 2-1. In this example, the lighter phase is the dispersed phase. So there are droplets of the light phase within a continuous heavy phase. When mixing is stopped, the droplets start to sediment to the top. At the boundary of the continuous phase the droplets coalesce to the bulk of the dispersed phase. Plotting the boundary between dispersed bulk and continuous phase over time, the coalescence curve can be constructed. Accordingly, the sedimentation curve is derived from the height parting the droplet free continuous phase from the sedimentation zone, where droplets still sediment towards their bulk. If the sedimentation is faster than the coalescence of droplets a dense packed zone is formed at the interface of the dispersion and the coalesced phase. In this zone drop-drop coalescence occurs, causing the drop diameter to increase to finally “dissolve” in the coalesced phase. Droplets may as well directly come into droplet-phase contact to “vanish” in the coalesced phase.

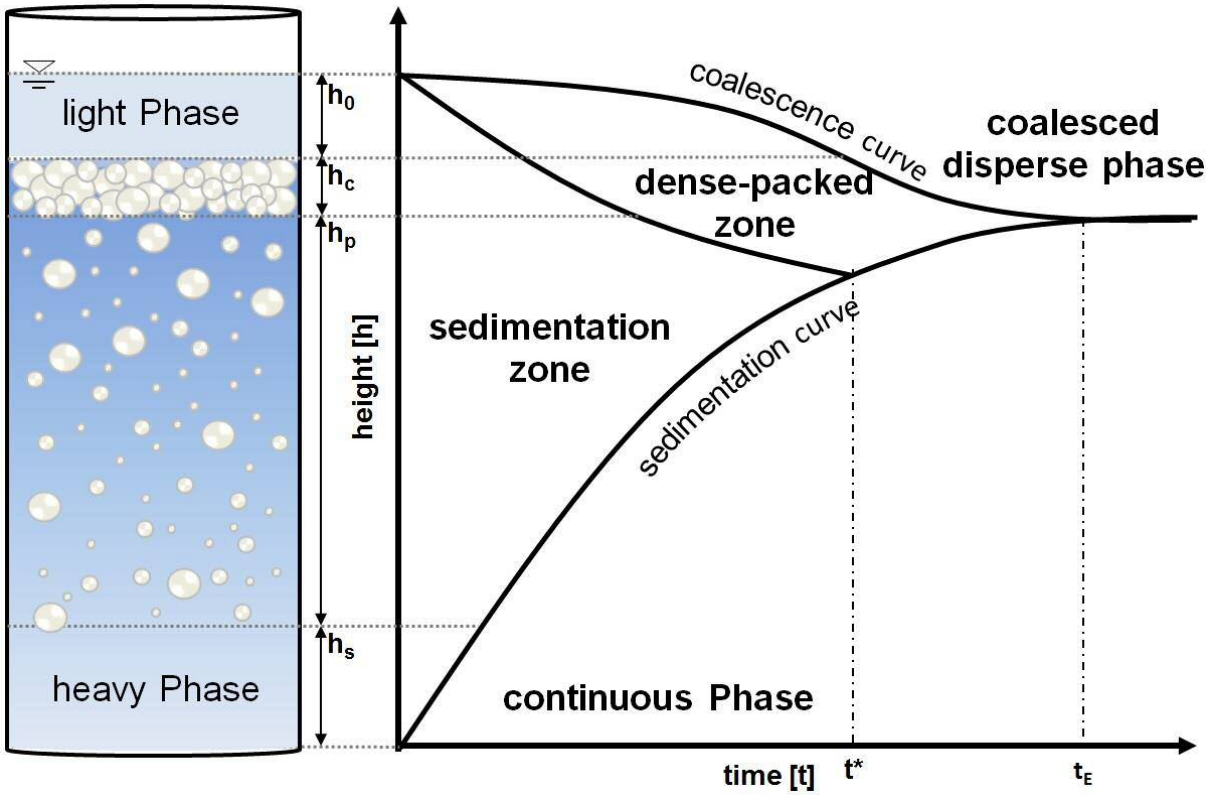

Fig. 2-1: Schematic representation of batch settling experiments

The basic height balances of batch settling were carried out by Jeelani and Hartland (1985). Before the free sedimentation finished the total height

$$h_{total} = h_0 + h_c + h_p + h_s \quad \text{for } t < t^* \tag{2-1}$$

has to be the sum of the height of the coalesced light phase h_o, the height of the continuous heavy phase h_s, the height of the sedimentation zone h_p and of the dense-packed zone h_c. After the free sedimentation process has ended at time t^* the term for the sedimentation zone is no longer required, resulting in

$$h_{total} = h_0 + h_c + h_s \quad \text{for } t \geq t^*. \tag{2-2}$$

The basic height balance was used and modified by many researchers (Henschke et al., 2002, Al-Zuhair, 2004, Frising et al., 2006).

The second characteristic time is the time t_E describing the moment when the two phases are completely separated.

2.2 Sedimentation of droplet

Small droplets show almost no inner circulation or deformation. Therefore, models for rigid spheres can be applied for them. The gravitational sedimentation of a rigid sphere is based on acting forces balance around which are the gravity force F_G, the drag force F_D and the buoyancy force F_B.

$$F_G = F_B + F_D \tag{2-3}$$

Stokes (1851) gives a complete description of drag force in a very slow steady relative motion of a rigid sphere with diameter d in an infinite fluid of viscosity η. Later, it is known as Stokes' law. The single rigid sphere is defined as dimensionless form (Rhodes, 2008):

$$\text{Reynolds number,}\quad \mathrm{Re}_\infty = \frac{\rho_c d v_\infty}{\eta_c} \tag{2-4}$$

$$\text{Archimedes number,}\quad \mathrm{Ar} = \frac{\rho_c \left|\rho_c - \rho_d\right| \cdot g d^3}{\eta_c^2} \tag{2-5}$$

$$\text{Drag coefficient,}\quad \mathrm{C_d} = R' \frac{2}{\rho_c v_\infty^2} \tag{2-6}$$

$$\text{Ljascenko number,}\quad \mathrm{Lj} = \frac{4}{3}\frac{\mathrm{Re}}{C_d} = \frac{v_\infty^3}{\nu \cdot g} \cdot \frac{\rho_c}{\rho_d - \rho_c} \tag{2-7}$$

Where ρ_c, η_c and v_∞ are the density and viscosity of continuous phase, and the relative velocity of a rigid sphere. R' is the resistance force per unit area of the rigid sphere.

Under the Stokes' law region, the terminal velocity of single rigid sphere relative to the continuous phase is given by (Richardson and Zaki, 1954):

$$v_\infty = \frac{\Delta\rho \cdot g \cdot d^2}{18\eta_c} \tag{2-8}$$

When many rigid spheres flow in the fluid close to each other the motion of each sphere is influenced by the presence of the other. The simple analysis for a single rigid sphere is no longer valid. However, it can be adapted to a model for multiple rigid spheres system.

The sedimentation swarm of droplets was studied by many researchers. Richardson and Zaki (1954) had considered the effect of packing on the sedimentation velocity of droplet which can explain only the systems with a dispersed phase fraction (ε_0) less than or equal to one. Their sedimentation velocity is expressed as follows:

$$v_s = v_{s,\infty}(1-\varepsilon_0) \tag{2-9}$$

where $v_{s,\infty}$ is free drop velocity.

However, this equation cannot be used to explain the sedimentation behavior in all cases, especially with a system of polydispersed droplets. Therefore, Mersmann (1980) and Andersson (1961) had modified the sedimentation velocity to the following equation:

$$v_s = v_{s,\infty}(1-\varepsilon_0)^m \tag{2-10}$$

where m is the hindered sedimentation parameter which is defined as a function of sauter mean diameter ($d_{32,0}$) and the properties of the system. The hindered sedimentation parameter has a theoretical value in a range of 2.3 – 4.6.

Since sedimentation and coalescence occur simultaneously, the effect of coalescence must be considered. Reddy and Fogler (1981) found that during the sedimentation step the coalescence can occur in two cases which are resulted from the difference in droplet velocity and from Brownian motion. Moreover, only drop-drop coalescence resulting from Brownian motion can be expected in the beginning of the sedimentation with the assumptions that the emulsion is monodisperse and all droplets are equal in size. Later, Nadiv and Semiat (1995) have modified Equation 2-10 to the following equation:

$$v_s = v_{s,\infty}(1-\varepsilon_0)\left(1+\frac{t^2 \cdot t_{s,\infty}^2}{h_0^2} n\varepsilon_0\right) \tag{2-11}$$

where h_0 is the inertial dispersion height and n is the impact of the dispersed phase fraction on binary coalescence. The second term in Equation 2-11 is indicating the effect of binary coalescence and is used to describe the colliding droplets coalesce after a long period of holding time.

Others have considered the coalescence effect during the sedimentation process using a changing mean diameter with which the sedimentation velocity can be calculated. For example, Jeelani, Pandit and Hartland (1990) presented the sedimentation velocity at low Reynolds numbers in the following equation:

$$v_s = \frac{dh_s}{dt} = v_0\left(\frac{d}{d_0}\right)^2 = \frac{|\rho_c - \rho_d| g\, d_{32,0}^2 (1-\varepsilon_0)^2}{18\eta_c(1+4.56\varepsilon_0)}\left(\frac{d}{d_0}\right)^2 \tag{2-12}$$

where v_0 the is initial sedimentation velocity, d_0 is the initial mean diameter and $|\rho_c - \rho_d|$ is the density difference of two liquids.

Later, Henschke et al. (2002) gave a complete overview of the description of drop sedimentation during the settling experiment. It is assumed that there is no coalescence in the sedimentation zone and the droplets are mono-disperse. Since the sedimentation curve almost represents a linear curve, the swarm sedimentation velocity (v_s) of the droplets can be determined from the slope of the sedimentation curve. The Sauter mean diameter ($d_{32,0}$) can be calculated from the sedimentation curve during free sedimentation with appropriate models accounting especially for local hold-up.

$$v_s = \frac{\mathrm{Re}_s\, \eta_c(1\text{-}\varepsilon_0)}{\rho_c d_{32,0}} \tag{2-13}$$

when $\varepsilon_0 = \dfrac{V_d}{V_d + V_c}$ is the local hold-up.

V_d and V_c are total volumes of dispersed phase and continuous phase, respectively.

Henschke et al. (2002) used the sedimentation model of Pilhofer and Mewes (1979)

$$\mathrm{Re}_s = \frac{3qK_{HR}^{1.5}}{c_w}\left(\frac{\varepsilon_0}{1-\varepsilon_0}\right)^{0.55}\left[\left(1 + Ar\,\frac{c_w(1-\varepsilon_0)^{2.55}}{10.8q^2K_{HR}^{1.5}\varepsilon_0^{1.55}}\right)^{0.5} - 1\right] \tag{2-14}$$

This model is valid for Archimedes number (Ar)

$$\mathrm{Ar} = \frac{\rho_c|\rho_c - \rho_d| g\, d_{32,0}^3}{\eta_c^2} \tag{2-15}$$

larger than 1 and hold-up between 0.06 to 0.55. The Hadamard–Rybczynski factor (K_{HR}) is defined

$$K_{HR}=\frac{3(\eta_c+\eta_d)}{2\eta_c+3\eta_d} \tag{2-16}$$

The parameter q can be calculated from

$$q=\frac{1-\varepsilon_0}{2\varepsilon_0 K_{HR}}\exp\left(\frac{2.5\varepsilon_0}{1-0.61\varepsilon_0}\right),\ \varepsilon_0<0.55 \tag{2-17}$$

$$q=\frac{2.2(1-\varepsilon_0)}{\varepsilon_0 K_{HR}}\exp\left(\frac{0.4\varepsilon_0}{1-0.61\varepsilon_0}\right),\ \varepsilon_0\geq 0.55 \tag{2-18}$$

The friction coefficient is a function of the Reynolds number in an infinitely extended fluid

$$c_w=\frac{\mathrm{Ar}}{6\,\mathrm{Re}_\infty^2}-\frac{3}{K_{HR}\,\mathrm{Re}_\infty} \tag{2-19}$$

For the Reynolds number developed

$$\mathrm{Re}_\infty=9.72\cdot\left[(1+0.01\cdot\mathrm{Ar})^{4/7}-1\right] \tag{2-20}$$

a model was developed by Ishii and Zuber (1979).

2.3 Coalescence

Hartland and Jeelani (1988), Hartland and Vohra (1978), Jeelani and Hartland (1985) and Henschke et al. (2002) give a complete fundamental modeling of drop-drop and drop-interface coalescence in batch settling. As depicted in Fig. 2-1 the height of the dense-packed zone can be calculated from the initial filling height after mixing is stopped (h_0), the height of the dispersed phase (h_p), the initial hold-up and the hold-up of the dense-packed zone. But with settling experiments in a settling cell the dense-packed zone cannot be investigated, since the boundary between sedimentation zone and dense-packed zone is rarely visible. However, the height of the dense-packed zone can be obtained numerically by the settler program.

The coalescence process itself can be divided into three consecutive stages as shown in Fig. 2-2:

- (I) The drop approaches to the interface of its own phase by the force balance of weight and buoyancy force, drag force as well as inertial force. The drop and the interface deform.

- (II) Drop and interface enclose a thin layer of continuous phase which has to drain to critical low thickness.
- (III) The film tears and the drop coalesces with the interface.

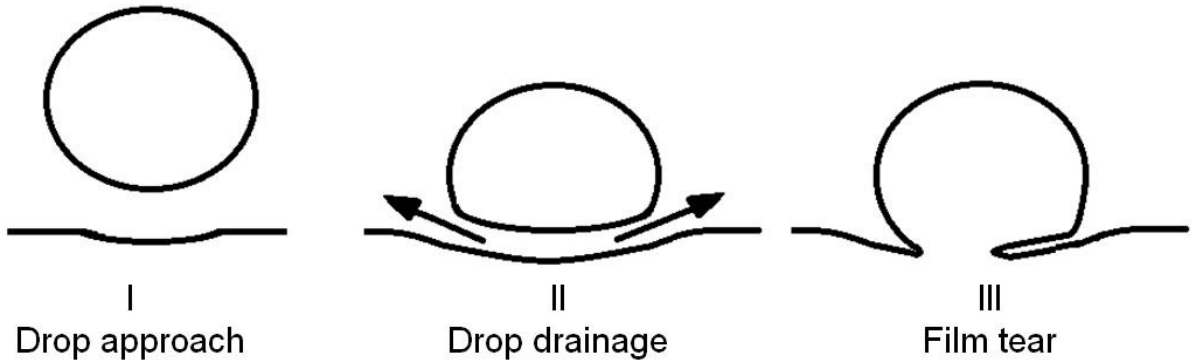

Fig. 2-2: The coalescence of drop according to Henschke, 1994.

In the first stage of droplet coalescence, the drop approaches the bulk phase. The undistorted droplet and interface of the bulk phase can be observed at first. When droplet and interface are close enough, both of them will be distorted. Therefore, the drainage of the continuous film between droplet and bulk phase occurs (II) (Aarts and Lekkerkerker, 2008). In the third stage (film tear or film breakup), the mechanism of the breakup of the film between droplet and bulk phase cannot be clearly explained in molecular fluid. Therefore Aarts and Lekkerkerker used thermal capillary waves to observe the breakup of the film. In the case of organic mixture, the minimal van der Waals force between droplet and bulk phase can be observed (Israelachvili, 1992). Consequently the neck of connection between droplet and bulk interface grows linearly with time.

Close-packed models of drops

It is important to identify the location where the coalescence is initially occurred. This can be done by observing the settling behavior. Coalescence occurs when drops are approaching and getting closer to each other until the distance between droplets is almost zero. This takes place in the close-packed zone. Therefore, the close-packed models can be used to determine the location where the coalescence occurs. Once the location is determined, the hold-up can be determined as well. Therefore, the close-packed models can describe the relationship of distance between drops and hold-up.

Since the hold-up depends on the drop volume per total volume and hence directly on the (average) distance between the drops, the distance between droplets must be calculated accurately by using a close-packed model. Three close-packed models have been investigated in this work: a cubic close packing, a body-centered tetragonal close packing and a hexagonal close packing. These three close-packed models are derived based on the same general equations for the hold-up:

$$\varepsilon_0 = \frac{nV_{drop}}{V_{total}}, \tag{2-21}$$

where ε_0 is local hold-up, V_{drop} the volume of a drop, n the number of the drop and V_{total} the total volume. This equation is only valid for mono-sized droplets. By assuming the droplets to be spheres the volume of drop is defined as:

$$V_{drop} = \frac{\pi d^3_{32,0}}{6} \tag{2-22}$$

Punsang et al., (2014) explained the droplet packed in the dense-packed zone using three different pack models of rigid sphere, which are a hexagonal close packing, body-centered tetragonal packing and cubic close-packing.

Model 1: Cubic close-packed model

As shown in Fig. 2-3, the droplet packing according to the cubic close-packed model has the least density compared to other packing models. The general equation for cubic close-packed model is defined in equation 2-23. The ratios between drop distance (s) and drop diameter ($d_{32,0}$) is simply obtained by substituting equation 2-22 and 2-24 into equation 2-23 and the result is written in equation 2-25.

$$\varepsilon = \frac{8\frac{1}{4\cdot 2}V_{drop}}{V_{total}} \tag{2-23}$$

where

$$V_{total} = \left(d_{32} + s\right)^3 \tag{2-24}$$

$$\frac{s}{d_{32}} = \frac{0.805996}{\varepsilon^{1/3}} - 1 \tag{2-25}$$

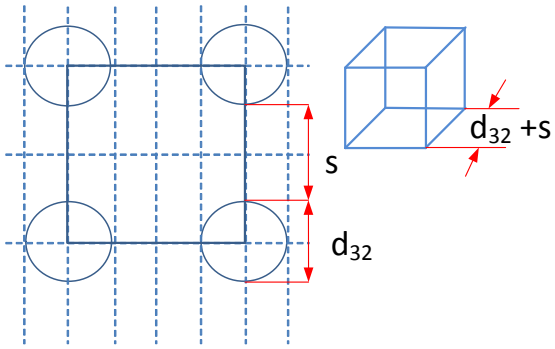

Fig. 2-3: Schematic representation of the cubic close-packed model (Punsang et al., 2014)

Model 2: Body-centered tetragonal close-packed model

A body-centered tetragonal close packing is displayed in Fig. 2-4 and its general equation is given in equation 2-26. The ratio of s/d_{32} is written as shown in equation 2-28.

$$\varepsilon = \frac{\left(8 \cdot \frac{1}{8} + 1\right) V_{drop}}{V_{total}} \tag{2-26}$$

where

$$V_{total} = \left(d_{32} + s\right)^3 \sqrt{3} \tag{2-27}$$

$$\frac{s}{d_{32}} = \frac{0.0845583}{\varepsilon^{1/3}} - 1 \tag{2-28}$$

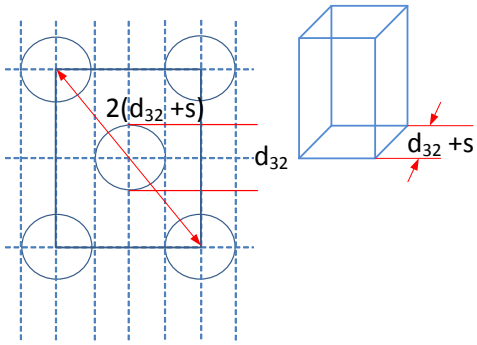

Fig. 2-4: Schematic representation of the body-centered tetragonal close-packed model (Punsang et al., 2014).

Model 3: Hexagonal close-packed model

The most dense packing can be achieved with a hexagonal close packing as depicted in Fig. 2-5. The general equation and the ratios s/d_{32} are defined in equation 2-29 and 2-31, respectively.

$$\varepsilon = \frac{(3+3+3)V_{drop}}{V_{total}} \tag{2-29}$$

where

$$V_{total} = (d_{32}+s)^3 \cdot \frac{9}{2}\sqrt{2} \tag{2-30}$$

$$\frac{s}{d_{32}} = \frac{0.9047}{\varepsilon^{1/3}} - 1 \tag{2-31}$$

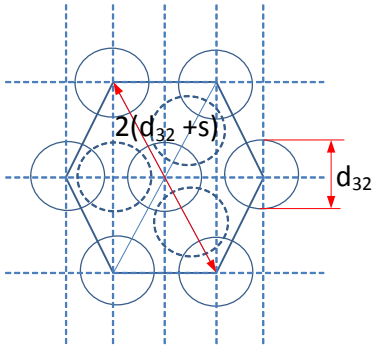

Fig. 2-5: Schematic representation of the hexagonal close-packed model (Punsang et al., 2014).

As illustrated in Fig. 2-3 to Fig. 2-5, these three models are different in the packing as well as the density and void fraction. This results in a difference in hold-up. Table 2.1 presents the packing density and void faction of close-packed models. The values were calculated based on the general equation 2-21 for the case when the distance between droplets is zero and the droplets are still in a spherical shape. The results show that the hexagonal close-packed model has the highest packing density whereas cubic close-packed model has the lowest.

Table 2.1: Packing density and void fraction according to close-packed models (Dullien, 1992)

Model	**Packing density**	**Void fraction**
Cubic close-packed model	0.5236	0.4764
Body-centered tetragonal close- packed model	0.6046	0.3954
Hexagonal close-packed model	0.7405	0.2595

2.4 Influence of electrolyte and viscosity on settling

The effects of salt (electrolytes) on the extraction process have been studied for long time. The admixture of inorganic salt to a mixture of water and a water-miscible organic solvent may cause separation of the solvent from the mixture and the formation of a two-phase system (Frankforter and Cohen, 1914). Sometimes this phenomenon is called "salt-induced phase separation". Observations of this "salting-out" phenomenon were made for a number of water-miscible organics such as acetone, methanol, ethanol, and acetonitrile. The degrees of phase separation were changed due to the different salts and different salt concentrations. At high salt concentrations usually salting out occurs. This behavior may also be used to increase the efficiency of the extraction with nonpolar, immiscible organic solvents as well.

There are several research studies about the influence of electrolytes on coalescence. In 1990, the effect of electrolytes on the coalescence of oil droplets in aqueous solution was studied by Stevens et al. The results showed that the effect of electrolytes is very small in the case of nonpolar organic liquids but for the case of polar organic liquids, the coalescence time is longer when the concentration of electrolytes increases. (Stevens et al., 1990) The effect of electrolytes on organic liquids for the coalescence of droplets was studied again in 1998 by Chen et al. for a methyl isobutyl ketone system. From the observations, the results are similar to the results from Stevens et al. This study is about the case of electrolytes of triple valent cations and anions such as $AlCl_3$, $LaCl_3$ or Na_3PO_4 in MIBK. Increasing the electrolyte concentration causes the coalescence of aqueous droplets to be much faster and of organic droplets to be much slower. (Chen et al., 1988) In 1998, Pfennig and Schwerin also studied the influence of electrolytes on liquid-liquid extraction in 1-butanol+water system with volumetric phase ratio between organic and aqueous phase equal to 5/2. Their result showed that low concentrations of salts (1 mol/m^3) also affect the settling time, which increases by a factor of more than 1000 when adding salt into this system. But the settling time was reduced again at salt concentration between 10 and 100 mol/m^3. Fig. 2-6 represents the settling time of this system as a function of the salt concentration.

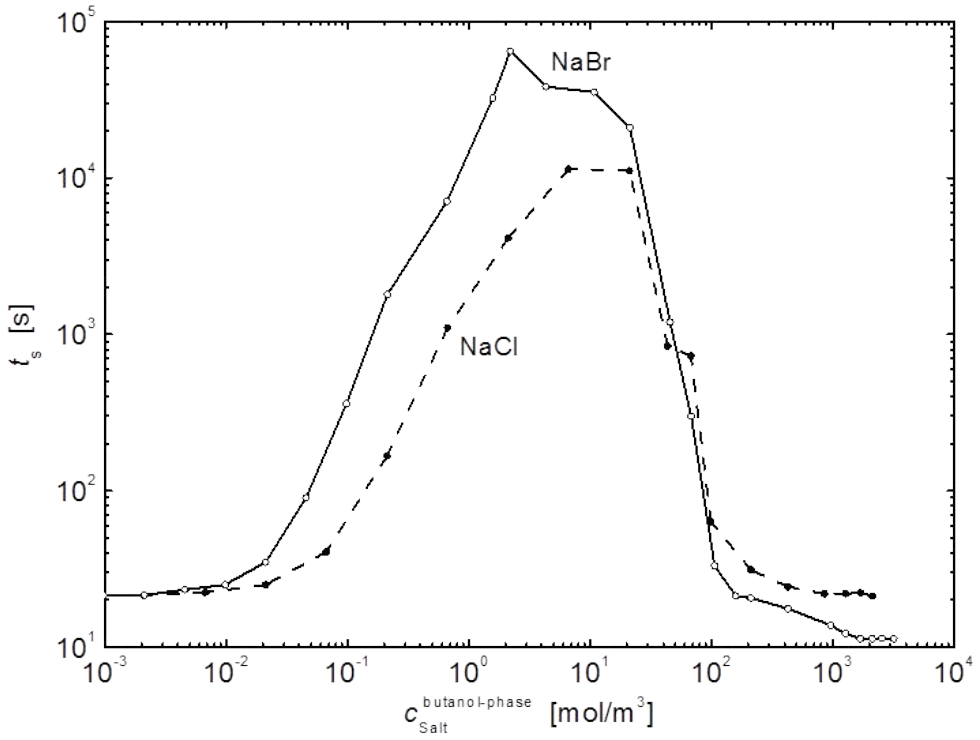

Fig. 2-6: Settling times for the system 1-butanol+water for a dispersed phase at 293 K with two salts added in varying concentrations (Pfennig and Schwerin, 1998)

The viscosity is as well an important property to affect the coalescence time in liquid-liquid extraction. Changing the viscosity of dispersed and continuous phase has an effect on mass transfer between the phases, and also affects the film drainage rate causing a change in the coalescence time as well (Bazhlekov et al., 2000; Chevaillier et al., 2006). There are three types of interfacial behavior during coalescence:

- Immobile interface; the viscosity of disperse phase is very large when compared with the continuous phase;
- Fully mobile interfaces; the viscosity of continuous phase is much higher compared with the disperse phase;
- Partially mobile interfaces; the viscosity ratio is temperate (10^{-2}…10^{2}). (Chester, 1991; Abid and Chester, 1994; Saboni et al., 1995)

In 2009, Wang et al. studied the effect of viscosity on the coalescence time. Their results showed that admixture of glycerol increases the viscosity of the water phase and decreases the interfacial tension and hereby the coalescence time also decreases (Wang et al., 2009).

2.4.1 DLVO theory

The electrolytes have an influence on the settling of droplets (Pfennig and Schwerin, 1998, Stevens et al., 1989, Chen et al., 1998, Pattarawut, 2010, Anursan et al., 2012, Effertz, 2011, Manodumrongthum, 2012, Mungma et al., 2014). This behavior is explained via the interaction force between two droplets (see Fig. 2-7) namely DLVO theory.

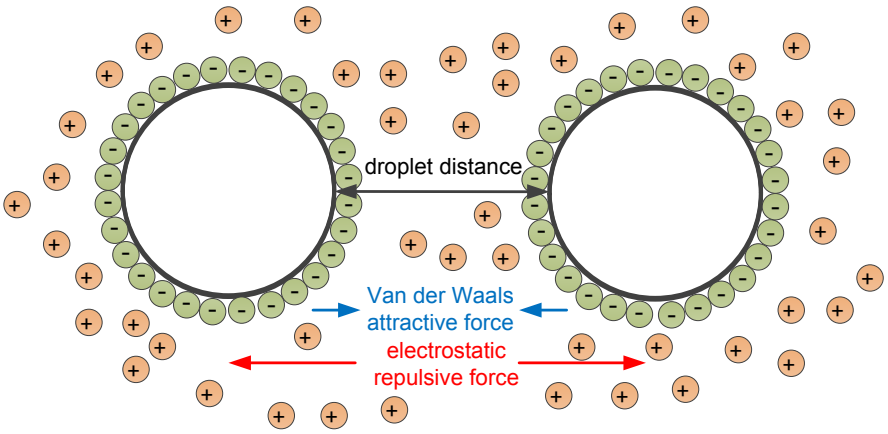

Fig. 2-7: DLVO theory: interaction forces between two droplets

This theory was given name from the initial letters of Derjaguin, Landau, Verwey and Overbeek (DLVO). It describes a balance between Van der Waals and electrostatic forces. The positive and negative electric charges and other properties are distributed over a surface uniformly. The total interaction force (F_T) between two droplets as a function of Van der Waals (F_{vdw}) and electrostatic (F_{el}) forces $F_T = F_{vdw} + F_{el}$.

Van der Waals force (F_{vdw}) is a function of Hamaker constant ($A_{1,2,3}$), drop diameter (R_0) and droplet distance (a)

$$F_{vdw} = \frac{\pi^2 A_{1,2,3} R_0}{12 a^2} \tag{2-32}$$

where the Hamaker constant ($A_{1,2,3}$) (Leite et al., 2012) between two droplets can be applied by

$$A_{1,2,3} = \frac{3}{4} k_B T \frac{\varepsilon_1 - \varepsilon_3}{\varepsilon_1 + \varepsilon_3} \frac{\varepsilon_2 - \varepsilon_3}{\varepsilon_2 + \varepsilon_3} + \frac{3 h v_e}{8\sqrt{2}} \frac{\left(n_1^2 - n_3^2\right)\left(n_2^2 - n_3^2\right)}{\sqrt{\left(n_1^2 + n_3^2\right)}\left(\sqrt{\left(n_1^2 + n_3^2\right)} + \sqrt{\left(n_2^2 + n_3^2\right)}\right)} \tag{2-33}$$

with the Boltzmann constant (k_B), the Planck constant (h), absorption frequency (v_e) the dielectric constants (ε_i), refractive index (n_i) (subscript 1 and 2 is for the droplet and 3 is the media).

Electrostatic force (F_{el}) is

$$F_{el} = 2\pi R_0 \varepsilon_0 \varepsilon_r \psi_0^2 \kappa \exp(-\kappa a) \tag{2-34}$$

where ε_0, ε_r, ψ_0 and a are permittivity of free space, dielectric constant, electrostatic potential difference and distance between two droplets, respectively. The Debye–Hückel screening length (κ^{-1}) is

$$\frac{1}{\kappa} = \sqrt{\frac{\varepsilon_r \varepsilon_0 k_B T}{2 N_A e^2 I}} = \sqrt{\frac{\varepsilon_r \varepsilon_0 R T}{2 F^2 C_0}} \tag{2-35}$$

with temperature (T), Avogadro constant (N_A), elementary charge (e), ionic strength of the electrolyte (I), Faraday constant (F), concentration (C_0) and gas constant (R).

3 Experimental setup

In this research programme two methods for investigating the phase separation process of low viscous and high viscous dispersions were performed. These are the optical technique and the ultrasonic technique which will be explained in the following.

3.1 Chemical system

In this chapter, the chemical systems which have been used in this research and the equipment are explained. Even small impurities have a big influence on the settling behavior of two-phase systems. A small amount of them will shift the settling time. To avoid the change of settling behavior and in order to make the result reproducible, all purchased chemicals which are used in this research have p.a. (pro analysis) grade quality. The water used in the experiments was either bi-distilled or ultrapure water generated with a Barnstead E-pure purification system. A list of the used chemicals is shown in Table 3-1.

Two different batches of MIBK and Cyclohexanone have been investigated in a standardized settling cell and an optical cell respectively to study the effect of impurity differences. It can be seen from Table 3-2, that the chemicals from different batches do not have the same settling time. Therefore, it is necessary to use the same batch for all comparison experiments.

Table 3-1: List of chemicals

Chemical	**Batch number**	**Company**
Methyl isobutyl ketone (MIBK)[2]	K42353646	Merck KGaA
Methyl isobutyl ketone (MIBK)	452193304	Carl Roth GmbH
Methyl isobutyl ketone (MIBK)	513208521	Carl Roth GmbH
Toluene[1,2]	-	AVT-TVT, RWTH-Aachen
Toluene	2F005908	AppliChem GmbH.
Cyclohexanone	472193603	Carl Roth GmbH
Cyclohexanone	013193603	Carl Roth GmbH
Cyclohexanone	193200133	Carl Roth GmbH
NaCl[2]	K41498446	Merck KGaA
NaCl	12E250019	VWR BDH Prolabo
Na_2SO_4[2]	K42353646	Merck KGaA
Polyethylene glycol (PEG 4000)[2]	1741722/100	Sasol GmbH
Polyethylene glycol (PEG 4000)	12H220008	VWR BDH Prolabo

[1]Distillated at AVT-TVT, RWTH-Aachen, [2]the chemicals have been on stock at AVT-TVT, RWTH-Aachen, Germany.

Table 3-2: Comparison of settling time from different chemical batches (production and company)

System (+water)	Equipment	Batch number	Settling time [s]
MIBK	Standardized settling cell	452193304	35
MIBK	Standardized settling cell	K42353646	19.3
Cyclohexanone +10wt% PEG4000	Optical cell	472193603, 12H220008	2517
Cyclohexanone +10wt% PEG4000	Optical cell	193200133, 12H220008	440

It is important that the liquids used in these experiments need to be saturated before the experiment takes place. Settling data for unsaturated phases can vary greatly because of mutual solubility. Therefore, the chemicals should be prepared one day before the experiment. The polyethylene glycol solution should not keep more than 5 days because it can change the physical properties by bacterial impact. The physical properties of the investigated systems can be found in appendix 8.3.

To enable investigation of the drop size distribution in high-viscosity systems, particles of two different polymer materials which are polyoxymethylene (POM) and polyamide 6.6 (PA66) obtained from Kugelfertigung Hoch KG, Germany, were used. The physical properties are shown in Table 3-3.

Table 3-3: Properties of particles[1].

Particle material	Density (g/cm^3)	Particle size (mm)	Approx. number of particles	Liquid absorption
Polyoxymethylene (POM)	1.4	2.0	4800	minimal absorption
		2.5	5000	
		3.0	4900	
		5.0	5000	
Polyamide 66 (PA66)	1.14	2.0	5000	slight absorption
		3.0	5000	
		5.0	5000	

[1]Data from (Kugelfertigung Hoch KG, 2012)

3.2 Optical methods

3.2.1 Standardized settling cell

Fig. 3-1a showed the batch-settling apparatus modified by Ruckes (2011) (the original design is by Henschke, 1994). It was used to investigate the influence of electrolyte and viscosity on settling. Fig. 3-1 represents the settling cell used to carry out the experiment.

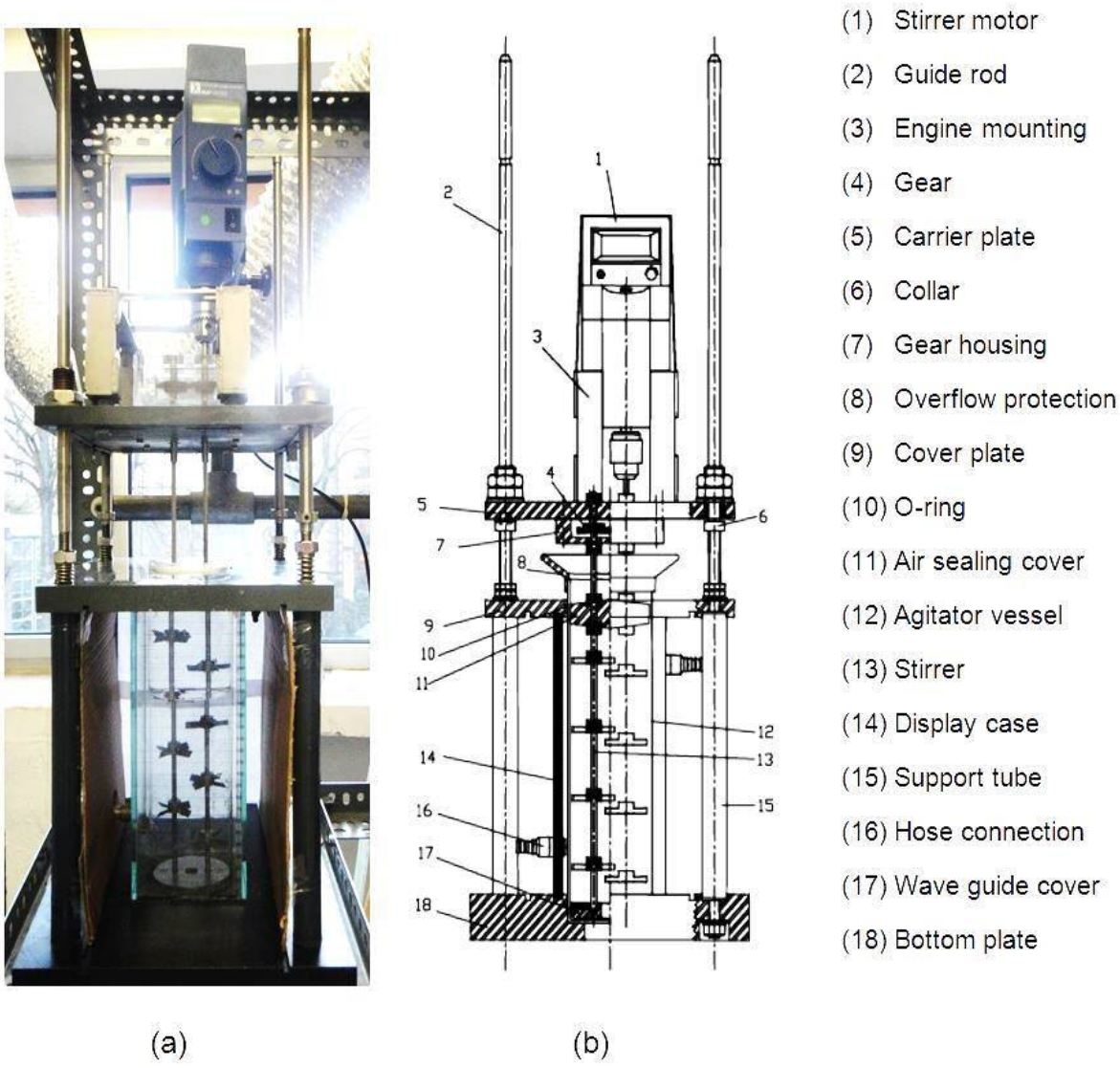

Fig. 3-1: (a) Picture of the settler cell (b) Schematic of the Settling apparatus (Anursan, 2012).

As shown in Fig. 3-2b, the settling cell consists of a double wall glass cylinder (12) with two counter rotating agitators (13) which are driven by a motor (1). On each agi-

tator a set of four four-bladed stirrers is fixed providing axial mixing in the system. The agitators rotate in different directions. The variable speed of the motor drive can be controlled from 50 rpm to 2000 rpm. In the experiments, the speed of the motor was always kept at 800 rpm according to Henschke (1994). The mixing time was set to 30 seconds (Henschke, 1994) and agitation time and the settling time were recorded with a stop watch. A cover plate (8) at the top of glass cylinder is used to prevent air from being mixed in. Cooling water from a thermostatic bath (14) is pumped through the double wall gap of the glass cylinder. It controls the temperature throughout the experiment. Temperature set point was 20 °C. A scale is attached to the cell for easy observation of the sedimentation and coalescence height over time. The experiments were recorded with a video camera (Sony-DCR-SR55). The arrangement of lighting and camera for the experimental setup is shown in Fig. 3-2. Two 250 Watt spotlights are placed in the front and behind the cell. To prevent reflection of light and in order to get better light diffusion, a matt paper is placed behind the cell and two black paper sheets are fixed on both cell sides. The experiment is finished when half of the boundary surface is covered with drops. The settling time is recorded. The data for the coalescence and sedimentation curve can be determined from the recorded video.

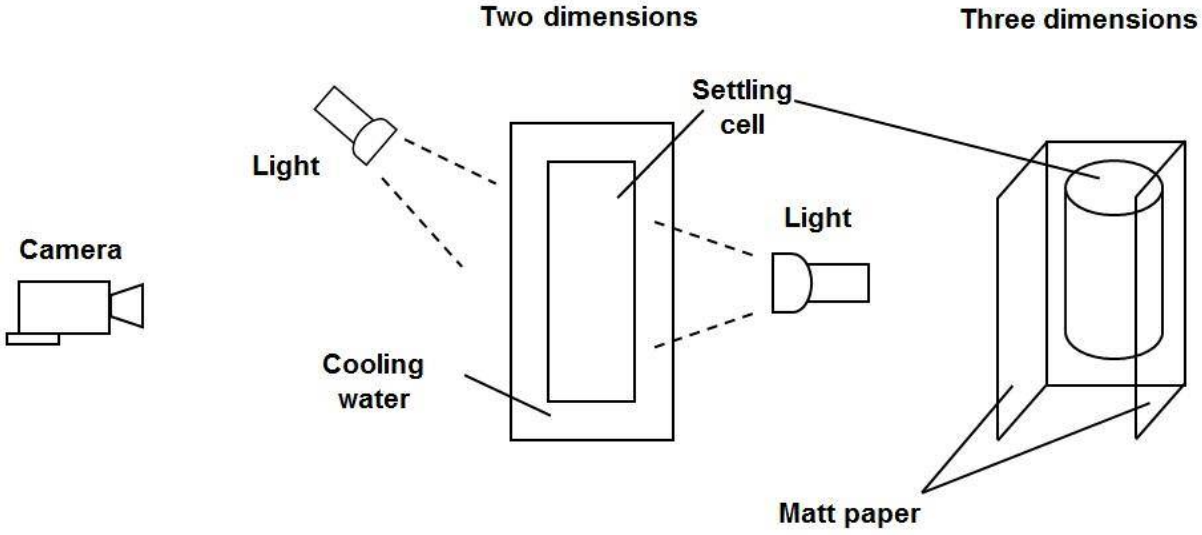

Fig. 3-2: Schematic of experimental setup: arrangement of lighting and camera (Anursan, 2012).

3.2.2 Optical cell

To match the dimensions of the decanter of the ultrasonic scanner, a new optical cell was constructed. A standardized mixing unit which has been modified from the standardized settling cell and the optical cell were used to study the behavior of liquid-liquid coalescence and sedimentation in laboratory scale. The external force input of the mixer provides sufficient mixing force to generate a dispersion between two liquid phases. The laboratory scale optical cell assembly consists of standardized mixing unit, a mixing motor, the optical cell and a water bath for controlling temperature as shown in Fig. 3-3.

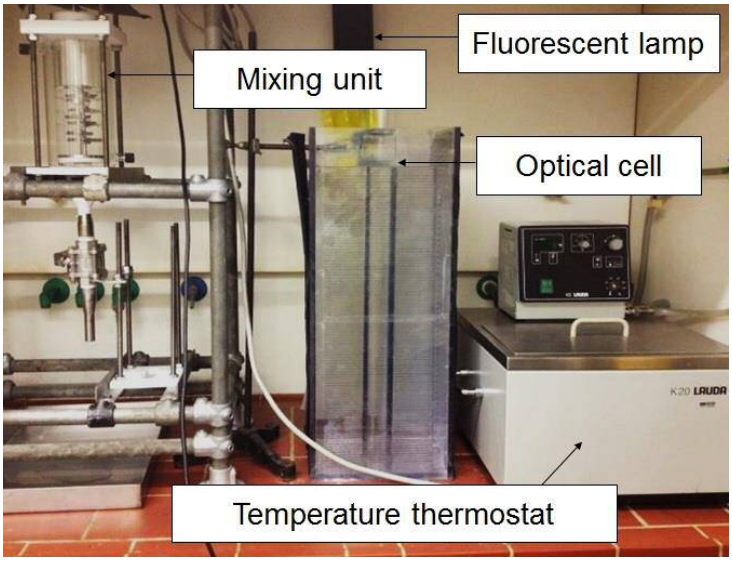

Fig. 3-3: Optical cell assembly

The standardized mixing unit consists of a double-wall vessel and two shafts with four propellers as in the standard settling cell. The vessel is made of borosilicate glass and can be connected to a thermostat. It has a cylindrical form with an inner diameter of 80 mm and a height of 220 mm. In the vessel, two rotating shafts driven by speed controlled motor are installed for mixing. Each shaft has four four-bladed diagonal stirrers, installed at different height. The propellers were mounted on different directions to completely mix two immiscible liquid. Importantly, one shaft rotates in clockwise direction while another rotates in counterclockwise. The mixing unit and schematic of propellers are shown in Fig. 3-4.

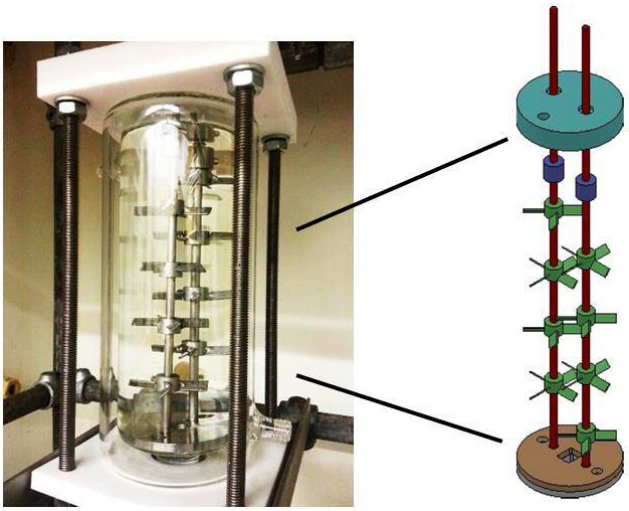

Fig. 3-4: Mixing unit and schematic of propeller.

The optical cell was used for monitoring phase separation. It consists of a cylindrical glass and a water bath which can be connected to a thermostat (see Fig. 3-3). The cylindrical glass, which has similar dimensions as the ultrasonic decanter, has an inner diameter of 56 mm and a height of 600 mm.

3.2.3 Internal cell

As for the optical cell, the saturated two-phase system is generated in the mixing unit (see Fig. 3-5) at a stirrer speed of 800 rpm for 30 seconds. Then a ball valve is quickly opened to feed the liquid into the settling glass with internals, which has been placed inside this lower cell beforehand (see Fig. 3-5a). The experiment is recorded via the settling time taken when half of the interface area is covered with a monolayer of drops. The data for the coalescence and sedimentation curve can be determined from the recorded video.

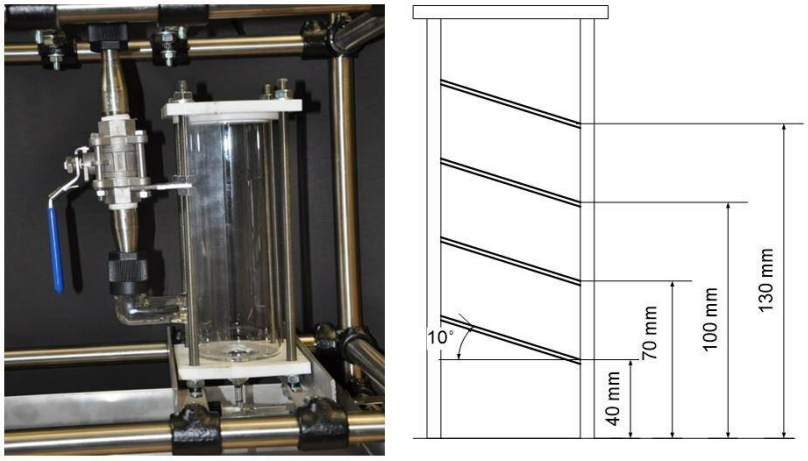

Fig. 3-5: Internal cell (a) settling glass (b) design of inclined plates in the settling cell (Mungma et al., 2014).

The inclined plates (see Fig. 3-5b) are made of stainless steel with a thickness of 2 mm and a diameter of 78 mm. The 10° inclined plates were placed in the settling cell in order to study the influence of internals on settling time of viscous system.

3.3 Ultrasonic scanner

An ultrasonic suspension analyzer, type SUSS-2008 from Rhosonics Analytical B.V., Netherlands, was used to investigate the behavior of sedimentation and coalescence in batch settling processes.

The ultrasonication equipment generates sound waves which pass the media sample perpendicular to the direction of phase separation. The speed of sound, attenuation and propagation vary with changing media composition (see Fig. 3-6). The wave is generated by the transducer (T) and passes the medium. As shown in 3-1 the attenuation coefficient α

$$\alpha = -\frac{1}{x}\ln\left(\frac{A_0}{A_t}\right) \tag{3-1}$$

can be calculated from the amplitude at initial position A_0, the amplitude at position A_t and the distance x. The generated sound waves are cyclic and have a typical sound velocity between 1,000 and 2,500 m/s.

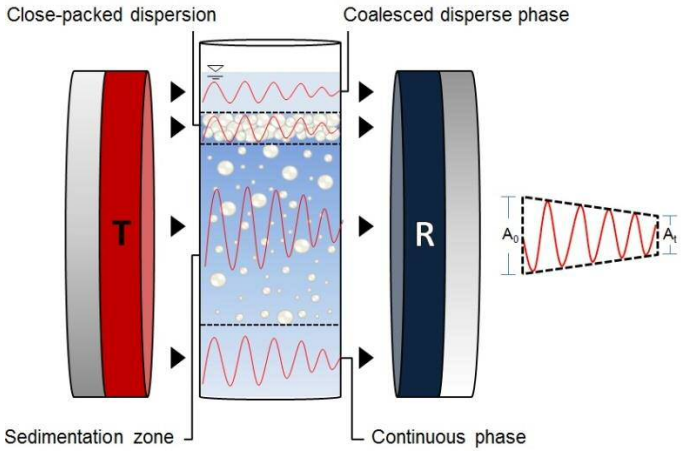

Fig. 3-6: Principle of ultrasonic scanner

The sound speed in the fluid is calculated in the scanning software by the Newton-Laplace equation which is a function of the physical properties bulk modulus K and density ρ.

$$c = \sqrt{\frac{K}{\rho}} \tag{3-2}$$

The changing speed of sound is representing the change in density and therefore, of the local hold-up.

This ultrasonic scanner consists of four main components (see Fig. 3-7): the temperature control unit, the decanter, the scanning ring and the data processing unit. The removable decanter, made from Polyphenylsulfide (PPS), is chemical resistant and allows an easy propagation of the sound wave. The suspension is filled into the decanter. The removable transmitter and receiver are mounted on the scanning ring. The scanning ring can move up and down along the decanter on linear guiding shafts. The desired temperature of the suspension is maintained via a water bath. Eight heater mats surround the bath. They are controlled by a PID controller (Rhosonics, 2012). The ultrasonic scanner can scan in one millimeter steps up to a maximum height of 500 mm. The scanning ring detects the sound speed of liquid suspension in the decanter only in the upward direction. The scanning time depends on the height set-up and the analyzer settings, e.g. maximum attenuation, signal filter and sound path. For the normal set-up, it will take about 20 to 40 s per data scan. The scanning ring has a transmitter to convert electric signals into sound waves. These are picked up by the receiver on the other side and converted back to electric signals (Rhosonics, 2012). The data processing unit processes the properties of the wave obtained by the receiver and generates a Microsoft Excel output file. The output data consists of scanning time (s), position (mm), temperature (°C), speed of sound wave (m/s), attenuation (dB) and gain (dB). The range of sound speed to be measured must be entered into the settings of the scanner prior the scanning. To ensure an accurate measurement, it is preferable that this range is as narrow as possible. The minimum and maximum sound speeds of the investigated systems are as following:

MIBK + water + PEG4000: 1300 m/s to 1700 m/s

Toluene + water + PEG4000: 1200 m/s to 1600 m/s

Cyclohexanone + water + PEG4000: 1400 m/s to 1700 m/s

Moreover, the scanning time must be set to be same as the observation time.

To measure the speed of sound during the dead time, the scanning time was set to 180 s. Also, it is very important to set up the scanning time until the settling time is finished.

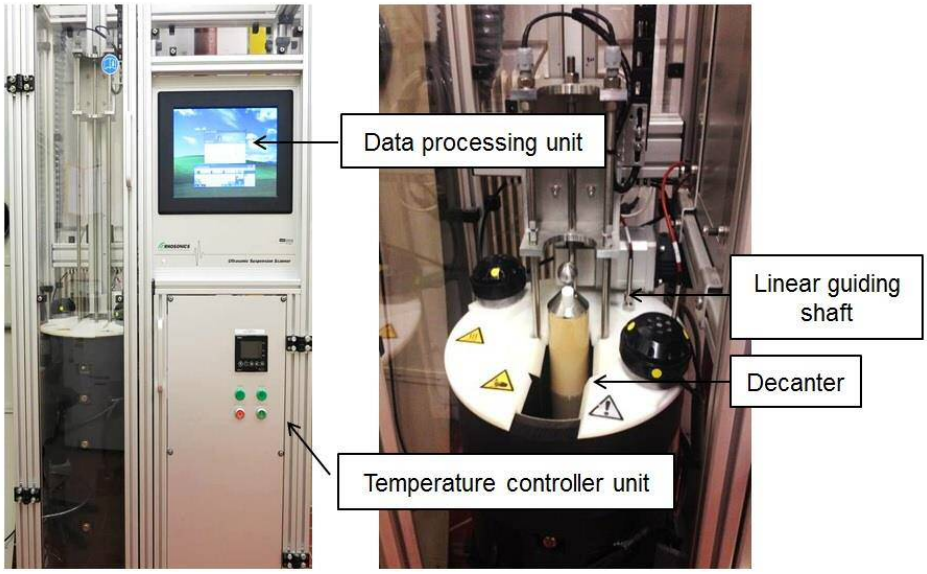

Fig. 3-7: Ultrasonic scanner Rhosonics SUSS-2008.

3.3.1 Measurement accuracy

Error, inaccuracy and imprecision of the equipment can cause problems. Especially, the sedimentation curve, coalescence curve and dense-packed zone curve are very sensitive to the speed signal. Therefore, an accuracy range of the sound-speed signal from an ultrasonic scanner has to be determined. A saturated pure phase is filled in the ultrasonic decanter. The speed of sound was measured every 1 mm position. The result is shown in Fig. 3-8. It can be seen from the result that the speed value of a saturated aqueous phase is maximum 1519.99, minimum 1518.40 and average 1519.19 m/s. The error of signal data is about ± 2 m/s. The limited accuracy data can be used for the minimum boundary for the hold-up calculation. In this research, the measurement accuracy has been tested in all experiments.

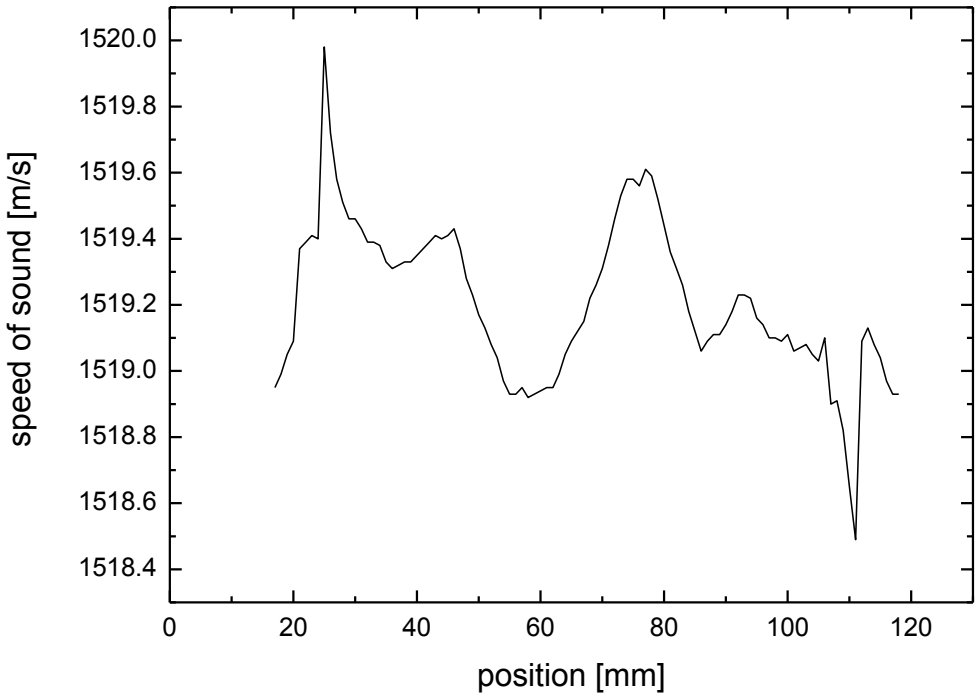

Fig. 3-8: Sound speed signal of the ultrasonic scanner.

3.3.2 Hold-up validation

In order to validate the hold-up from the speed of sound data, the speed of sound of known hold-ups was measured for every experimental system. The experiments were simply performed by mixing known volume ratio of organic and aqueous phase by the mixer at 800 rpm for 30 seconds and then the sound speed was measured with the ultrasonic scanner. The measuring time was 50 to 150 seconds because the speed of sound during the dead time was needed only. The hold-up to be analyzed lies between 0 and 1. The sound speed difference is represented as a function of hold-up

$$\left|c_{org} - c_{aq}\right| = f(\varepsilon) \tag{3-3}$$

Fig. 3-9 shows the relation between the speed of sound difference and the hold-up of the system cyclohexanone + water + 10wt% PEG4000. The analyzed hold-up values were 0, 0.05, 0.1, 0.25, 0.5, 0.71, 0.83, 0.91, and 1.

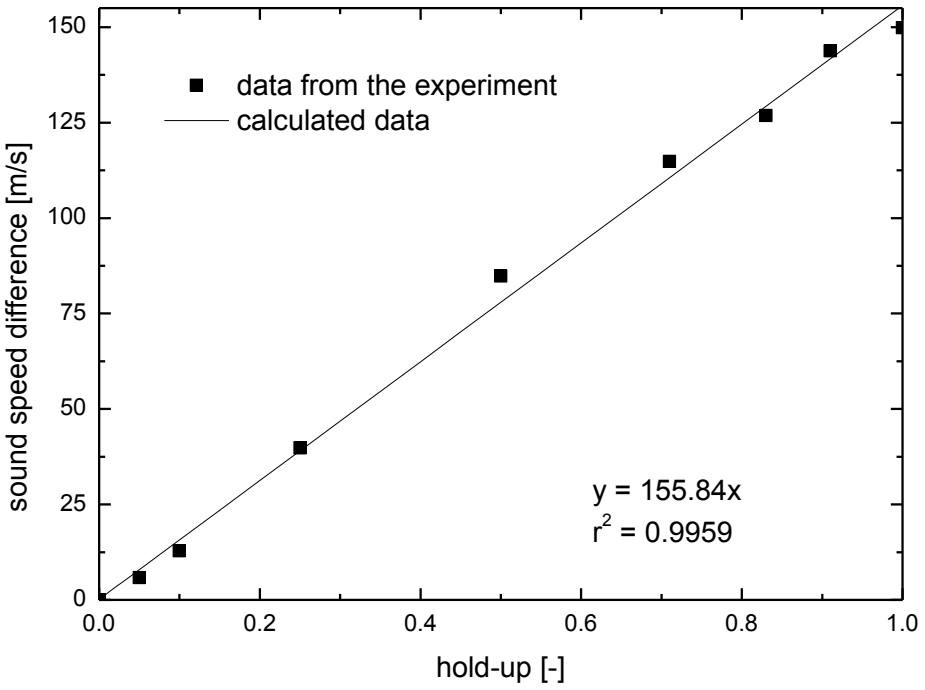

Fig. 3-9: Relation between speed of sound difference and hold-up; test system cyclohexanone + water + 10wt% PEG4000; temperature: 20°C

The speed of sound as a function of hold-up is

$$\Delta c = 155.84\varepsilon \tag{3-4}$$

where the coefficient of determination r^2 is 0.9959.

3.3.3 Influence of temperature on the speed of sound

As explained in topic 3.3, the temperature has a big influence on the sound speed. Hence, the relation between the speed of sound and the temperature was investigated. The sound speed was evaluated for both aqueous phase and organic phase for different temperature (20 to 40 ºC), as shown in Fig. 3-10. The sound speed increases with the temperature for the aqueous phase, while in the organic phase the sound speed decreases with the temperature. Thus, it is necessary to control the experimental temperature. In this research, the temperature is 25 ± 0.02 ˚C for all further experiment.

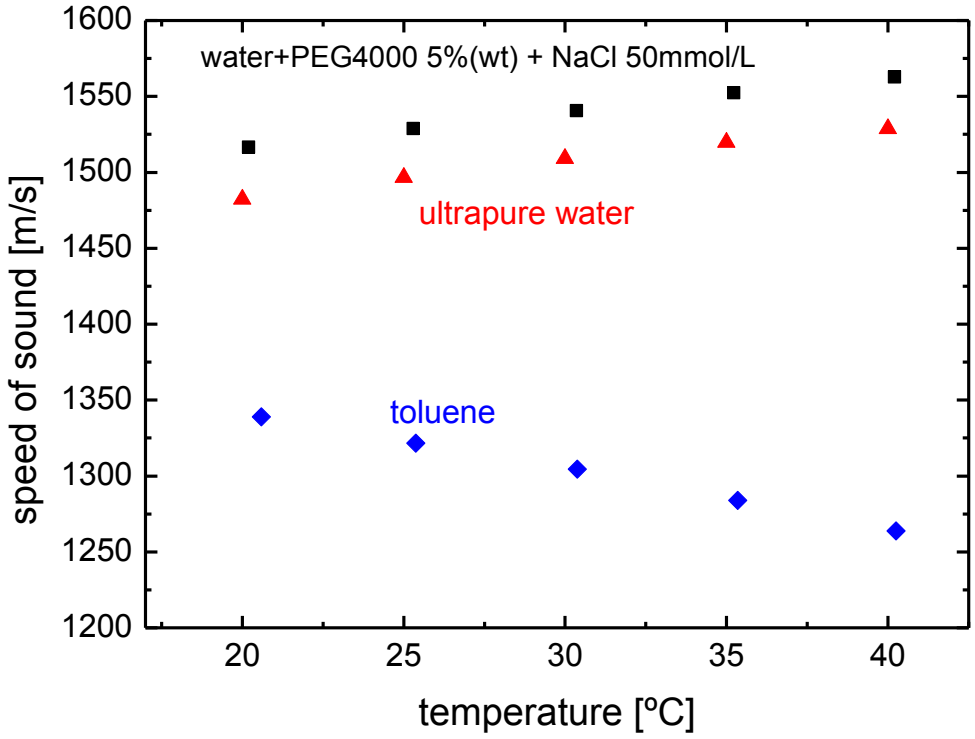

Fig. 3-10: Temperature influence in sound speed in organic and aqueous phases: toluene + water + 5wt% PEG4000 + NaCl 50 mmol/L.

3.4 Validation of optical cell and ultrasonic scanner

The optical cell (see Fig. 3-3) is used to validate the ultrasonic scanner (see Fig. 3-7) by comparing the results of both methods. As a test system Toluene + water was chosen. Toluene (analytical grade, batch nr. 2F005908) and NaCl (analytical grade, batch nr. 12E250019) were obtained from AppliChem GmbH and VWR BDH Prolabo, respectively. The aqueous phase viscosity was adjusted by adding polyethylene glycol with a specified mean molecular weight of 4000 g/mol obtained from VWR BDH Prolabo (batch nr. 12H220008). Ultrapure water was used in the experiments. The experiments were performed at a volumetric phase ratio between organic and aqueous phase (o/a) of 1/2. The aqueous solution was prepared by adding 50 mmol/L_{aq} of NaCl and 5 wt% of PEG 4000 to ultrapure water. Density and viscosity of the aqueous phase were 1008 kg/m^3 and 1.921 mPa s, respectively. PEG4000 and NaCl were added to increase the settling time of the system. The standardized mixing unit (see Fig. 3-4) was used for mixing toluene and water (with PEG 4000 and salt) at 800 rpm for 30 seconds. Then, the dispersion was transferred to either the optical cell or the ultrasonic decanter. The sedimentation and coalescence behavior of the system toluene + water in the optical cell was recorded on video for evaluation. The results from the optical cell were compared with the results of the ultrasonic equipment. Fig. 3-11 shows the data record from ultrasonic scanning and optical detection.

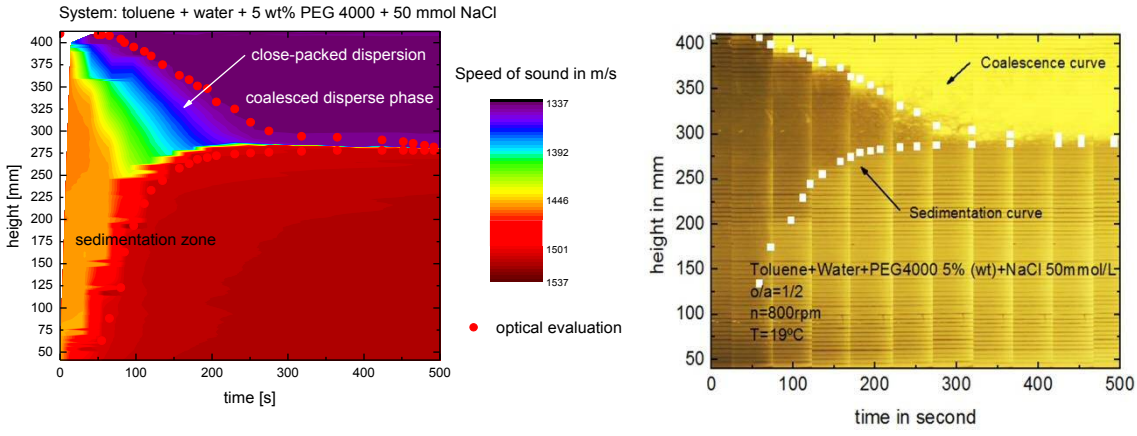

(a) (b)

Fig. 3-11: Comparison of ultrasonic scanning (a) with optical detection (b) (Aunyindee, et al., 2013).

In order to obtain the sedimentation and coalescence height with time, pictures from the video were taken and contrasted afterwards (see Fig. 3-11b). In this experiment toluene was the dispersed phase. The data from ultrasonic scanning are plotted in Fig. 3-11a.

The results show that the height of the sedimentation zone and the coalescence curve can be determined from time dependent speed of sound and height in the ultrasonic scanner. The curves are quantitatively identical with the settling trend observed in the optical cell. The ultrasonic technique can be used to determine the boundary between close-packed dispersion, coalescence and sedimentation zone, even in opaque systems where optical detection fails. It additionally allows quantitative evaluation of local hold-up in opaque systems.

4 Modeling of sedimentation

If a dispersion is separated by gravity, three zones are visible by optical evaluation, the continuous phase, the coalesced dispersed phase and a turbid zone including the sedimentation zone and the dense-packed zone. The boundaries between these zones are the sedimentation curve and the coalescence curve. If the sedimentation is faster than the coalescence of the droplets the dense packed zone is formed. In this zone drop-drop coalescence occurs, causing the drop diameter to increase. The information of the coalescence and sedimentation curve can then be used to design a settler

Henschke et al. (2002) consider only a monodisperse droplet size, while in reality a polydisperse distribution will occur. The very fine droplets do not sediment with the majority of droplets leading to a secondary sedimentation. Secondary sedimentation cannot be evaluated by optical techniques in most case.

The experiments clearly showed a hold-up variation within the sedimentation zone and the continuous phase, where in the optical cell only one line could be seen. Therefore, a new model approach was developed to describe this behavior.

4.1 Sedimentation model

The velocity of each droplet relative to the surrounding fluid depends on the droplet size. Small droplets have a lower velocity compared to bigger droplets. In the settling process the smallest droplets will therefore be part of the second sedimentation phase leading to a hold-up variation. In the beginning of a settling experiment the polydisperse droplets are equally distributed in the sedimentation zone.

Due to the faster sedimentation velocity of bigger droplets, separation zones of different sedimentation velocity are formed with time, containing only droplets below a certain size. This results in a change of the local hold-up. The hold-up and the drops sizes for different height elements are sketched in Fig. 4-1.

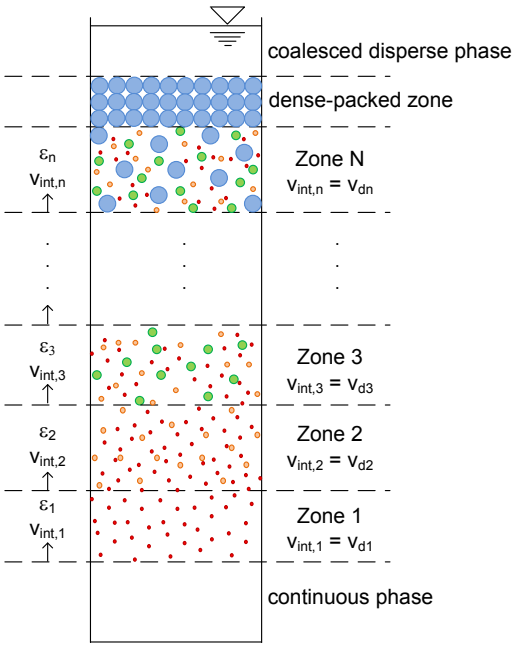

Fig. 4-1: Sedimentation of polydisperse droplets (Chuttrakul and Pfennig, 2014).

As a starting point for the modeling, a drop size distribution is assumed. This distribution may be varied to fit the model results to the experimental data. A set of drops is generated in the simulation which each droplet assigned randomly a position within the settling cell taking into account the average hold-up of the experiment. This corresponds to the situation directly after the mixing process, where different drop sizes can be found everywhere in the cell after stopping the mixer. By knowing the size and the position of all droplets, the local hold-up for all height elements can be calculated.

The model of Pilhofer and Mewes (1979) was used to determine the swarm drop velocity for each droplet depending on the drop size and the local hold-up. Here, it has to be taken into account that for every drop moving up some continuous phase has to move down due to continuity (see Fig. 4-2). This counter-current flow slows down the sedimentation speed. Some small droplets might even move down.

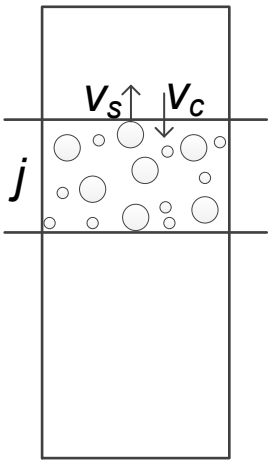

Fig. 4-2: Balance of droplets in sedimentation zone (Bol and Pfennig, 2014).

The relative velocity between the swarm drops and the continuous phase (v_{rs}) can be described as

$$v_{rsi,j} = v_{si,j} + v_{cj} \tag{4-1}$$

where i = drop class; i = 1, 2, 3…N; i = N is the biggest drop

j = sedimentation zone; j = 1, 2, 3…N; j = N is the top zone

v_s = actual velocity of the swarm drops

v_c = actual velocity of the continuous phase

At each sedimentation element j, the volume flow rate of the dispersed phase ($\dot{V}_d$) equals to the volume flow rate of the continuous phase ($\dot{V}_c$)

$$\dot{V}_{dj} = \dot{V}_{cj} \tag{4-2}$$

The volume flux $\dot{V}_d$ is a function of local hold-up ε and the ratio of drop hold-up ($\omega_{i,j} = \frac{\varepsilon_{i,j}}{\varepsilon_j}$)

$$\varepsilon_j \cdot A \cdot \sum_{i=1}^{N} v_{si,j}\omega_{i,j} = (1-\varepsilon_j)\cdot A \cdot v_{cj} \tag{4-3}$$

where ε = hold up; $\varepsilon = \frac{\text{volume of organic phase}}{\text{volume total}}$

Combining Equation 4-1 with Equation 4-3 results in

$$v_{cj} = \frac{\varepsilon_j A}{(1-\varepsilon_j)A} \sum_{i=1}^{N} (v_{rsi,j} - v_{cj}) \cdot \omega_{i,j} \tag{4-4}$$

Equation 4-4 is the $\frac{\varepsilon_j}{(1-\varepsilon_j)}$ time summation of multiplying the ratio of drop hold-up $\omega_{i,j}$ distributed over addition of $v_{rsi,j}$ and $-v_{cj}$

$$v_{cj} = \frac{\varepsilon_j}{(1-\varepsilon_j)} \sum_{i=1}^{N} v_{rsi,j}\omega_{i,j} - \sum_{i=1}^{N} v_{cj}\omega_{i,j} \tag{4-5}$$

The sum of the overall ratio of drop hold-up $\sum_{i=1}^{N} \omega_{i,j}$ of the continuous phase is 1. Then the velocity of the continuous phase is

$$v_{cj} = \varepsilon_j \cdot \sum_{i=1}^{N} v_{rsi,j}\omega_{i,j} \tag{4-6}$$

4.2 Fitting algorithm

The numerical is performed in a simulation program called PolySed. The algorithm of the program is shown in Fig. 4-3.

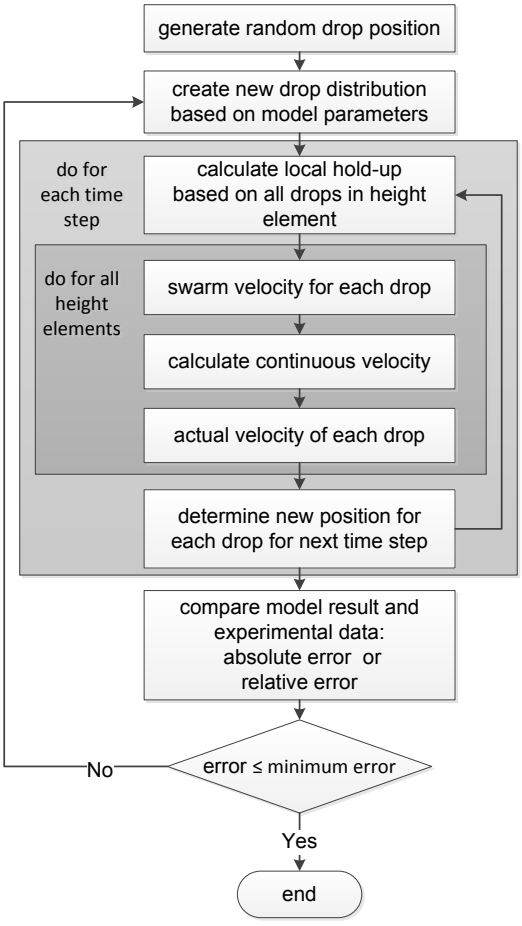

Fig. 4-3: Diagram of the PolySed algorithm (Bol and Pfennig, 2014).

The drop size distributions for polydisperse droplets in liquid/liquid system are usually found to be log normal having a narrow distribution (EL-Hamouz, 2009, Carlucci, 2010, Jurado et al., 2007, Singh et al., 2008). The log normal distribution function is given in terms of the drop diameter (d), the expectation value for diameter (μ) and the standard deviation for drop diameter (σ). In the PolySed, the three parameters will be assumed by the user before starting simulation and fitted to experimental results using the Levenberg–Marquardt algorithm.

$$q(x) = \frac{1}{\sigma \cdot d \cdot \sqrt{2 \cdot \pi}} \cdot \exp\left[-\frac{1}{2} \cdot \left(\frac{\ln(d) - \mu}{\sigma} \right)^2 \right] \tag{4-7}$$

In each time step and height element, the swarm droplet velocity (Equation 2-13), velocity of the continuous phase (Equation 4-6) and relative velocity (Equation 4-1) are calculated (see Fig. 4-2).

Based on the sedimentation velocity of a droplet, its new position will be calculated. Then, the hold up in each height element will be compared with the experimental result. Only the result in the sedimentation zone will be compared. The error between model and experimental data can be compared as absolute error

$$\Delta\varepsilon_{\text{abs,i}} = \left(\varepsilon_{\text{exp,i}} - \varepsilon_{\text{mod}}(m,n) \right) \tag{4-8}$$

or relative error

$$\Delta\varepsilon_{\text{rel,i}} = \frac{\left(\varepsilon_{\text{exp,i}} - \varepsilon_{\text{mod}}(m,n) \right)}{\varepsilon_{\text{exp,i}}} \tag{4-9}$$

with the experimental data point i accounting for height element m and time step n.

4.3 A rate based analytical approach

In many cases the sedimentation curve can be divided into three different parts, starting with a dead time (part I). The major part is the second one. In this part the sedimentation curve is linear. The drops can move up unhindered. The slope depends mainly on the drop size. In part III, the drop velocity is slowed down due to the increasing hold-up close to the main phase boundary. In Fig. 4-4 the three phases are indicated. More results can be found in appendix 8.6. The coalescence curve follows the same pattern, having a dead time, a linear part and a slow-down (retardation) zone. This behavior was found already by Henschke (1994) who considered only the linear part to determine the drop size with his settler program.

Many chemical reactions undergo a change of the reaction order from $n = 0$ to $n = 1$ during conversion. Photochemical reactions are representative for this type of reactions, easily to explain with the effect of depleting concentration on the exit intensity of a photometric device. At high concentration of the corresponding constituent and/or large path length the ingoing intensity is completely absorbed, effecting linear depletion. The reaction order is $n = 0$. With ongoing conversion, absorption along the optical path length decreases. The rate shifts from zero order to first order. The rate of hindered settling follows a very similar principle. But, as shown in Fig. 4-4, three different phases of “conversion” have to be considered since turbulences at the beginning of an experiment affect the settling and coalescence process. The kinetic approach for “reaction of shifting order” has to be adjusted to this phenomenon by application of a sigmoidal rate function (Siebenhofer, 2014).

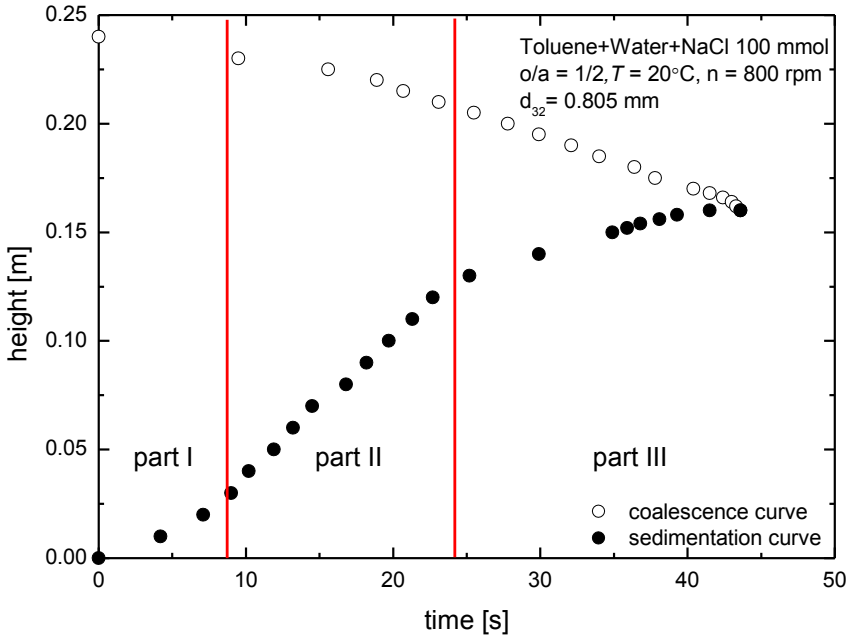

Fig. 4-4: Sedimentation behavior in the batch settling experiments

Phase separation is in strict accordance with this kinetic approach. In hindered settling, sedimentation, coalescence and dense-packed zone curves show the characteristic "S" shape which can quantitatively address the process on a physical base according to the basic function

$$S(t) = \frac{1}{1 + e^{-t}} \tag{4-10}$$

A modified sigmoid function can be used to explain the settling curve as a function of height (h) and time (t). According to equation 4-11 the sedimentation curve and secondary sedimentation can be described by the adjusted algorithm of the basic function

$$h(t) = \frac{h_{\text{heavy phase}}}{1 - b \cdot \exp(-c \cdot t)} \tag{4-11}$$

where b is a factor to scale the sedimentation velocity. It will depend on the drop size, the systems hold-up and the drag coefficient. The separation time is scaled by the factor c. It represents the compaction of the droplets close to the phase boundary which retards the sedimentation velocity and gives quantitative access to the specification of the dense packed zone. The height of the heavy phase $h_{\text{heavy phase}}$ can be directly determined from the phase volumes.

The coalescence curve can be described with a a corresponding function for descend according to

$$h(t) = h_{total} - \frac{h_{\text{light phase}}}{1 - b \cdot \exp(-c \cdot t)} \tag{4-12}$$

addressing the total height of the system and the height of the light phase. The function for the lines of same hold-up in the dense-packed zone is analogously constructed to the coalescence curve.

$$h(t) = h_{total} - \frac{\Delta h}{1 - b \cdot \exp(-c \cdot t)} \tag{4-13}$$

The height of the light phase has to be replaced by a variable height difference Δh which will depend of the sedimentation velocity and the coalescence rate.

5 Discussion of results

In industrial scale, impurities such as electrolytes even in trace amounts may have a significant impact on process operation and process efficiency. These impurities may change the settling behavior although their effect on the phase properties cannot be detected. For technically more relevant systems e.g. with high viscosity or impurities which is often encountered in the industries, systematic validation is still required. Moreover, the sedimentation of polydisperse droplets is clearly seen when the system has impurities and high viscosity. The influence of electrolyte and viscosity of the settling, the comparison of sedimentation of polydisperse droplets modeling with experimental result, the coalescence of droplets in dense-packed zone, and the influence of internals in high-viscosity systems will therefore be explained.

5.1 Influence of electrolyte and viscosity on settling

Many researchers (Frankforter and Cohen, 1914, Stevens et al., 1990, Chen et al., 1988, Pfennig and Schwerin, 1998, Effertz, 2011, Anursan et al., 2012) have reported that a small amount of electrolyte in the system will change the settling behavior.

Pfennig and Schwerin, 1998 studied the influence of salts on the electrostatic potential based on the DLVO theory. Different types of salts (different oxidation number) and variations in salt concentration affect the electrostatic potential of each phase, which results in a change of the coalescence behavior.

Hence, two salts with different oxidation numbers were chosen to determine their influence on the settling time in the system toluene (distillate) + bi-distilled water in a standardized settling cell. For NaCl (Nr. K41498446) the oxidation number equals 1 and for Na_2SO_4 (Nr. K42353646) it equals 2. The concentration of both salts was varied from 50 to 500 mmol/L of water (Anursan et al., 2012).

The experimental results (see Fig. 5-1, more results are recorded in appendix 8.6) indicate that at a phase ratio of (o/a) 1/2 the influence of NaCl on the settling time of the toluene + water system is larger than the influence of Na_2SO_4. For a volume phase ratio (o/a) of 1/2 the results from both salts show that the settling time increases with increasing salt concentration. The theory behind this effect is that at small salt concentrations an increase of the concentration leads to a further increase in the set-

tling time. For salt concentrations above a certain limit of 200 mmol/L Na_2SO_4 and 100 mmol/L NaCl a further increase of the salt concentration does not affect the settling time further.

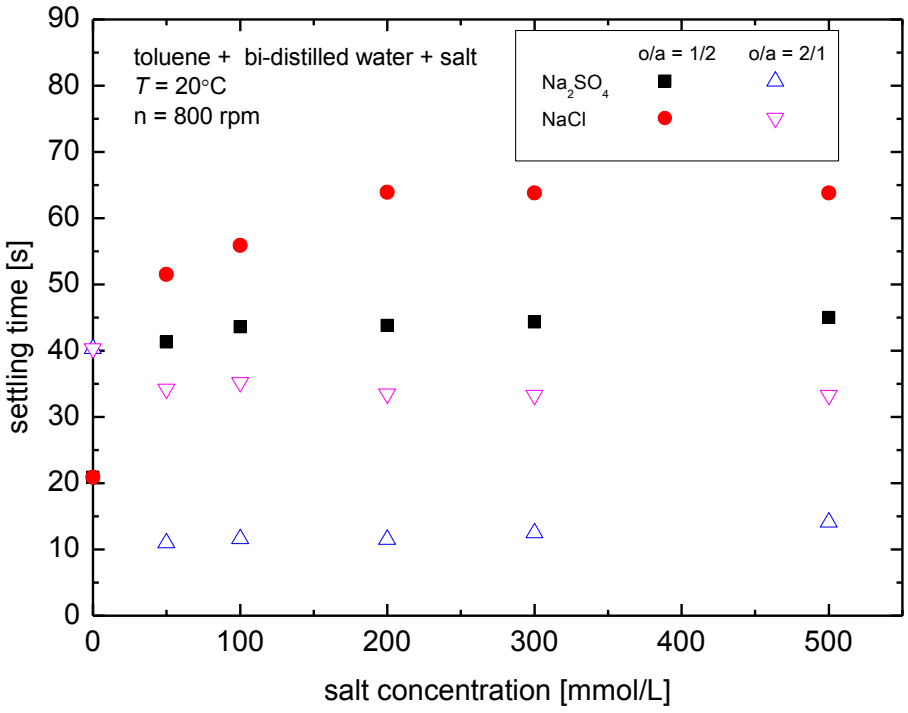

Fig. 5-1: Influence of salt on settling time with volume phase ratio 1:2 and 2:1, toluene + bi-distilled water (Anursan et al., 2012).

In the case of the volume phase ratio (o/a) of 2/1, it was observed that sodium sulfate has a higher effect than sodium chloride. The settling time decreases with increasing concentration of sodium chloride and it becomes nearly constant for salt concentration above 200 mmol/L. For sodium sulfate, the settling time is rapidly declining when 50 mmol/L of the salt were added. For Na_2SO_4-concentrations above 100 mmol/L only a slight effect on the settling time could be observed.

These results agree with the investigated behavior for the MIBK + water system (see Fig. 5-2), investigated by Effertz (2011) and Tantichumnan (2014).

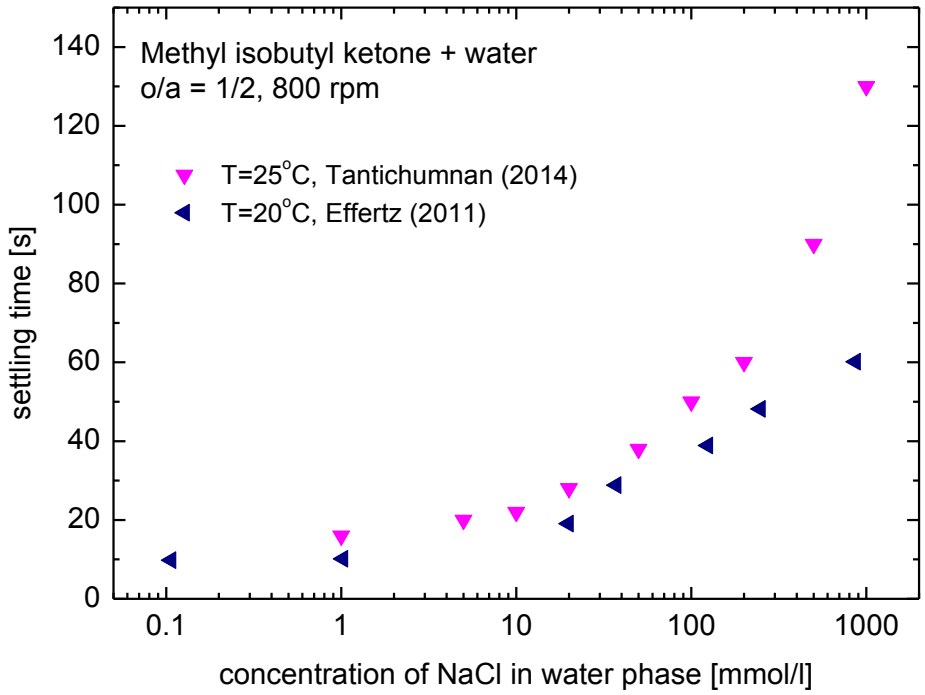

Fig. 5-2: Influence of salt on settling time of MIBK and water

However, it can be seen that the influence of salt is much stronger with the system of MIBK than toluene at the same salt concentration. With the DLVO theory, it can be explained that the electrostatic force in MIBK system has a stronger influence than within the toluene system at comparable conditions. The force is not only depending on the droplet distance (a) but also on the electrostatic potential difference (ψ) which is difficulty to measure (see Equation 2-34). Alternatively, Stevens et al. (1990) and Chen et al. (1988) found that the electrolyte has more influence on a polar solvent than on a non-polar solvent. This also agrees with the result for the MIBK (polarity 27) and toluene system (polarity 9.9) (Smallwood, 1996).

In those experiments where the viscosity of the aqueous phase was varied with PEG4000 (Nr. 1741722/100), the concentration of NaCl and Na_2SO_4 were fixed at 100 mmol/L of water. Two volume phase ratios (o/a) 1/2 and 2/1 were studied. The physical properties of the investigated system can be found in appendix 8.3.

The coalescence and sedimentation curve for the volume phase ratio (o/a) of 1/2 are shown in Fig. 5-3. The results from both salts show a similar behavior. The organic phase (toluene) is dispersed in the aqueous phase (water + PEG4000 + salt) and the

increased viscosity leads to higher settling times. This behavior can be explained by Equation 2-13. Especially the Archimedes number (Equation 2-15) depends on the physical properties of the system, therefore by increasing the concentration of PEG4000 the physical properties and subsequently the settling time of the system change.

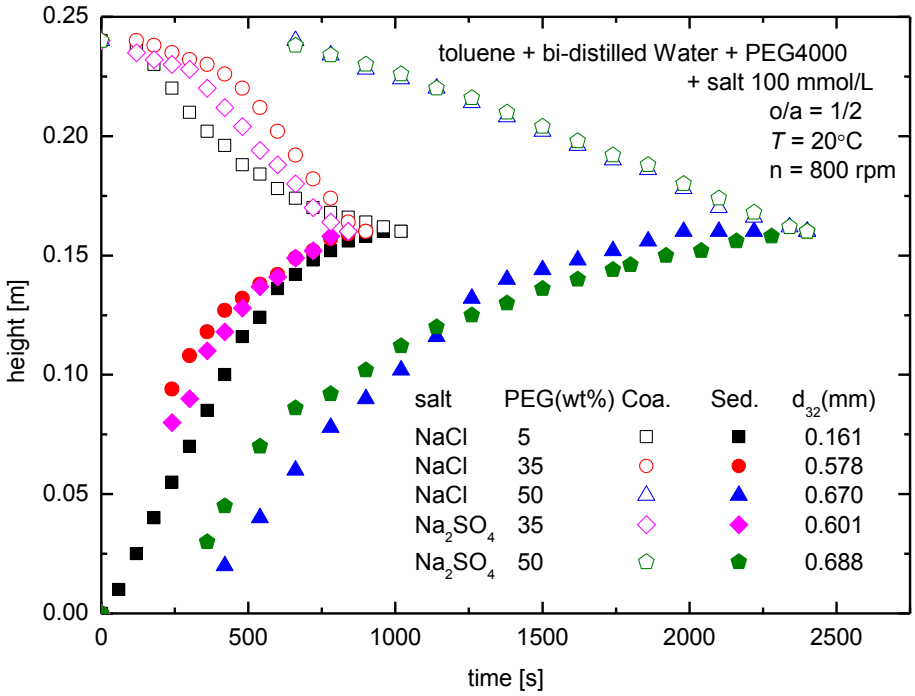

Fig. 5-3: Comparison of settling curves; system: toluene + water; o/a = 1/2 and different weight percent of PEG4000 (Nr. 1741722/100); NaCl and Na_2SO_4: 100 mmol/L (Anursan et al., 2012).

Both salts NaCl and Na_2SO_4 show a similar tendency regarding the increased viscosity. Therefore, it can be concluded that the effect of different kind of salts on the settling time is much less pronounced compared to the influence of the viscosity.

Fig. 5-4 shows the influence of the viscosity on the settling curve of the toluene-water system for both investigated salts for the volume phase ratio (o/a) of 2/1. The results from both cases show a similar effect: the settling time increases when 5 wt% and 20 wt% PEG4000 are added to the system. The rate of the droplet rise decreases as the viscosity increases (see Equation 2-13), therefore a longer settling time is required. In the case of 35 wt% and 50 wt% PEG4000, the organic phase changed to be

the continuous phase whereas the aqueous phase became the disperse phase. This behavior also describe by Ngan et al. (2009) when the phase inversion occurs during liquid–liquid dispersion. Moreover, the addition of 35 wt% and 50 wt% PEG4000 in aqueous phase caused a decrease in the settling time, because the aqueous droplets are bigger than the toluene droplets.

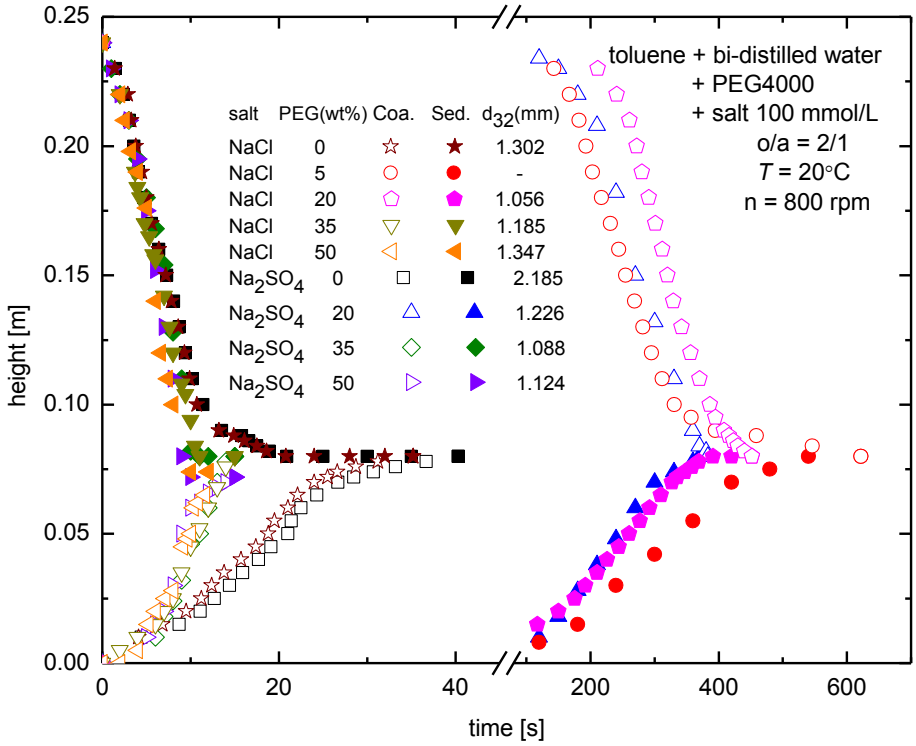

Fig. 5-4: Comparison coalescence and sedimentation curve; system: toluene + water; o/a = 2/1; different concentrations of PEG4000 and 100 mmol/L NaCl and Na_2SO_4 (Anursan et al., 2012).

It can be concluded from the results that the selected electrolytes NaCl and Na_2SO_4 had essentially no effect on the settling time in viscous systems of toluene. The settling time of MIBK and water system at varying NaCl concentrations in the optical cell has a similar trend with results of a previous work of Anursan et al. (2012) as shown in Fig. 5-5. As viscosity and NaCl concentration are increased, the settling time is expected to be increased as well. This has been observed for systems with 5 wt% and 10 wt% PEG4000. However, at 15 wt% PEG4000 the influence of viscosity dominated the influence of electrolyte resulting in constant settling time as NaCl concentration increased.

It can be concluded that the electrolyte has more influence on the settling time in low viscosity systems while high viscosity is the dominating factor. With increasing aqueous phase viscosity the settling velocity of droplet swarms will significantly slow down.

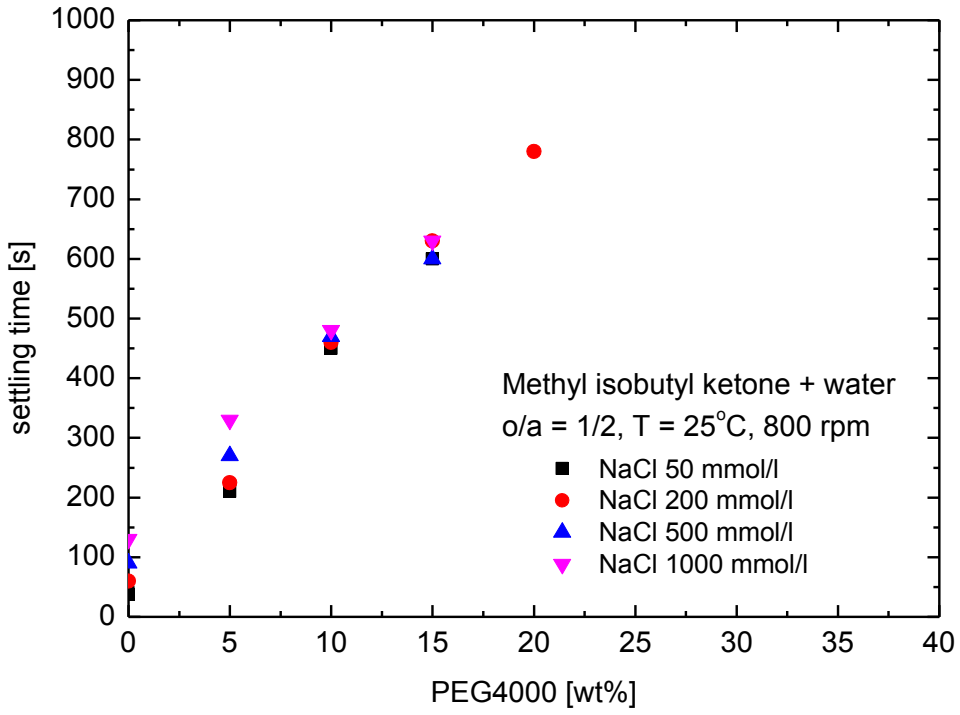

Fig. 5-5: Influence of aqueous phase viscosity on settling time of MIBK and water with different wt%PEG4000 (Nr.12H220008) and NaCl (Nr.12E250019) concentration, o/a = 1/2 (Tantichumnan, 2014).

The important factor that can change the settling time is the droplet size. Bigger drop size will have faster settling time than smaller drop size. This corresponds to the principle that the drop size determines the rate of the drop. Normally, large drops and large contact area reduce the film drainage rate and results in large coalescence time compared to small drops (Pattarawut, 2010 and Mungma et al., 2014). The droplet size decreases as the viscosity of the aqueous phase increases and causes a longer settling time (the drop settling rate is lower) (Nevers and Wu, 1971). The viscosity acts as a damping mechanism for the drag force throughout the film-thinning process. Therefore, smaller droplets are formed and the generation of large droplets is obstructed (Schoolenberg and During, 1998).

5.2 Sedimentation of polydisperse droplets

To develop a model describing the sedimentation of polydisperse droplets, experiments with polydisperse droplets have been performed. A clear sedimentation trend has been found in the system cyclohexanone + water (Chuttrakul and Pfennig, 2014), MIBK + water (Tantichumnan, 2014, Pungsang et al., 2014) and toluene + water (Aunyindee et al., 2013). The polydisperse droplet settling behavior of liquid-liquid system was studied with the ultrasonic scanner. The result was compared to the simulation result. In order to investigate polydisperse sedimentation without superpositioned effects of the droplets themselves, the sedimentation of rigid spheres was studied as well. The rigid spheres are polymer particles of specified size and density.

5.2.1 Sedimentation of polydisperse particles in high-viscosity systems

To determine the influence of sedimentation without superimposed effects like mass transfer or coalescence in high-viscosity systems, solid particles of known size and density were added to the water phase. The aqueous phase has an increased viscosity due to the addition of different PEG4000 concentrations. Two types of solid particles made of POM and PA66 were used. Three difference sizes of particles, the void fraction and the viscosity were varied as well. The mixing cell consisted of a 3 liter beaker and a 3 blade impeller size 10 mm x 100 mm (Nr. C 474-08 and Nr. C 443-10, BOHLENDER GmbH.). The motor speed was varied to find the appropriate solid phase dispersed in the liquid. The settling experiments were done using the optical cell. The results were recorded with the video camera. Fig. 5-6 shows a screen shot in 2 second steps. The sedimentation curves for POM particles at ε_0 = 0.15 in water + 50 wt% PEG-4000 system are clearly visible.

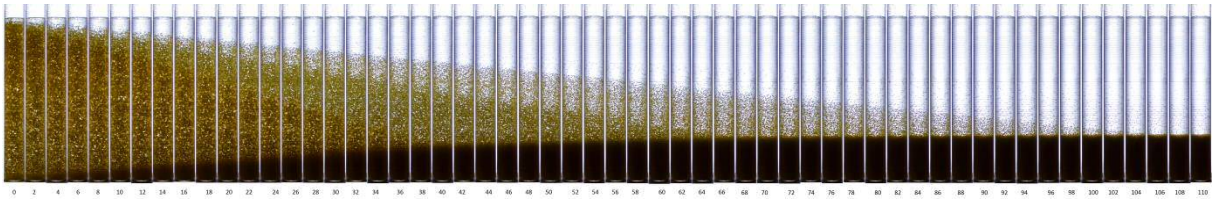

Fig. 5-6: Settling curves of POM particles at ε_0 = 0.15 in water + 50 wt% PEG-4000; recorded with 2 second screen shot technique (Findlay, 2013).

Fig. 5-7 shows the three interfaces for each of the void fractions producing a linear slope from just after the initial height until they reach the sediment indicating a Type 1 settling regime. This is most likely due to the low particle void fractions used in the experiments (Rhodes, 2008) preventing the buildup of a region of high concentration just before the sediment.

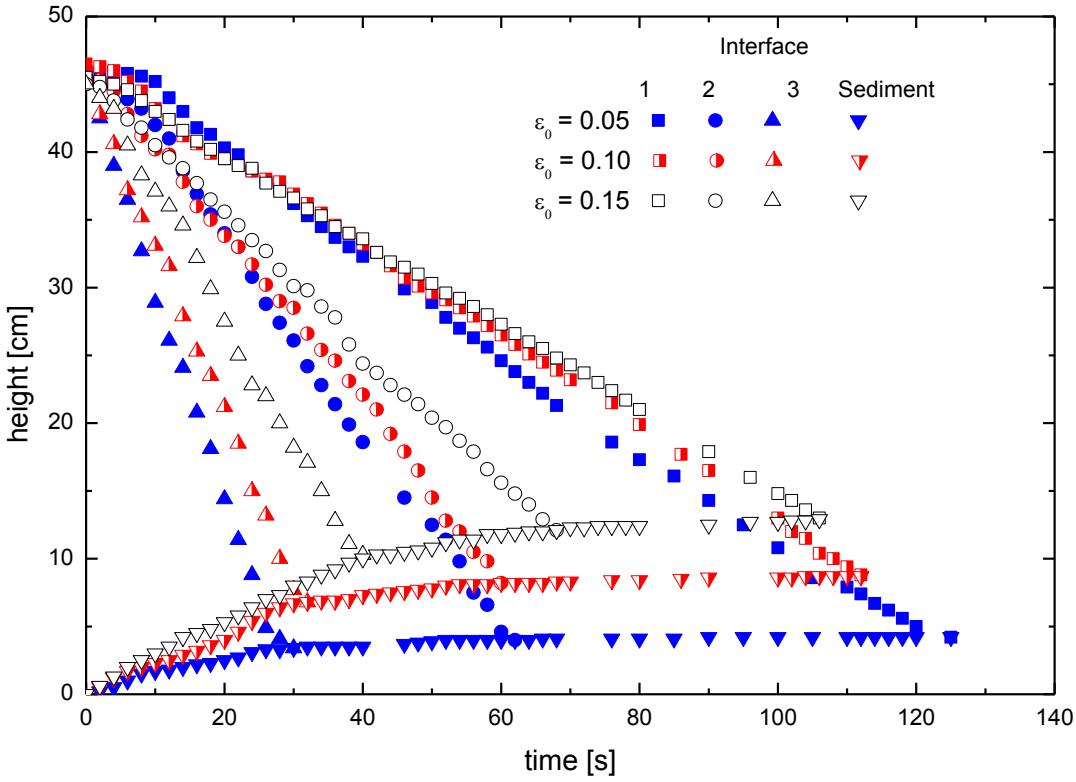

Fig. 5-7: Comparison of interface and sediment curves for POM particles at ε_0 = 0.15, 0.10 and 0.05 in water + 50 wt% PEG-4000 (Findlay, 2013).

Due to the faster sedimentation rate of bigger particles, separation zones of different sedimentation velocity are formed with time, containing only particles below a certain size. This results in a change of the local hold-up (more results can be found in appendix 8.4.).

5.2.2 Sedimentation of polydisperse droplets

Due to the limitation of the optical cell (see Fig. 3-3), the settling behavior cannot be seen and evaluated when the system is opaque. An alternative technique to evaluate the sedimentation and coalescence behavior is the ultrasonic scanner. Due to the low scanning speed of the equipment (see more information in topic 3.3), the

investigated system should have a settling time of more than 3 minutes. Knowledge about the influence of electrolyte and viscosity on settling (see topic 5.1) is useful for this experiment.

The ultrasonic suspension analyzer, type SUSS-2008 from Rhosonics Analytical B.V., Netherlands, is depicted in Fig. 3-7. With this equipment, the settling and the dead time of the system and the hold-up as a function of time and height can be identified. To be analyzed in the ultrasonic scanner, chemicals have to be filled into a decanter. The decanter has a height of 500 mm and a volume of 1250 ml. It is mounted in the middle of the water bath. The scanner ring with the ultrasound sensors is placed around it. When the measurements start, the scanner ring is moving down to the bottom. While moving up in 1 mm steps, the speed of sound is measured. Due to technical limitations, the zero position cannot be set to the bottom of the decanter. Therefore, a piece of stainless steel was put inside the decanter to shift up the level of the dispersion.

The data of the ultrasonic suspension analyzer (type SUSS-2008) are exported into an Microsoft Excel file as shown in Fig. 5-8. It contains for all measurement points the data for time (s), position (mm), the temperature (°C), the speed of sound (m/s) and the attenuation. The speed of sound and the attenuation will depend on the investigated liquid system. The analyzing program was originally designed to support Microsoft Office in Dutch language. Therefore, some time it changes the experimental data to date (see the attenuation in Fig. 5-8).

The data file also contains information regarding errors. The following error codes are possible (for more information see the Manual of the ultrasonic suspension analyzer, type SUSS-2008 from Rhosonics Analytical B.V., Netherlands (Rhosonics, 2012)).

1 Next of previous position has an error.
65 Signal to low for measurement.
Probe is not in a liquid, bad cable/connection, probe contaminated or probe defective
66 To much noise in signal.
67 Ultrasonic error
68 Ultrasonic error
69 Ultrasonic error
70 Ultrasonic error
Bad cable/connection or Probe contaminated

Minimum and maximum speed setting in the liquid edit menu are to large or to small

71 No trigger in window

72 Wave form error

73 Wave form error

74 Wave form error

Minimum and maximum speed setting in the liquid edit menu are to large or to small

Bad cable/connection or Probe contaminated

Data from measurement points with error code might be not reliable. In this research, all the error data have been cut out.

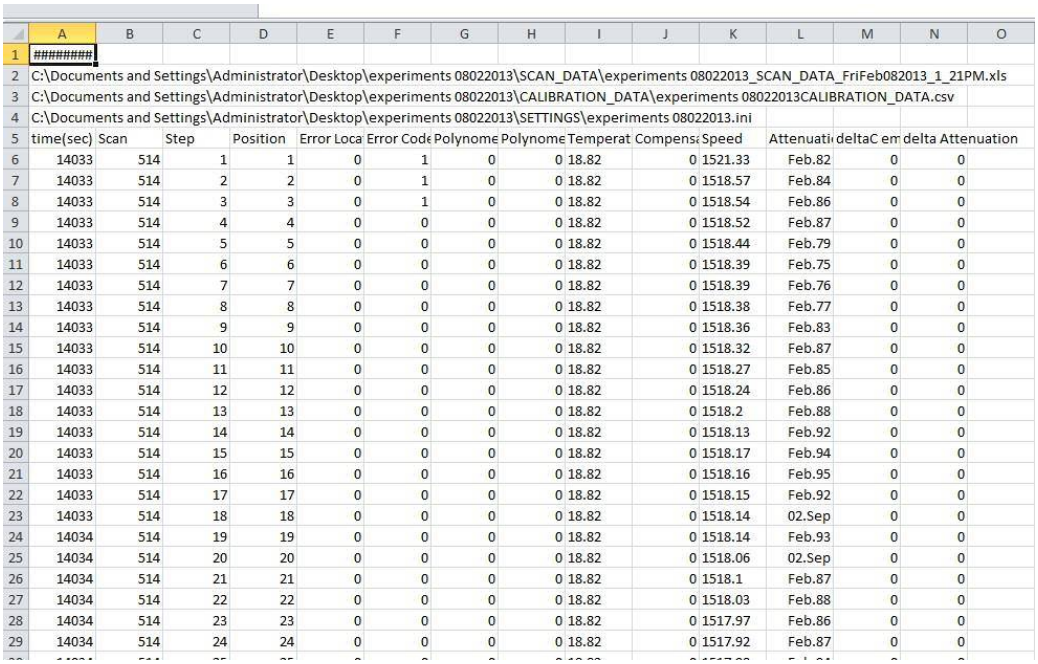

	A	B	C	D	E	F	G	H	I	J	K	L	M	N	O
1	#########														
2	C:\Documents and Settings\Administrator\Desktop\experiments 08022013\SCAN_DATA\experiments 08022013_SCAN_DATA_FriFeb082013_1_21PM.xls														
3	C:\Documents and Settings\Administrator\Desktop\experiments 08022013\CALIBRATION_DATA\experiments 08022013CALIBRATION_DATA.csv														
4	C:\Documents and Settings\Administrator\Desktop\experiments 08022013\SETTINGS\experiments 08022013.ini														
5	time(sec)	Scan	Step	Position	Error Loca	Error Code	Polynome	Polynome	Temperat	Compensa	Speed	Attenuati	deltaC em	delta Attenuation	
6	14033	514	1	1	0	1	0	0	18.82	0	1521.33	Feb.82	0	0	
7	14033	514	2	2	0	1	0	0	18.82	0	1518.57	Feb.84	0	0	
8	14033	514	3	3	0	1	0	0	18.82	0	1518.54	Feb.86	0	0	
9	14033	514	4	4	0	0	0	0	18.82	0	1518.52	Feb.87	0	0	
10	14033	514	5	5	0	0	0	0	18.82	0	1518.44	Feb.79	0	0	
11	14033	514	6	6	0	0	0	0	18.82	0	1518.39	Feb.75	0	0	
12	14033	514	7	7	0	0	0	0	18.82	0	1518.39	Feb.76	0	0	
13	14033	514	8	8	0	0	0	0	18.82	0	1518.38	Feb.77	0	0	
14	14033	514	9	9	0	0	0	0	18.82	0	1518.36	Feb.83	0	0	
15	14033	514	10	10	0	0	0	0	18.82	0	1518.32	Feb.87	0	0	
16	14033	514	11	11	0	0	0	0	18.82	0	1518.27	Feb.85	0	0	
17	14033	514	12	12	0	0	0	0	18.82	0	1518.24	Feb.86	0	0	
18	14033	514	13	13	0	0	0	0	18.82	0	1518.2	Feb.88	0	0	
19	14033	514	14	14	0	0	0	0	18.82	0	1518.13	Feb.92	0	0	
20	14033	514	15	15	0	0	0	0	18.82	0	1518.17	Feb.94	0	0	
21	14033	514	16	16	0	0	0	0	18.82	0	1518.16	Feb.95	0	0	
22	14033	514	17	17	0	0	0	0	18.82	0	1518.15	Feb.92	0	0	
23	14033	514	18	18	0	0	0	0	18.82	0	1518.14	02.Sep	0	0	
24	14034	514	19	19	0	0	0	0	18.82	0	1518.14	Feb.93	0	0	
25	14034	514	20	20	0	0	0	0	18.82	0	1518.06	02.Sep	0	0	
26	14034	514	21	21	0	0	0	0	18.82	0	1518.1	Feb.87	0	0	
27	14034	514	22	22	0	0	0	0	18.82	0	1518.03	Feb.88	0	0	
28	14034	514	23	23	0	0	0	0	18.82	0	1517.97	Feb.86	0	0	
29	14034	514	24	24	0	0	0	0	18.82	0	1517.92	Feb.87	0	0	

Fig. 5-8: Output file from ultrasonic suspension analyzer (type SUSS-2008).

Fig. 5-9 shows the settling properties of toluene (Nr. 2F005908) + water + PEG4000 5 wt% (Nr. 12H220008) + NaCl 50mmol/L (Nr. 12E250019) with a phase ratio o/a=1/2. By analyzing the data, the range of speed of sound for the continuous phase, the coalescence dispersed phase and the sedimentation zone were determined. The speed of sound in each phase is following:

- coalesced dispersed phase $v < 1342\,\text{m/s}$
- sedimentation zone $1405 < v < 1502\,\text{m/s}$
- continuous phase $v > 1518\,\text{m/s}$

The results show that the height of the sedimentation zone and the coalescence curve can be determined from time and height dependent speed of sound with the ultrasonic scanner. Ultrasonic scanning technology can be used to determine the boundary between close-packed dispersion, coalescence and sedimentation zone, even in opaque systems where optical detection fails. It additionally allows quantitative evaluation of local hold-up as well as indications for drop-size distributions in opaque systems. The data below a height of 41 mm cannot be evaluated because of the limitation of the equipment's scanning range. Later, a metal piece with a height of 51 mm was put inside to shift the liquid phase up. It can be seen from the result that there is hold-up shift where usually only one sedimentation curve is visible. This indicates that there are droplets of different size settling.

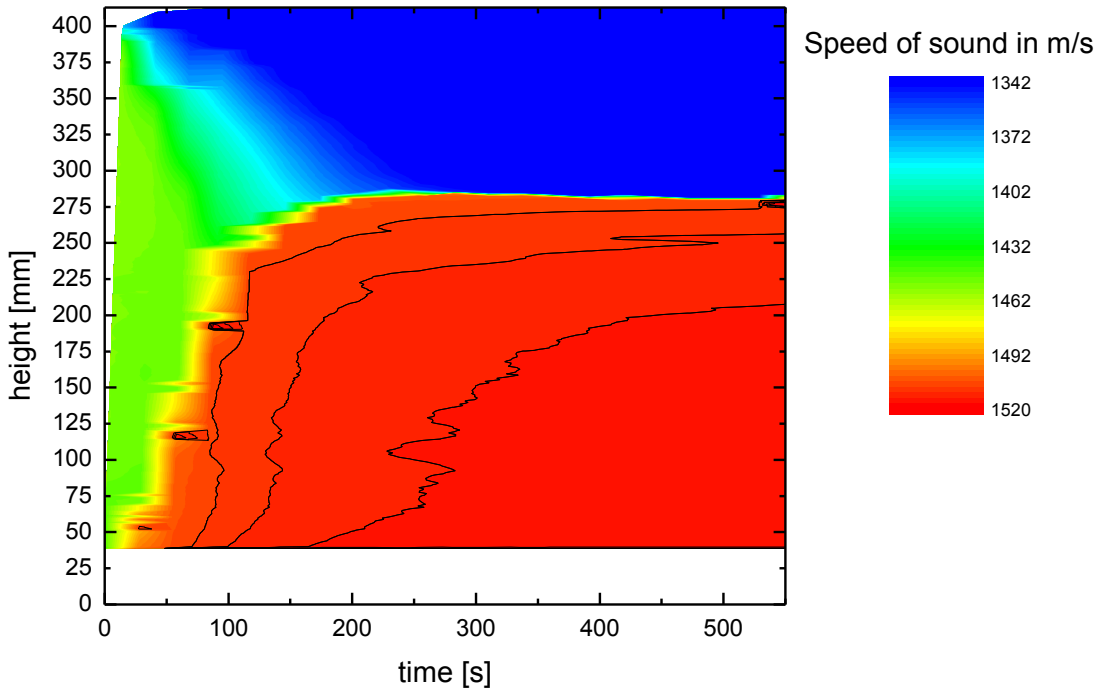

Fig. 5-9: Sedimentation of polydisperse droplets; system: toluene + water + PEG4000 5 wt% + NaCl 50mmol/L; o/a=1/2 (Aunyindee et al., 2013).

The positions of all droplets in the sedimentation zone for the systems of MIBK (Nr. 452193304) and water with and without NaCl (Nr. 12E250019) were plotted over the range of scanning time as shown in Fig. 5-10 and Fig. 5-11, respectively. In addition, the difference in drop sizes is illustrated by contouring the speed of sound. The

sound speed is plotted in these two graphs in steps of 3 m/s. This corresponds to a hold-up step of approximately 1%. The two figures indicate that more than one sedimentation zones is observable and that the sedimentation behavior is distinguishable for both systems (without NaCl and with NaCl 200 mmol/L). Therefore, it can be confirmed that the system MIBK + water + PEG4000 (Nr. 12H220008) is a polydisperse system (more results can be found in appendix 8.4).

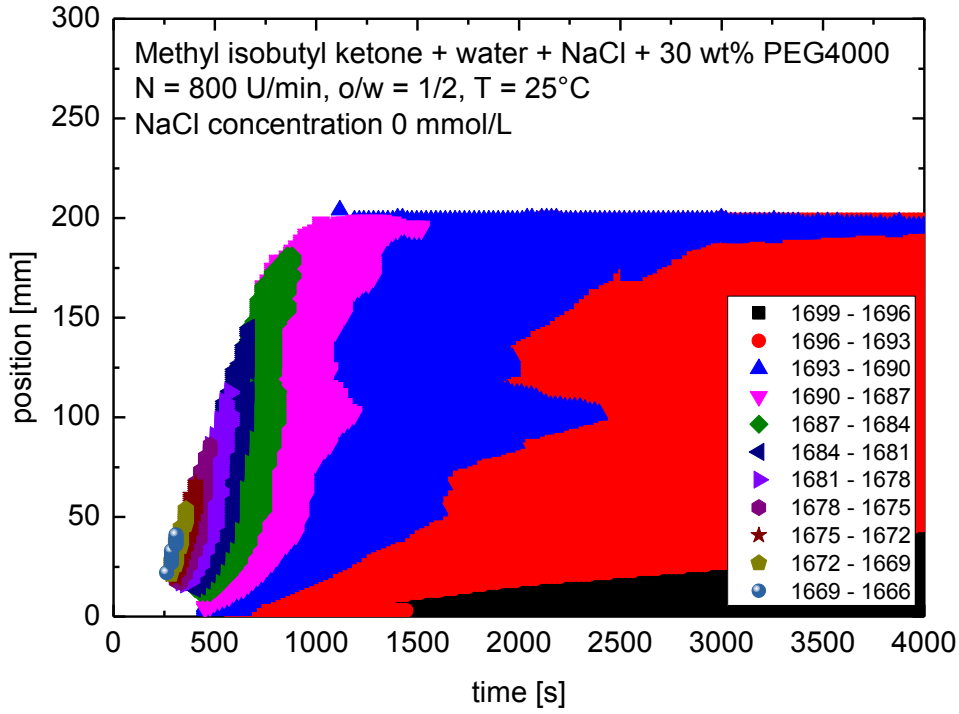

Fig. 5-10: Sedimentation zone of MIBK and water with 30 wt%PEG4000 and without NaCl concentration, o/a = 1/2 (Tantichumnan, 2014).

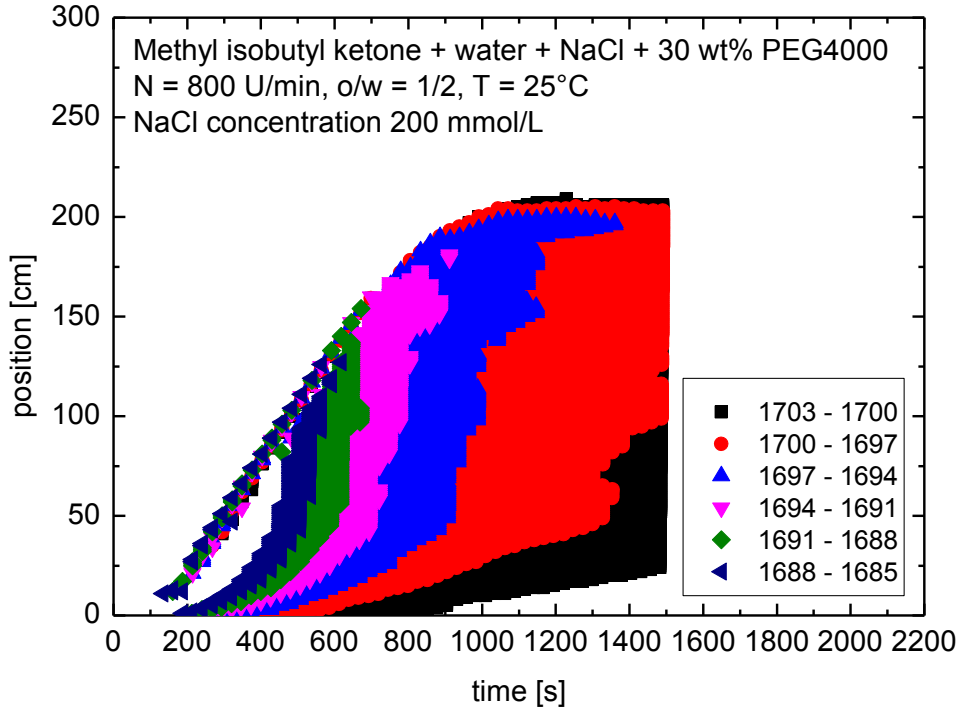

Fig. 5-11: Sedimentation zone of MIBK and water with 30 wt%PEG4000 and NaCl concentration 200 mmol/L, o/a = 1/2 (Tantichumnan, 2014).

Fig. 5-12 shows the hold-up over time for the system cyclohexanone + water +5 wt% PEG4000. By analyzing the data, the range of speed of sound for the continuous phase, the coalesced dispersed phase and the sedimentation zone were determined. The speed of sound in each phase is the following:

- coalesced dispersed phase: $v < 1454 \pm 1\,\mathrm{m/s}$
- sedimentation zone: $1454 < v < 1574 \pm 1\,\mathrm{m/s}$
- second sedimentation zone: $1574 < v < 1600 \pm 1\,\mathrm{m/s}$
- continuous phase: $v > 1600 \pm 1\,\mathrm{m/s}$.

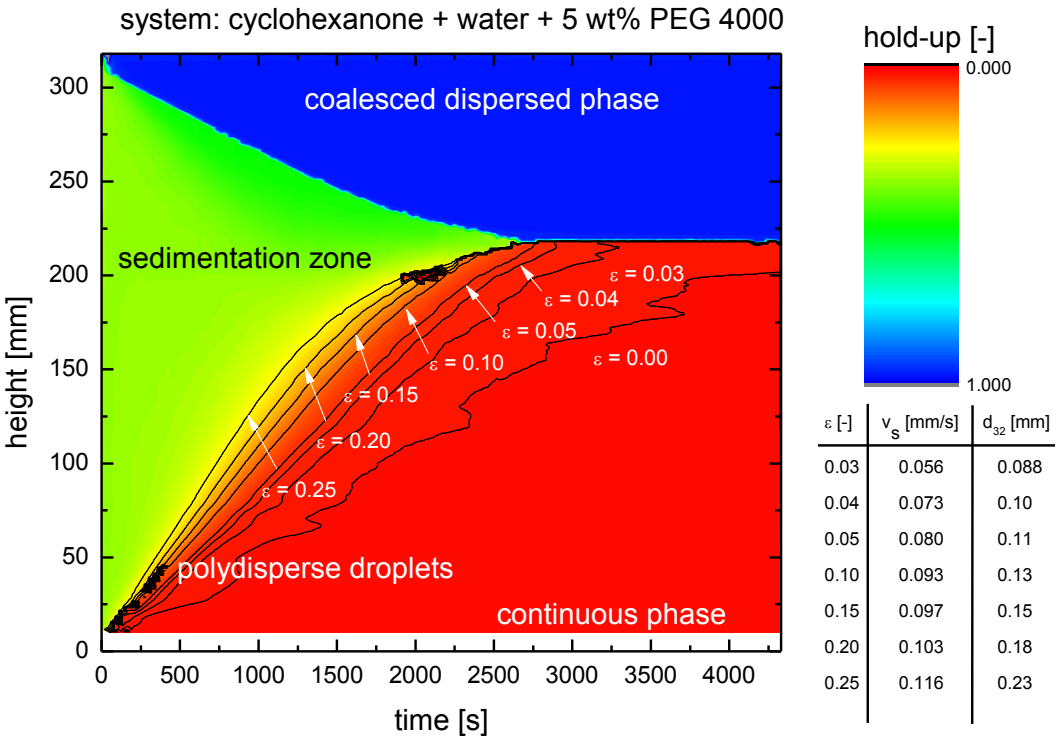

ε [-]	v_s [mm/s]	d_{32} [mm]
0.03	0.056	0.088
0.04	0.073	0.10
0.05	0.080	0.11
0.10	0.093	0.13
0.15	0.097	0.15
0.20	0.103	0.18
0.25	0.116	0.23

Fig. 5-12: Experimental result from ultrasonic analyzer: hold-up over time, system: cyclohexanone + water +5 wt% PEG4000 (Chuttrakul and Pfennig, 2014).

A clearly visible sedimentation of polydisperse droplets was found in this system. The hold-up in the dense-pack zone is about 0.74 for monodisperse (Henschke, 1994) and 0.85 to 0.9 for polydisperse droplets (Pilhofer and Mewes, 1979). In Fig. 5-12, the hold-up in dense-pack zone is 0.4 to 0.6 which is less than the values given in the literature. This finding can be used in the future to optimize the separation models.

The swarm sedimentation velocity (v_s) and the Sauter mean diameter (d_{32}) were calculated from Equation 2-13. The data beyond 10 mm cannot be determined because of the metal piece. With polydisperse droplets different sedimentation velocities occur in the same fluid. In gravity settling the velocity of each droplet relative to the surrounding fluid depends on the droplets size. In the beginning of a settling experiment the polydisperse droplets are assumed to be equally distributed in the sedimentation zone. With time separation zones of different sedimentation velocity are formed, containing only droplets of certain size, which change the local hold-up. Regions of close-packed dispersion could not always be identified clearly (Chuttrakul and Pfennig, 2014, Chuttrakul et al., 2014).

5.2.3 Comparison between model and experiment results

The experimental data from ultrasonic scanner are used to simulate the behavior of the sedimentation of polydisperse droplets using the PolySed program. The model determines the swarm drop velocity for each droplet depending on the drop size and the local hold-up. It does not only take into account the movement of every drop, but also the countercurrent flow of the continuous phase to fulfill continuity. The experiment with the most clear sedimentation of polydisperse droplets was used for comparison between the simulation program and the experimental data. The results of the simulation are depicted in Fig. 5-13.

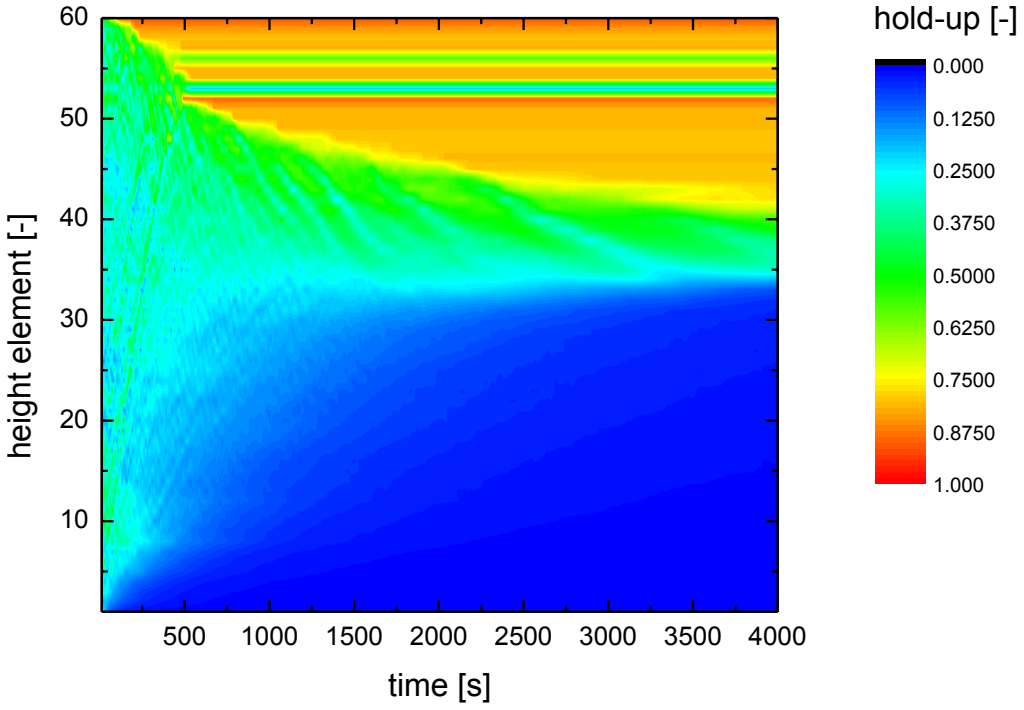

Fig. 5-13: Result from PolySed program; system: cyclohexanone + water +5 wt% PEG4000.

The modeled data displays a similar behavior to the data obtained from the ultrasonic scanner. There is a clear hold-up change from the continuous phase to the sedimentation zone visible. The hold-up is increasing from 0.1 to 0.3. This simulation does not take into account for the effects of coalescence. Therefore, in the top part above height element 30, the generated droplets are accumulated. The accumulated droplets increase the local hold-up in the upper height elements and reduce the sedimen-

tation velocity in that zone. This leads to even further accumulation and hold-up greater than 100% can appear.

To avoid the non-realistic drop accumulation, the droplets that reach the coalescence curve zone can be withdrawn from the simulation as shown in Fig. 5-14. However, the model still does not take into account the drop-drop coalescence behavior in the dense-packed zone (see topic 5.3).

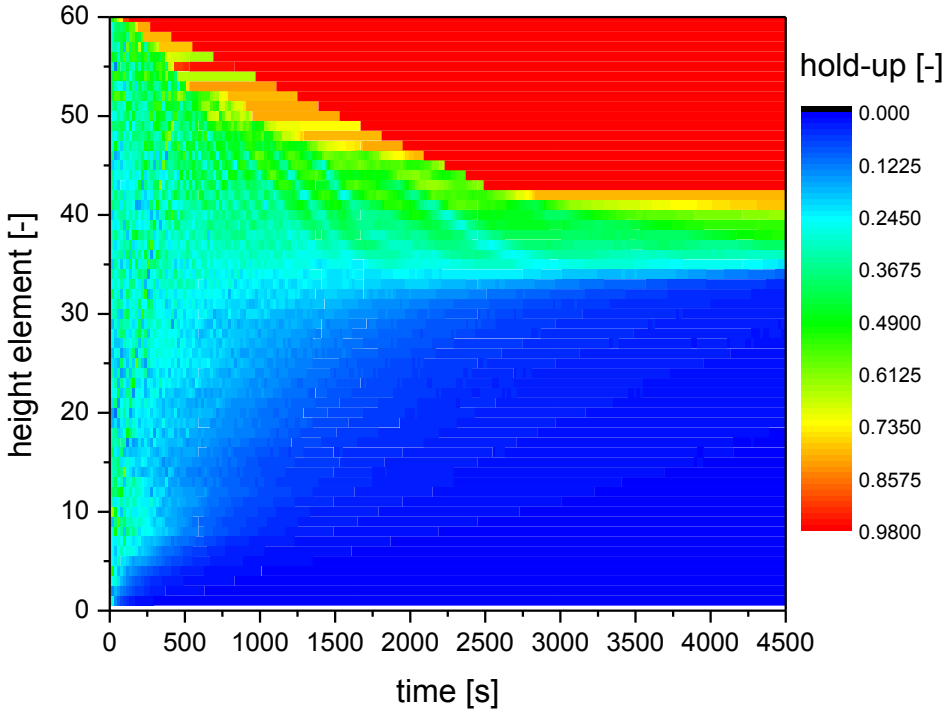

Fig. 5-14: Result from PolySed program, droplet leave; system: cyclohexanone + water +5 wt% PEG4000.

The drop distribution used in this simulation is depicted in Fig. 5-15. The maximum drop size was 1 mm. The drop distribution was assumed to be a lognormal distribution. The expected value of the corresponding normal distribution was $\mu = 0\,\text{mm}$. The standard deviation of the drop diameter was $\sigma = 0.029\,\text{mm}$.

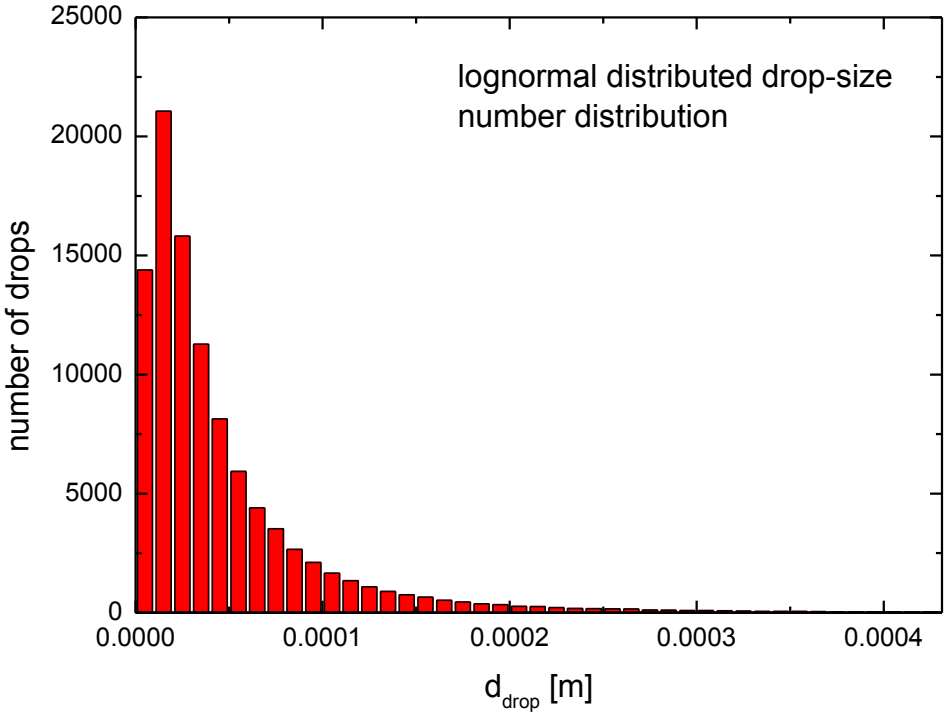

Fig. 5-15: Generated lognormal drop distribution; system: cyclohexanone + water + 5 wt% PEG4000.

The modeled data displays a similar behavior to the data obtained from the ultrasonic scanner. There is a clear hold-up change from the continuous phase to the sedimentation zone visible. The hold-up is increasing from 0.1 to 0.9 here. Only the lower part (0.1 m) of the simulation was compared with the experimental results. The absolute error $\Delta\varepsilon_{abs}$ between the simulated and measured hold-up is shown in Fig. 5-16.

The developed model proves to be principally suitable to describe the experimental data. The different hold-up regions are caused by drop-size distributions, where each drop has a different settling rate. Of course the selected drop distribution will have a significant influence on the model results. In a next step the provided drop distribution model should be improved to achieve a better agreement between model and experiment. The model parameters can then be fitted to the experiment to obtain information regarding the actual drop distribution.

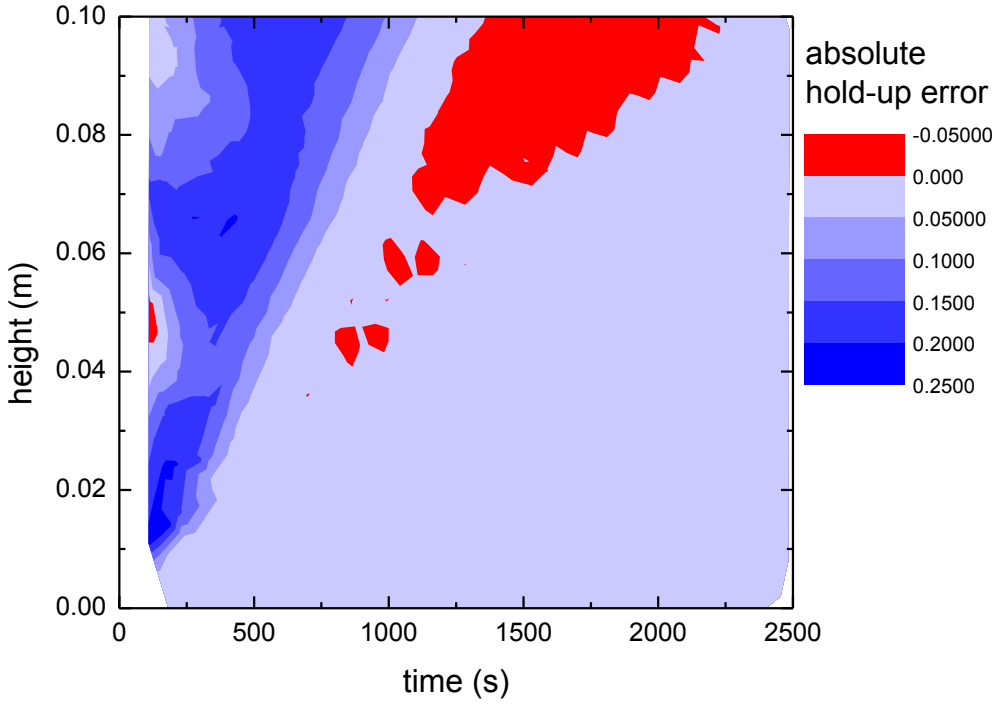

Fig. 5-16: Absolute error in hold-up between simulation and experiment

5.3 Coalescence in dense-packed zone

The aim of this part is to investigate the behavior of drop-drop coalescence in the dense-packed zone, applied for the Henschke model.

5.3.1 Evaluation of Henschke's model with experimental data

The settler program base on previous works of Henschke, 1994 was written to simulate the behavior of sedimentation and coalescence of swarm droplets. The model assumes that all droplets are similar in size and velocity in the range of the free sedimentation zone where hardly any drop-drop coalescence takes place (Henschke, 2002). The sedimentation, coalescence and dense-packed curves are determined by the program. The results from the program compared with experimental data from the ultrasonic scanner are shown in Fig. 5-17 (more results can be found in appendix 8.5)

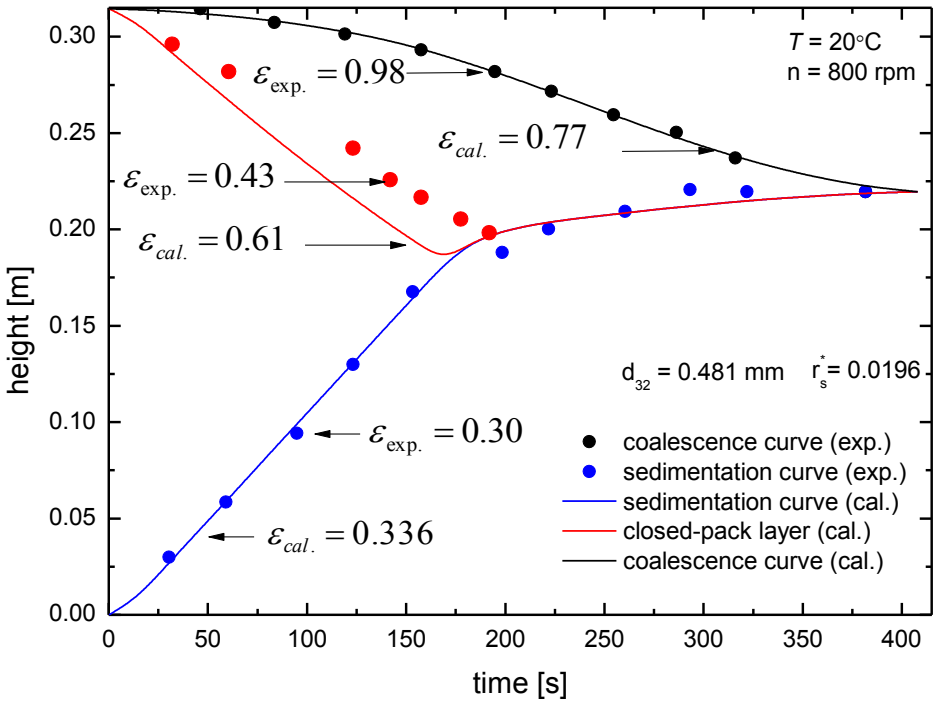

Fig. 5-17: Comparison between Henschke model and experimental data; system: toluene and water with 15 wt% PEG4000 and 50 mmol of NaCl (Punsang, 2014).

Since the settler program fits its sedimentation and coalescence parameters to the sedimentation and coalescence curve the calculated curves match the experimentally visible curves. However, the hold-up at the interfaces calculated by Henschke's model differ from the experimental hold-up determined by ultrasonic scanner. The settle program computes a hold-up $0.61 < \varepsilon_{cal.} < 0.77$, while the hold-up in the experiment $0.43 < \varepsilon_{exp.} < 0.98$ varies over a larger scale. This hold-up variation could not be detected before by using only optical evaluation. Here the model has to be adopted in future, taking into account that the drop-size is in fact polydisperse.

5.3.2 Coalescence behavior of droplets in dense-packed zone

The data of the ultrasonic scanner experiments show, that the hold-up in the dense-packed zone is changing with height and time (see Fig. 5-18). In order to find an analytical description for the hold-up change in that region, the hold-up data are plotted in the following as a function of the height for different times. Due to the movement of the scanner ring, the data are not available for all times and heights.

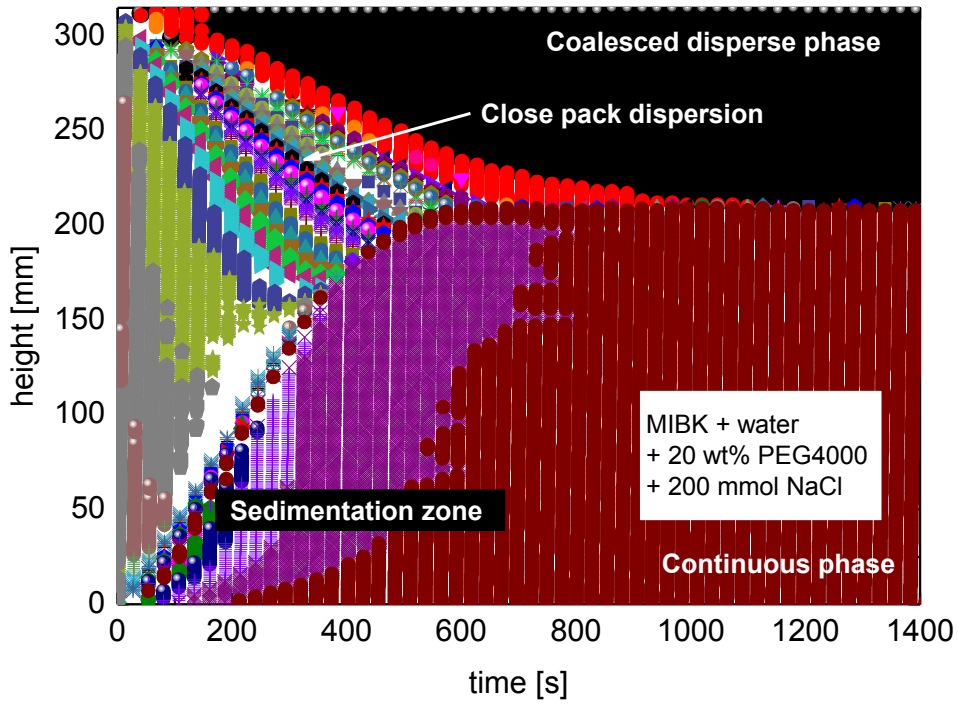

Fig. 5-18: 1% hold-up changing with height and time (Punsang et al., 2014).

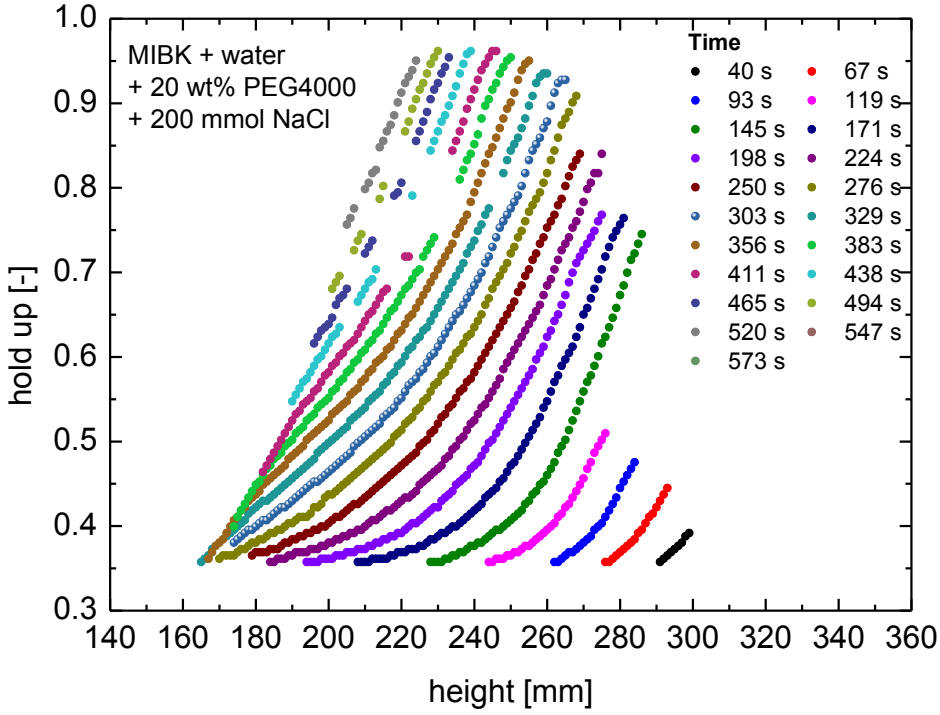

Fig. 5-19: Hold-up shifting along the height in the close-packed zone (Punsang et al., 2014).

In Fig. 5-19 the data of the clear dense-packed for the system MIBK + water + 20 wt% PEG4000 + 200 mmol of NaCl zone are shown. Two different shapes of gradients can be observed. For a better visualization the data are split up into two diagrams in the following. The time where the free sedimentation is ending is $t^* = 356\,\mathrm{s}$. All data for $t < t^*$ are plotted in Fig. 5-20 and all data for $t \geq t^*$ in Fig. 5-21.

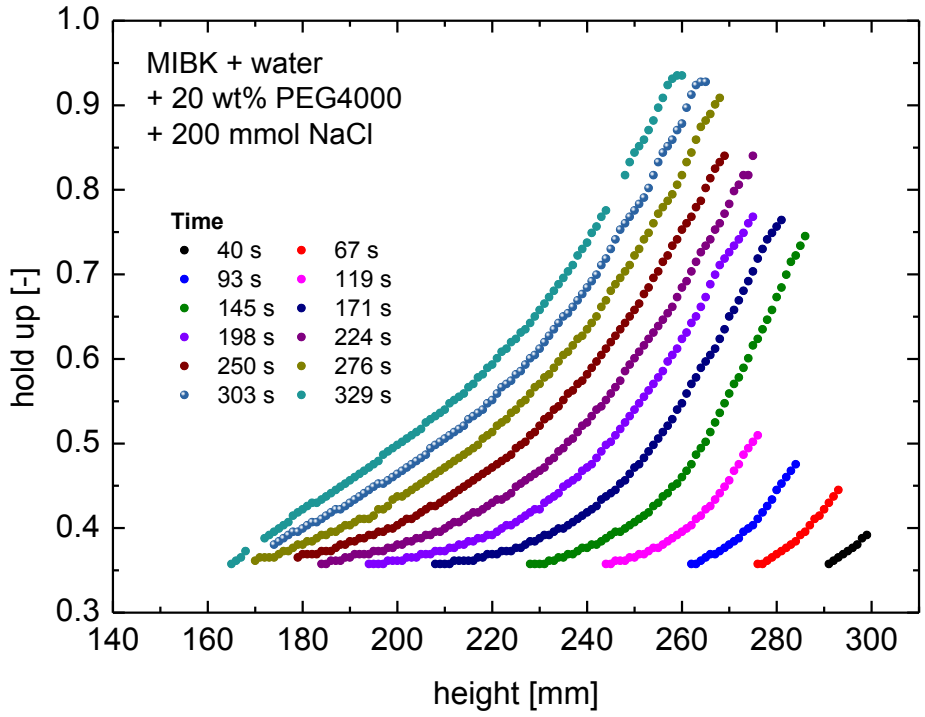

Fig. 5-20: Hold-up shifting along the height in the close-packed zone at $t < t^*$ (Punsang, 2014).

It can be seen from Fig. 5-20 that the functions for the hold-up are similar for the different times. For hold-up below 0.74 the trend line is curved. Above that hold-up the lines are more linear and almost parallel for the different times. In real processes the drop size will be distributed. Distributed sizes usually allow a higher hold-up before coalescence due to the better usage of space compared to monosized droplets. This leads to a less likely coalescence events. Coalescence between droplets is possible to occur when the droplets move up and are so close to each other that there is no distance between them. The force inside the dense-packed zone causes droplets to combine. Once coalescence occurs, most of droplets will grow at the same rate and have a similar size. It can be observed that beyond a hold-up of 0.74, the trend of gradients starts to change to linear.

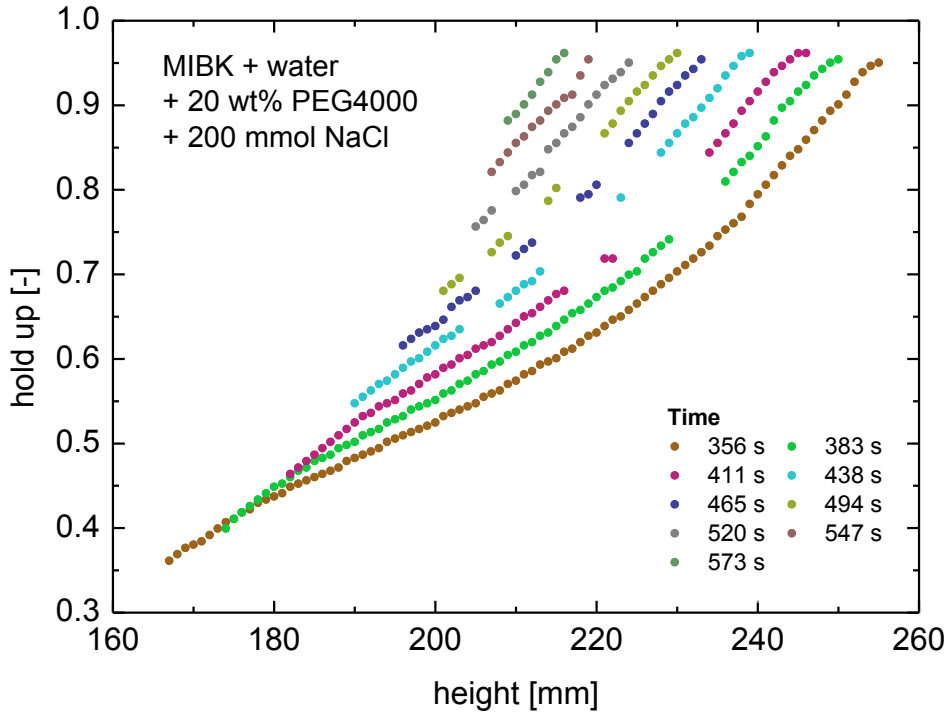

Fig. 5-21: Hold-up shifting along the height in the close-packed zone at $t \geq t^*$ (Punsang, 2014).

After free sedimentation is finished ($t \geq t^*$), only drop-drop coalescence occurs in this period. Consequently, most of all droplets are already in the same drop size, so the trend of gradients becomes nearly a straight line. This can be explained by the three pack models of rigid sphere which are a hexagonal close packing (hold-up 0.74), a body-centered tetragonal packing (hold-up 0.6) and a cubic close-packing (hold-up 0.52) (see chapter 2.3). Trends of the gradients for all close-packed models are similar. Therefore, the densest packing, the hexagonal close packing, was chosen. The distance between droplets is shortest here, so a strong drop deformation can take place. The result is shown in Fig. 5-22. The relationship of hold-up and height in the dense-packed zone can be described well by a polynomial function as presented in Table 5-1.

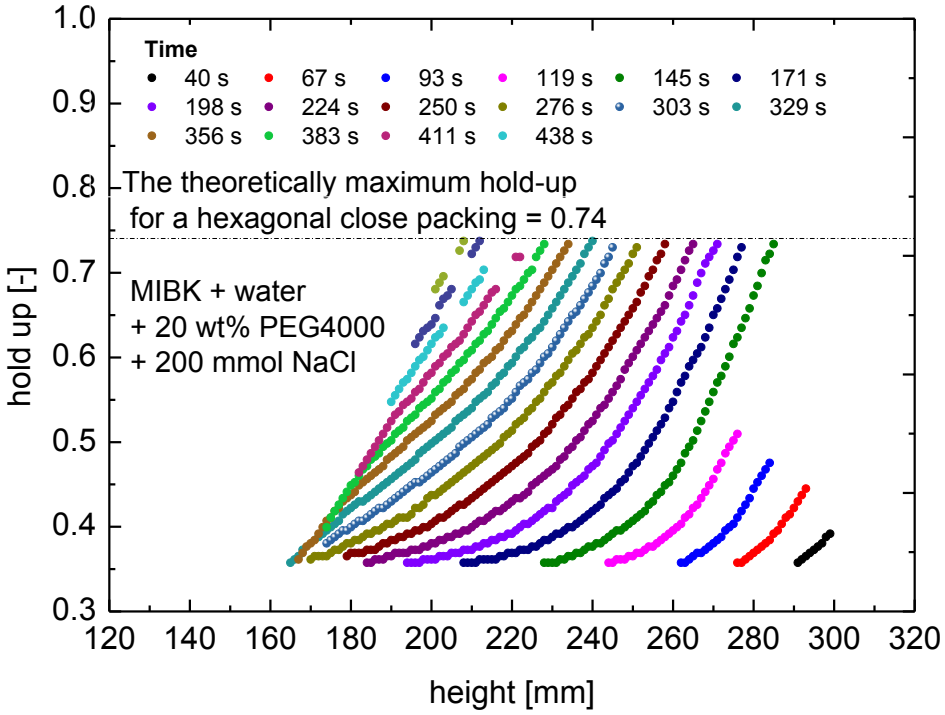

Fig. 5-22: Hold-up shifting along the height in the close-packed zone for the hold-up lower than the theoretical maximum hold-up based on a hexagonal close-packed model (Punsang, 2014).

Table 5-1: Fit equation of the hold-up shifting along the height in the close-packed zone

Close packed model	Time [s]	Equation	R^2
hexagonal close packed model	40	$\varepsilon = 0.0001 \cdot h^2 - 0.0807 \cdot h + 11.647$	0.9961
	67	$\varepsilon = 0.0002 \cdot h^2 - 0.0935 \cdot h + 12.948$	0.999
	93	$\varepsilon = 0.0002 \cdot h^2 - 0.1006 \cdot h + 13.389$	0.9983
	119	$\varepsilon = 0.0002 \cdot h^2 - 0.0768 \cdot h + 9.7659$	0.9983
	145	$\varepsilon = 0.0001 \cdot h^2 - 0.0625 \cdot h + 7.6179$	0.9986
	171	$\varepsilon = 1E\text{-}04 \cdot h^2 - 0.0417 \cdot h + 4.8644$	0.9984
	198	$\varepsilon = 8E\text{-}05 \cdot h^2 - 0.031 \cdot h + 3.4898$	0.9984
	224	$\varepsilon = 6E\text{-}05 \cdot h^2 - 0.0234 \cdot h + 2.571$	0.9986
	250	$\varepsilon = 5E\text{-}05 \cdot h^2 - 0.0189 \cdot h + 2.0464$	0.9991
	276	$\varepsilon = 4E\text{-}05 \cdot h^2 - 0.0143 \cdot h + 1.5201$	0.9988
	303	$\varepsilon = 3E\text{-}05 \cdot h^2 - 0.0085 \cdot h + 0.9281$	0.9992
	329	$\varepsilon = 1E\text{-}05 \cdot h^2 - 0.0008 \cdot h + 0.1425$	0.9986
	356	$\varepsilon = -9E\text{-}06 \cdot h^2 + 0.008 \cdot h - 0.7348$	0.9978
	383	$\varepsilon = -3E\text{-}05 \cdot h^2 + 0.0156 \cdot h - 1.5071$	0.9974
	411	$\varepsilon = -6E\text{-}05 \cdot h^2 + 0.0313 \cdot h - 3.0906$	0.9986
	438	$\varepsilon = -7E\text{-}05 \cdot h^2 + 0.0354 \cdot h - 3.5125$	0.9967

h: height, ε: hold-up

The relationship between and height for the hold-up higher than the theoretical maximum hold-up of a hexagonal close-packed model is shown in Fig. 5-23. The coales-

cence of droplets will take place in this range since the droplets are closed to each other. Force due to the accumulation of droplets causes the deformation resulting in the coalescence of droplets. The relationship can be fitted with the exponential function as displayed in Table 5-2. Similar results were found for other systems as well (more results can be found in appendix 8.4).

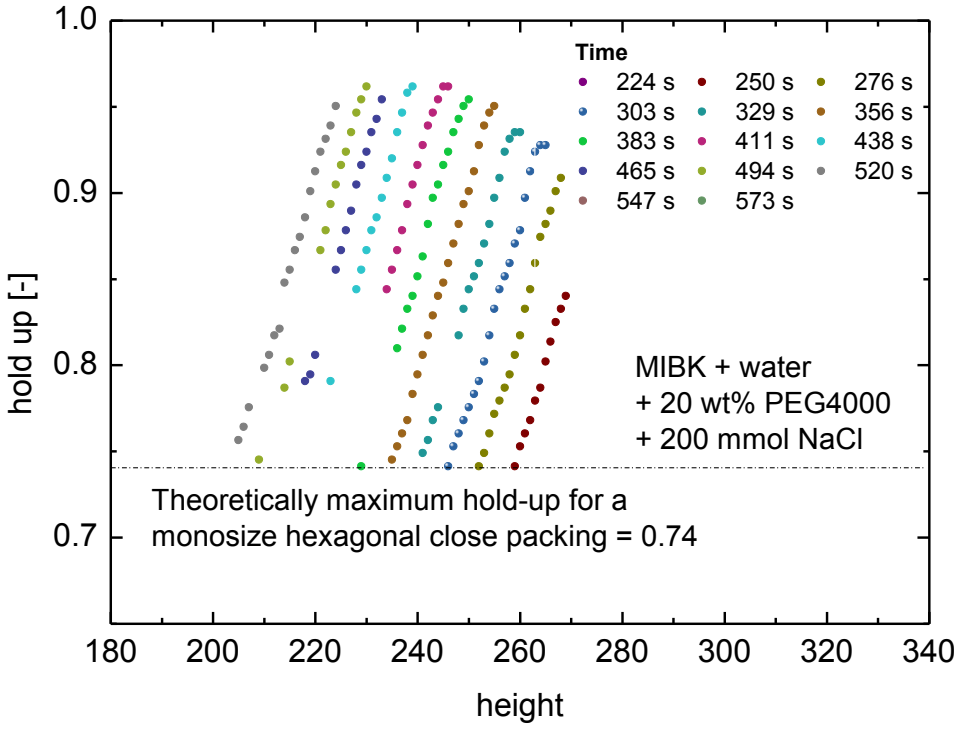

Fig. 5-23: Hold-up shifting along the height in the close-packed zone for the hold-up higher than the theoretical maximum hold-up based on a hexagonal close packed model (Punsang, 2014).

Table 5-2: Fit equation for the hold-up along the height in the close-packed zone for the hold-up higher than the theoretical maximum hold-up

Close packed model	Time [s]	Equation	R^2
hexagonal close packed model	224	$\varepsilon = 0.0209e^{0.0134 \cdot h}$	0.9878
	250	$\varepsilon = 0.0209e^{0.0134 \cdot h}$	0.9878
	276	$\varepsilon = 0.0262e^{0.0132 \cdot h}$	0.9957
	303	$\varepsilon = 0.0356e^{0.0123 \cdot h}$	0.9981
	329	$\varepsilon = 0.0413e^{0.012 \cdot h}$	0.9978
	356	$\varepsilon = 0.0458e^{0.0119 \cdot h}$	0.9974
	383	$\varepsilon = 0.0505e^{0.0118 \cdot h}$	0.9968
	411	$\varepsilon = 0.0552e^{0.0117 \cdot h}$	0.9978
	438	$\varepsilon = 0.0587e^{0.0117 \cdot h}$	0.9983
	465	$\varepsilon = 0.0585e^{0.012 \cdot h}$	0.9985
	494	$\varepsilon = 0.0567e^{0.0123 \cdot h}$	0.9986
	520	$\varepsilon = 0.0586e^{0.0125 \cdot h}$	0.9948
	547	$\varepsilon = 0.0771e^{0.0114 \cdot h}$	0.9874
	573	$\varepsilon = 0.0573e^{0.0131 \cdot h}$	0.9951

h: height, ε: hold-up

5.4 Comparison between analytical settling model and experimental results

As described in chapter 4.3 the sedimentation curve and the coalescence curve can be described by sigmoidal curves. In Fig. 5-24 the experimental data for the system MIBK + water + 20 wt% PEG4000 + 200 mmol of NaCl zone are shown. These are the optically visible main sedimentation curve, a secondary sedimentation curve of tiny droplets and the coalescence curve. Since the hold-up profile in the dense packed zone shows a sigmoidal structure as well (see Fig. 5-18) it is described with a similar function. The sedimentation curve, coalescence curve and dense-packed zone curve are calculated from equation 4-11, 4-12 and 4-13 respectively. The parameters *b* and *c* are fitted to the experimental data. It can be seen from the result that the modified sigmoid function can well approach the experimentally obtained settling curve.

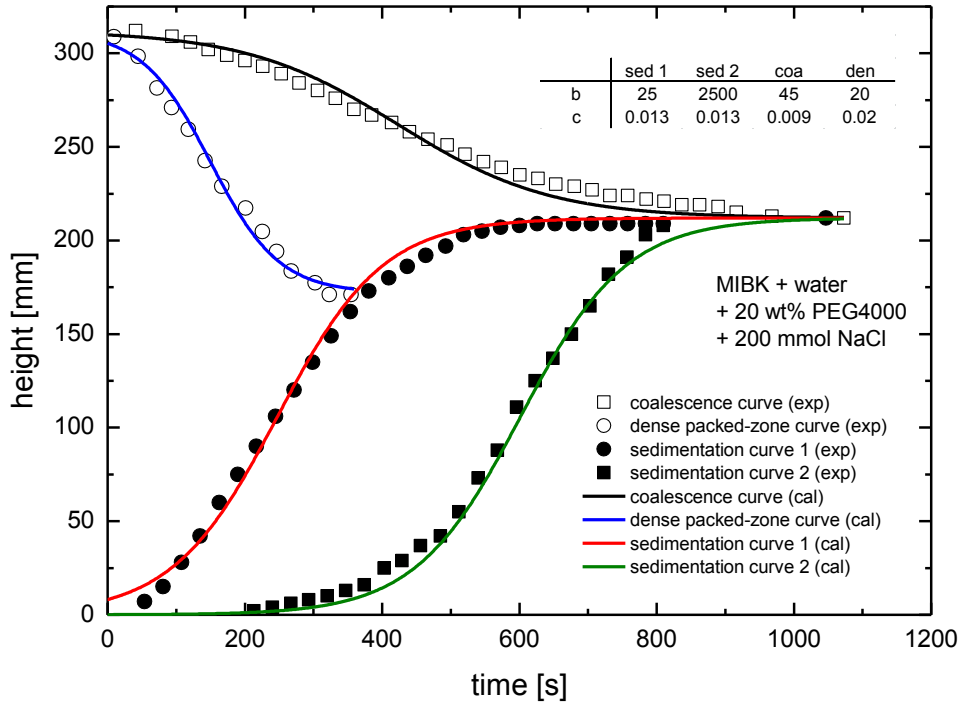

Fig. 5-24: Comparison between rate based settling model and experimental result.

5.5 Influence of internals in high-viscosity systems

It is known that internals have a strong influence on phase separation. To study the influence of internals in high-viscosity systems, a suitable internal for the settling cell was designed and built (see Fig. 3-5). The viscosity of the aqueous phase was increased by adding polyethylene glycol with the molecular weight 4000. Mungma et al. (2014) found that adding PEG4000 to the aqueous phase does not only change the viscosity but also the interfacial tension, having a significant impact on drops size. The influence of the internals was studied for inclined plates. The results are showed in Fig. 5-25 (more results can be seen in appendix 8.7). Unlike the phase separation without internals there are multiple coalescence and sedimentation curves. The upwardly moving drops are hindered in their movement by the plates and therefore accumulate below the plates.

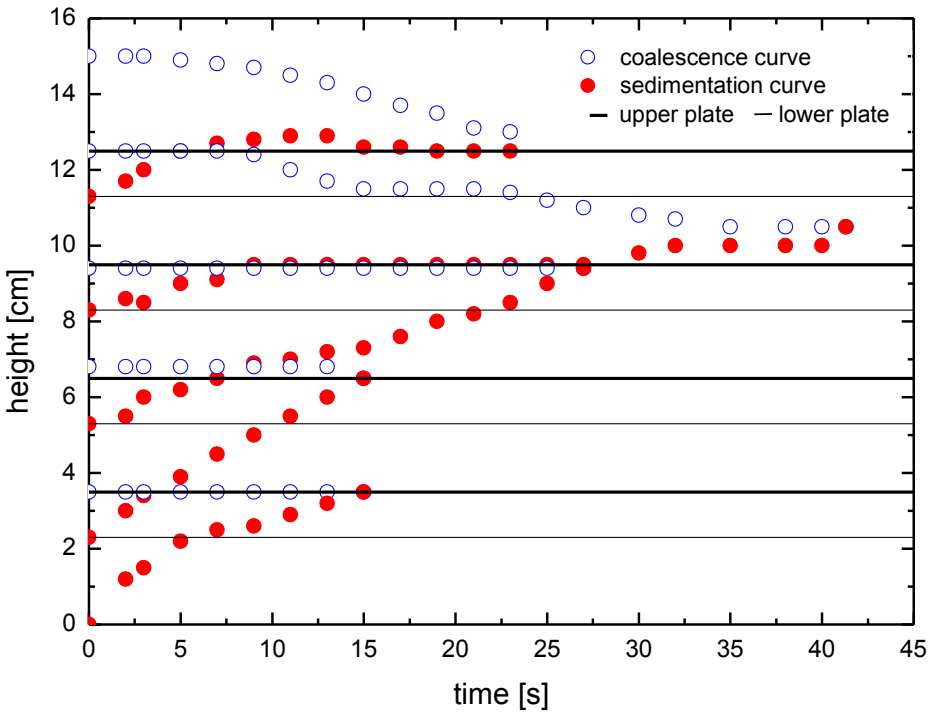

Fig. 5-25: Experimental variations in the heights of sedimenting and coalescing interfaces with 4 inclined plates; system: cyclohexanone+water +4 wt% PEG 4000, o/a = 1/2 (Mungma, 2013).

Hence, coalescence does not only take place in the upper part of the cell, but over the total height. This speeds up the coalescence process in general. In Fig. 5-26 the

normalized settling time τ is plotted as a function of plate distance and phase ratio. The normalized settling time is defined as

$$\tau = \frac{t_{\text{end,with internals}}}{t_{\text{end,without internals}}}. \tag{5-1}$$

Higher-viscosity systems have longer settling and dead times than lower-viscosity systems. Higher viscosity systems lead to smaller droplet sizes. When comparing viscous system separation with and without internal plates, it was found that internal plates enhance the separation significantly. It can be seen that the settling time is decreased for systems with internals in all experiments up to 40%.

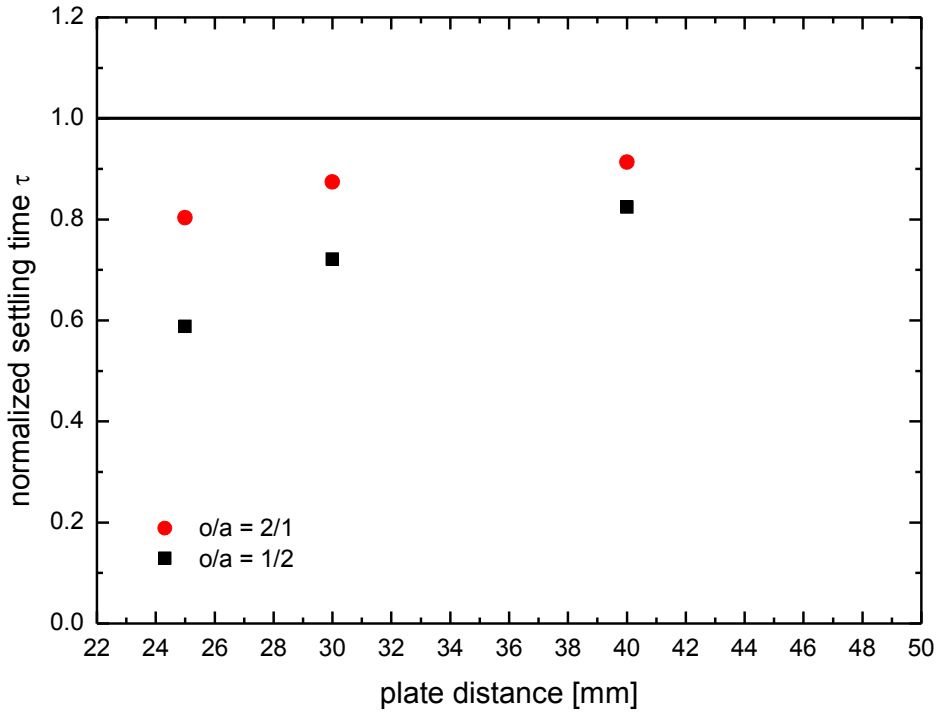

Fig. 5-26: Variation of the normalized settling time of cyclohexanone + water + 4 wt% PEG 4000 versus plate distance (Mungma et al., 2014).

At the same time a clear difference between the phase ratios can be seen. The phase ratio of the organic and aqueous phase is one parameter which affects the direction of phase dispersion. For high ratios the aqueous phase will disperse, while for low ratios the organic phase will disperse. Therefore, it is clear that the settling time may be affected in different magnitudes.

6 Summary

In this work the separation of two phase systems was studied in order to gain information that will help to improve the design of industrial settlers. The influence of high viscosity and electrolyte on the settling process was investigated. The novel ultrasonic scanning technology was used to characterize systems where the established optical investigation was not applicable.

The influence of electrolytes on the settling time depends on the type of salt and the investigated system. The electrolyte has more influence on the settling time in low viscosity systems while in high viscosity systems the viscosity is the dominating factor. With increasing viscosity of the aqueous phase the settling velocity of droplet swarms will significantly slow down. Moreover, the droplet size decreases as the viscosity of the aqueous phase increases and causes a longer settling time. The effect of interface tension and its depletion with admixture of hydrocarbon based constituents of course also acts on drop size. However, at constant mixing rate the viscosity is governing drop formation and size. Higher viscosity systems lead to smaller droplet sizes. For constant density of phases higher-viscosity systems have (expectedly) longer settling and dead times than lower-viscosity systems. When comparing viscous system separation with and without internals, it was found, as expected from sedimentation basics, that internals enhance the phase separation significantly. The knowledge about these influence factors allows the selection of suitable systems for further analysis with the ultrasonic scanner.

In the industry opaque systems may frequently occur. These systems cannot be investigated with the optical method. Therefore, a new technology, the ultrasonic scanner was introduced. The ultrasonic scanner generates and receives sound waves. The sound waves are altered by the medium they are passing and thus can be used to obtain the local hold-up with time for a separating system. The height of the sedimentation zone and the coalescence curve can be determined from time dependent speed of sound and height. The curves are quantitatively identical with the settling trend observed in the optical cell. Ultrasonic scanning technique can be used to determine the boundary between close-packed dispersion, coalescence and sedimentation zone, even in opaque systems where optical detection fails. It additionally allows quantitative evaluation of local hold-up in opaque systems.

The ultrasonic scanner data showed hold-up changes in the continuous phase which are optically not identifiable, most likely caused by secondary sedimentation of tiny droplets. Sedimentation experiments with polydisperse particles showed that due to the faster sedimentation rate of bigger particles, separation zones of different sedimentation velocity are formed with time, containing only particles below a certain size. This means that for polydisperse droplets different sedimentation velocities occur in the same fluid.

Previous models in settler design base on the assumption of monodisperse droplets. Hence a new model was developed to describe the settling behavior of polydisperse swarm drops. In gravity settling the velocity of each droplet relative to the surrounding fluid depends on the droplets size. In the beginning of a settling experiment the polydisperse droplets are assumed to be equally distributed in the sedimentation zone. With time separation zones of different sedimentation velocity are formed, containing only droplets of certain size, which change the local hold-up. Regions of close-packed dispersion could not always be identified clearly. The model parameters can then be fitted to the experiment to obtain information regarding the actual drop distribution.

The hold-up change in dense-packed zone could not be modeled with just one function. At the lower part of the dense-packed zone, the droplets still remain distant to neighboring droplets so coalescence does not occur in this zone. In the upper part, the droplets are close to each other (almost no distance between droplets) causing the droplets to coalesce. This information can be used in the future to model the coalescence of droplet in the dense-packed zone.

However, it was found that sigmoidal functions, deduced from kinetics, can be used to describe the settling curves and coalescence curves as a function of height and time as well. The parameters of these functions address the different phases of settling and coalescence.

7 Nomenclature

Symbol	Unit	Definition
a	m	Droplet distance
A_0	m	Amplitude at initial position
A_t	m	Amplitude at position t
$A_{1,2,3}$	[-]	Hamaker constant
Ar	[-]	Archimedes number
c	m/s	Speed of sound wave
c_{org}	m/s	Speed of sound wave in organic phase
c_{aq}	m/s	Speed of sound wave in aqueous phase
C_0	mol/m^3	Concentration
Cd	[-]	Drag coefficient
c_w	[-]	Friction coefficient
d	m	Diameter
$d_{32,0}$	mm	Sauter mean diameter
d_0	mm	Initial mean diameter
e	C	Elementary charge
F	[-]	Faraday constant
F_B	N	Buoyancy force
F_D	N	Drag force
F_{el}	N	Electrostatic force

F_G	N	Gravity force
F_T	N	Total interaction force
F_{vdw}	N	Van der Waals force
g	m/s^2	Gravitational constant
h	[-]	Planck constant
h_o	mm	Height of the coalesced light phase
h_s	mm	Height of the continuous heavy phase
h_p	mm	Height of the sedimentation zone
		Inertial dispersion height
h_c	mm	Height of the dense-packed zone
h_{total}	mm	Sum of the total height
I	mol/m^3	Ionic strength of the electrolyte
k_B	[-]	Boltzmann constant
K_{HR}	[-]	Hadamard-Rybczynski factor
K	Pa	Bulk modulus
m	[-]	Hindered sedimentation parameter
n	[-]	Impact of the dispersed phase fraction on binary coalescence
		Number of drop
n_i	[-]	Refractive index
N_A	[-]	Avogadro constant
R	JK^{-1}mol^{-1}	Gas constant

R'	N/m^2	Resistance force per unit area of the rigid sphere
Re	[-]	Reynolds number
Re_∞	[-]	Reynolds number in an infinitely
Re_s	[-]	Reynolds number of dispersed droplets
R_0	m	Drop radius
r^2	[-]	Coefficient of determination
r_s^*	[-]	Henschke's coalescence parameter
s	mm	Distance between drops
t	s	Time
t^*	s	Time at the end of free sedimentation
t_E	s	Settling time
T	[-]	Transducer
	°C or K	Temperature
v	m/s	speed of sound in the media
v_e	1/s	Absorption frequency
v_c	m/s	Actual velocity of the continuous phase
v_{rs}	m/s	relative velocity between the swarm drops and the continuous phase
v_s	m/s	Sedimentation velocity
		Actual velocity of the swarm drops
$v_{s,\infty}$	m/s	Free drop sedimentation velocity
v_0	m/s	Initial sedimentation velocity

v_∞	m/s	Relative velocity
V_c	m^3	Total of continuous phase
$\dot{V}_c$	m^3/s	Volume flow rate of the continuous phase
V_d	m^3	Total volumes of dispersed phase
$\dot{V}_d$	m^3/s	Volume flow rate of the dispersed phase
V_{drop}	mm^3	Volume of drop
V_{total}	mm^3	Total volume
x	m	Distance

Greek Symbols

Symbol	**Unit**	**Definition**
ρ	g/cm^3	Density
ρ_c	g/cm^3	Density of the continuous phase
ρ_d	g/cm^3	Density of the dispersed phase
η	Pa·s	Dynamic viscosity
η_c	Pa·s	Dynamic viscosity of the continuous phase
μ	m	Expectation value for diameter
ε_0	[-]	Local hold-up
	F/m	Permittivity of free space
$\Delta\varepsilon_{abs,i}$	[-]	Absolute error at data point i
$\Delta\varepsilon_{rel,i}$	[-]	Relative error at data point i

$\varepsilon_{cal.}$	[-]	Hold-up calculated via settle program
$\varepsilon_{\mathrm{exp,i}}$	[-]	Hold-up of experimental data point i
$\varepsilon_{\mathrm{mod}}(m,n)$	[-]	Hold-up of model for height element m and time step n
ε_r	[-]	Dielectric constants
κ^{-1}	[-]	Debye–Hückel screening length
α	[-]	Attenuation coefficient
$\omega_{i,j}$	[-]	Ratio of drop hold-up
σ	m	Standard deviation for drop diameter

8 Appendix

8.1 Geometric data of internal cell

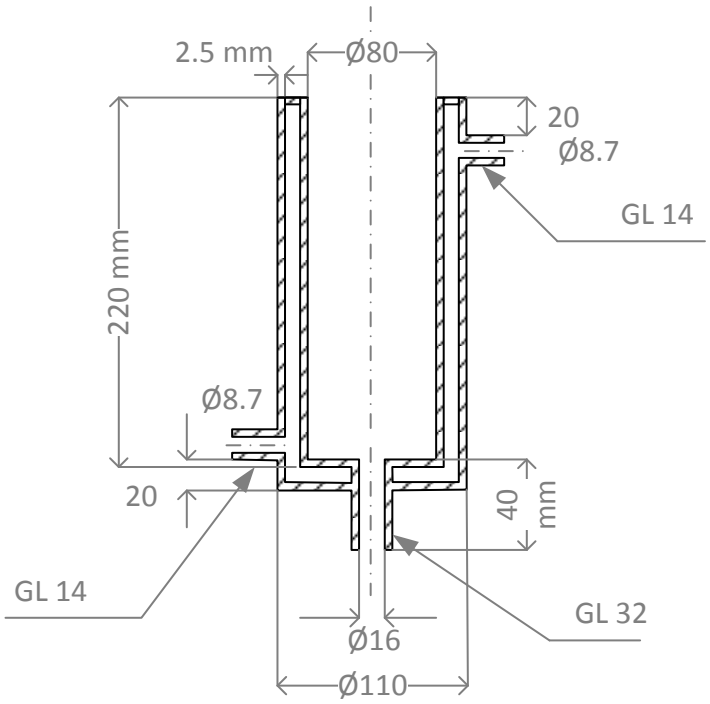

Fig. 8-1: Mixing unit cell

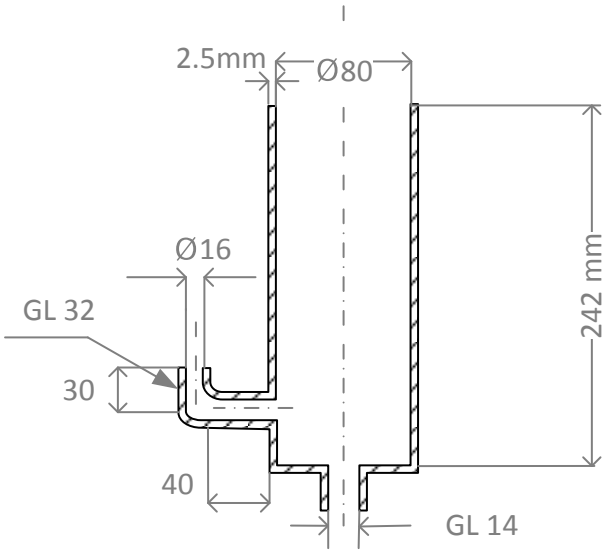

Fig. 8-2: Internal cell

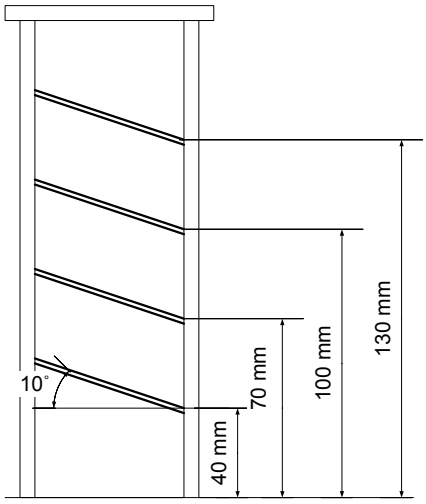

Fig. 8-3: design of inclined plates in the settling cell

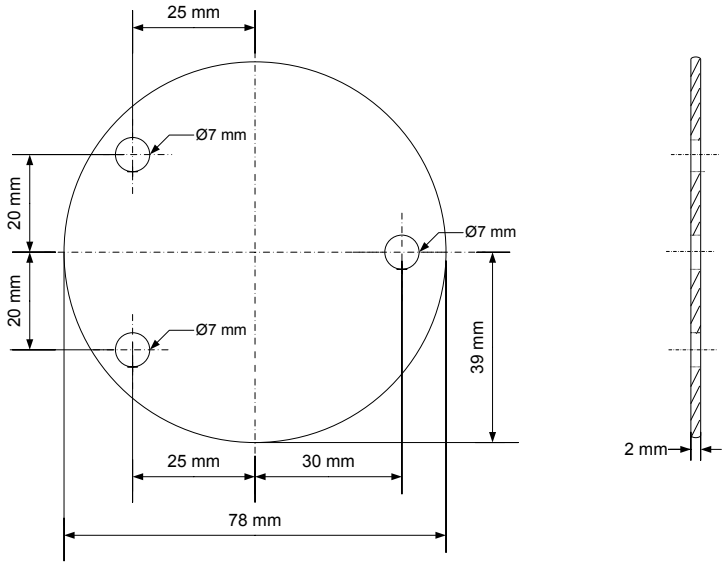

Fig. 8-4: Inclined plate geometry

8.2 Geometric data of optical cell

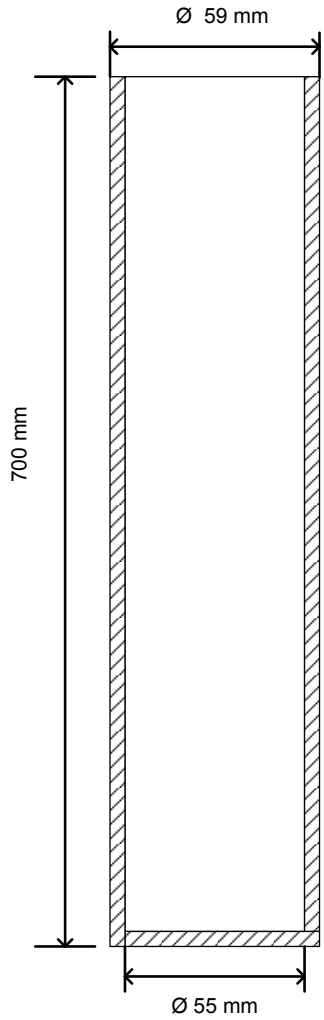

Fig. 8-5: Optical cell geometry

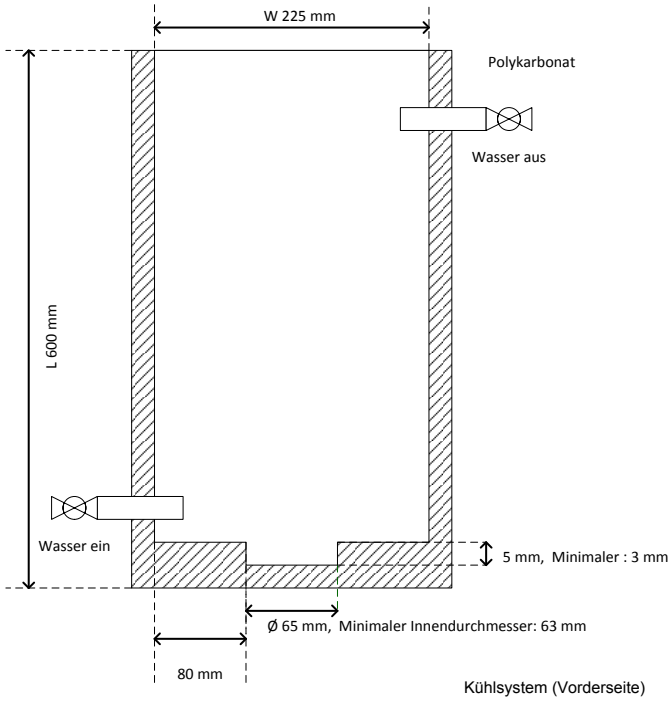

Fig. 8-6: Cooling system geometry (front)

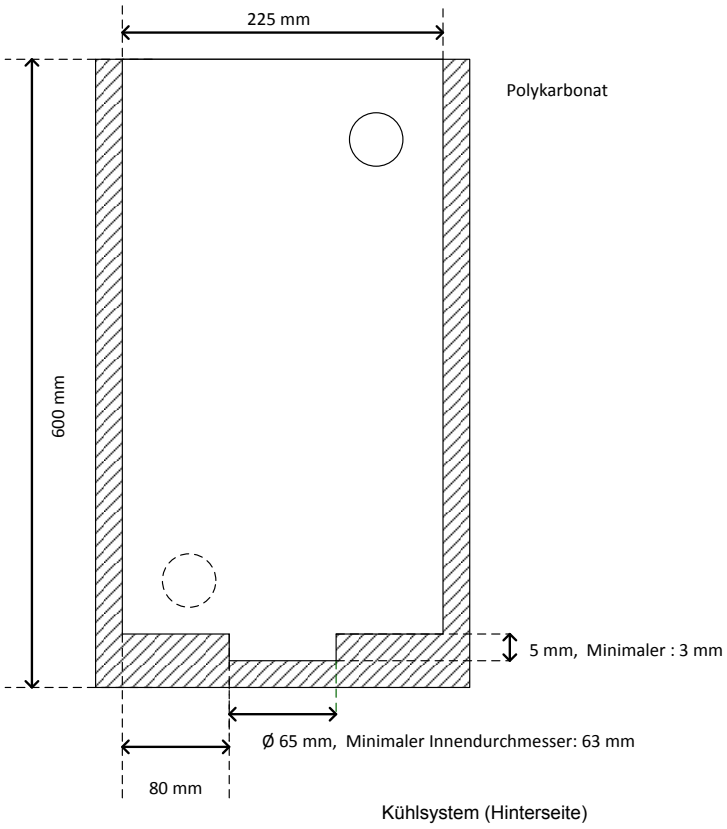

Fig. 8-7: Cooling system geometry (side)

8.3 Physical properties of the chemical systems

System	PEG4000 (wt%)	Salt (mmol/L)	$Viscosity_{org}$ (Pa·s)	$Density_{org}$ (g/cm^3)	$Viscosity_{aq}$ (Pa·s)	$Density_{aq}$ (g/cm^3)	Interfacial tension (mN/m)
Toluene (Distillate)	-	-	0.000597	0.867	0.00135	0.998	34.025
Toluene (Distillate)	-	50 (NaCl)	0.000597	0.867	0.00104	1.0003	38.673
Toluene (Distillate)	-	100 (NaCl)	0.000597	0.867	0.00105	1.0019	40.638
Toluene (Distillate)	-	200 (NaCl)	0.000597	0.867	0.00105	1.0065	40.363
Toluene (Distillate)	-	300 (NaCl)	0.000597	0.867	0.00106	1.0106	41.094
Toluene (Distillate)	-	500 (NaCl)	0.000597	0.867	0.00108	1.0190	38.515
Toluene (Distillate)	5	-	0.000597	0.867	0.00162	1.0064	20.998
Toluene (Distillate)	5	50 (NaCl)	0.000597	0.867	0.00162	1.0083	21.093

System	PEG4000 (wt%)	Salt (mmol/L)	$Viscosity_{org}$ (Pa·s)	$Density_{org}$ (g/cm^3)	$Viscosity_{aq}$ (Pa·s)	$Density_{aq}$ (g/cm^3)	Interfacial tension (mN/m)
Toluene (Distillate)	5	100 (NaCl)	0.000597	0.867	0.00163	1.0104	21.101
Toluene (Distillate)	5	200 (NaCl)	0.000597	0.867	0.00164	1.0142	20.857
Toluene (Distillate)	5	300 (NaCl)	0.000597	0.867	0.00165	1.0177	21.393
Toluene (Distillate)	5	400 (NaCl)	0.000597	0.867	0.00165	1.0219	21.039
Toluene (Distillate)	5	500 (NaCl)	0.000597	0.867	0.00166	1.0257	20.326
Toluene (Distillate)	20	100 (NaCl)	0.000597	0.867	0.00776	1.0355	18.494
Toluene (Distillate)	35	100 (NaCl)	0.000597	0.867	0.02721	1.0628	15.606
Toluene (Distillate)	50	100 (NaCl)	0.000597	0.867	0. 1061	1.0869	3.574

System	PEG4000 (wt%)	Salt (mmol/L)	$Viscosity_{org}$ (Pa·s)	$Density_{org}$ (g/cm^3)	$Viscosity_{aq}$ (Pa·s)	$Density_{aq}$ (g/cm^3)	Interfacial tension (mN/m)
Toluene (Distillate)	-	50 (Na_2SO_4)	0.000597	0.867	0.00106	1.0046	35.880
Toluene (Distillate)	-	100 (Na_2SO_4)	0.000597	0.867	0.00119	1.0110	36.755
Toluene (Distillate)	-	200 (Na_2SO_4)	0.000597	0.867	0.00123	1.0233	38.755
Toluene (Distillate)	-	300 (Na_2SO_4)	0.000597	0.867	0.00123	1.0358	39.233
Toluene (Distillate)	-	500 (Na_2SO_4)	0.000597	0.867	0.00139	1.0587	39.447
Toluene (Distillate)	5	100 (Na_2SO_4)	0.000597	0.867	0.00199	1.0183	20.476
Toluene (Distillate)	20	100 (Na_2SO_4)	0.000597	0.867	0.00916	1.0368	16.135
Toluene (Distillate)	35	100 (Na_2SO_4)	0.000597	0.867	0.03684	1.0681	14.591

System	PEG4000 (wt%)	Salt (mmol/L)	$Viscosity_{org}$ (Pa·s)	$Density_{org}$ (g/cm^3)	$Viscosity_{aq}$ (Pa·s)	$Density_{aq}$ (g/cm^3)	Interfacial tension (mN/m)
Toluene (Distillate)	50	100 (Na_2SO_4)	0.000597	0.867	0.12003	1.0927	0.216
Toluene (2F005908)	5	50 (NaCl)	0.0005930	0.866	0.001910	1.008	18.79
Toluene (2F005908)	10	50 (NaCl)	0.000560	0.8667	0.00270	1.0171	10.95
Toluene (2F005908)	15	50 (NaCl)	0.0005650	0.8662	0.00436	1.0252	10.20
MIBK (K42353646)	-	-	0.00063	0.803	0.001082	0.998	10.8
MIBK (452193304)	5	50 (NaCl)	0.0005420	0.8044	0.0014163	1.0058	8.52
MIBK (452193304)	5	200 (NaCl)	0.0005836	0.8043	0.0015890	1.0138	8.76
MIBK (452193304)	5	500 (NaCl)	0.0005643	0.8043	0.0016826	1.0327	10.06

System	PEG4000 (wt%)	Salt (mmol/L)	$Viscosity_{org}$ (Pa·s)	$Density_{org}$ (g/cm^3)	$Viscosity_{aq}$ (Pa·s)	$Density_{aq}$ (g/cm^3)	Interfacial tension (mN/m)
MIBK (452193304)	5	1000 (NaCl)	0.0005643	0.8038	0.0015798	1.0694	10.18
MIBK (452193304)	10	50 (NaCl)	0.0005211	0.8123	0.0028598	1.0242	8.46
MIBK (452193304)	10	200 (NaCl)	0.0005211	0.8123	0.0028176	1.0310	8.70
MIBK (452193304)	10	500 (NaCl)	0.005211	0.8123	0.0031828	1.0456	8.98
MIBK (452193304)	10	1000 (NaCl)	0.005211	0.8123	0.0032528	1.0703	9.18
MIBK (452193304)	15	50 (NaCl)	0.005506	0.8123	0.0046994	1.0332	8.28
MIBK (452193304)	15	200 (NaCl)	0.005506	0.8123	0.0050315	1.0393	8.51
MIBK (452193304)	15	500 (NaCl)	0.005506	0.8123	0.0052243	1.0528	8.71

System	PEG4000 (wt%)	Salt (mmol/L)	$Viscosity_{org}$ (Pa·s)	$Density_{org}$ (g/cm^3)	$Viscosity_{aq}$ (Pa·s)	$Density_{aq}$ (g/cm^3)	Interfacial tension (mN/m)
MIBK (452193304)	15	1000 (NaCl)	0.005506	0.8123	0.0052968	1.0766	8.93
MIBK (452193304)	20	200 (NaCl)	0.005506	0.8123	0.0083694	1.0484	8.59
MIBK (452193304)	30	200 (NaCl)	0.005506	0.8123	0.0195940	1.0661	8.06
Cyclohexanone (472193603)	-	-	0.00227	0.950	0.00295	1.010	2.61
Cyclohexanone (013193603)	-	-	0.002416	0.960	0.001417	1.015	4.02
Cyclohexanone (013193603)	4	-	0.002416	0.960	0.00207	1.019	3.19
Cyclohexanone (013193603)	13	-	0.002416	0.960	0.00487	1.023	3.08
Cyclohexanone (013193603)	19	-	0.002416	0.960	0.00978	1.029	2.92

System	PEG4000 (wt%)	Salt (mmol/L)	$Viscosity_{org}$ (Pa·s)	$Density_{org}$ (g/cm^3)	$Viscosity_{aq}$ (Pa·s)	$Density_{aq}$ (g/cm^3)	Interfacial tension (mN/m)
Cyclohexanone (193200133)	10	-	0.001848	0.9523	0.002683	1.0134	3
Cyclohexanone (193200133)	15	-	0.0018094	0.9517	0.003918	1.0221	3.15

8.4 Experimental data: polydisperse sedimentation

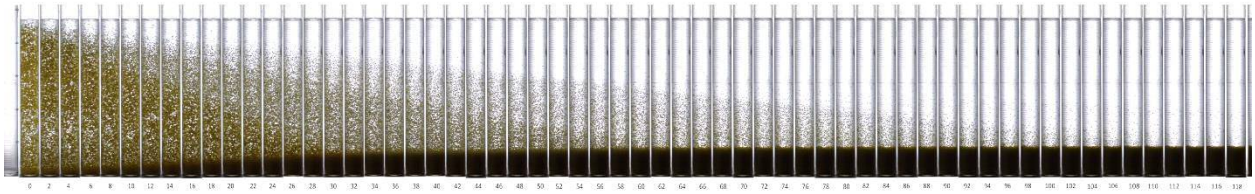

Fig. 8-8: Settling curves of POM particles at ε_0 = 0.10 in water + 50 wt% PEG-4000; recorded with 2 second screen shot technique

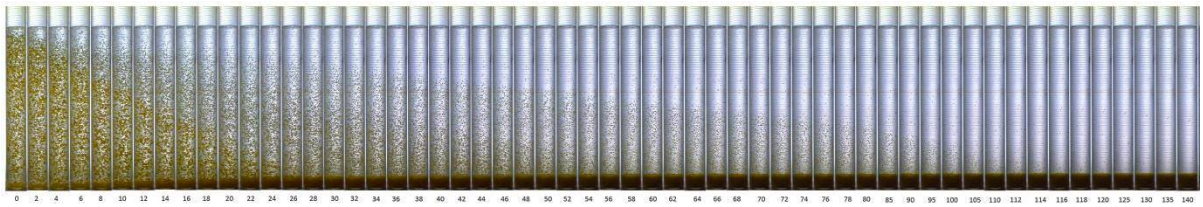

Fig. 8-9: Settling curves of POM particles at ε_0 = 0.05 in water + 50 wt% PEG-4000; recorded with 2 second screen shot technique

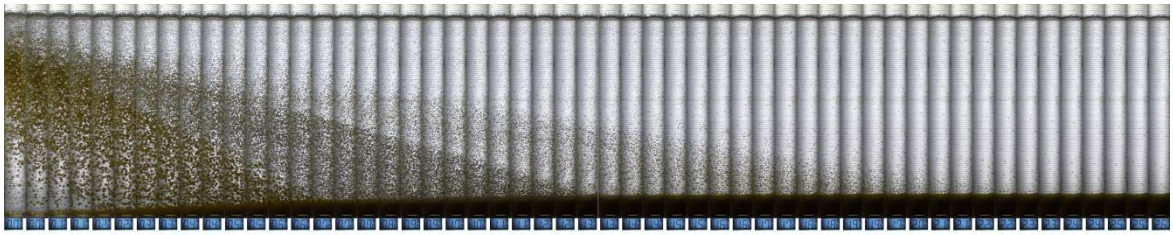

Fig. 8-10: Settling curves of POM particles at ε_0 = 0.05 in water + 30 wt% PEG-4000; recorded with 0.5 second screen shot technique

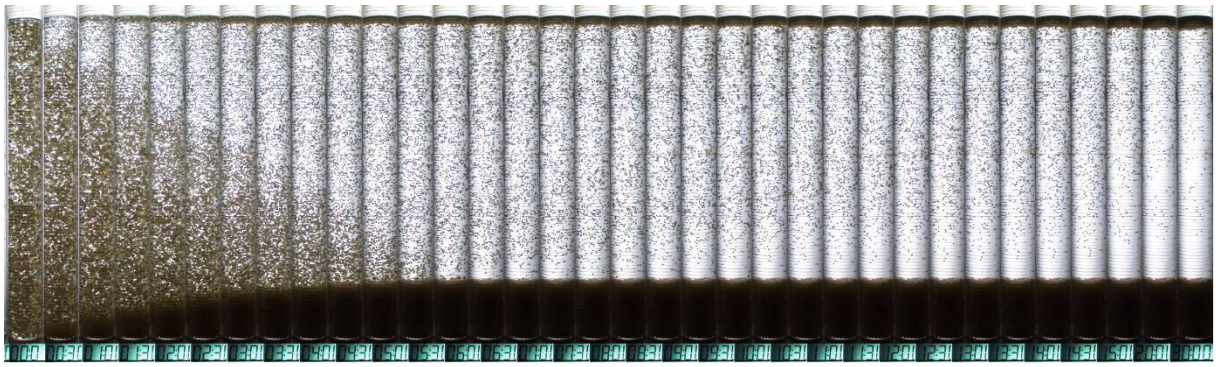

Fig. 8-11: Settling curves of PA particles at ε_0 = 0.10 in water + 50 wt% PEG-4000; recorded with 0.5 second screen shot technique

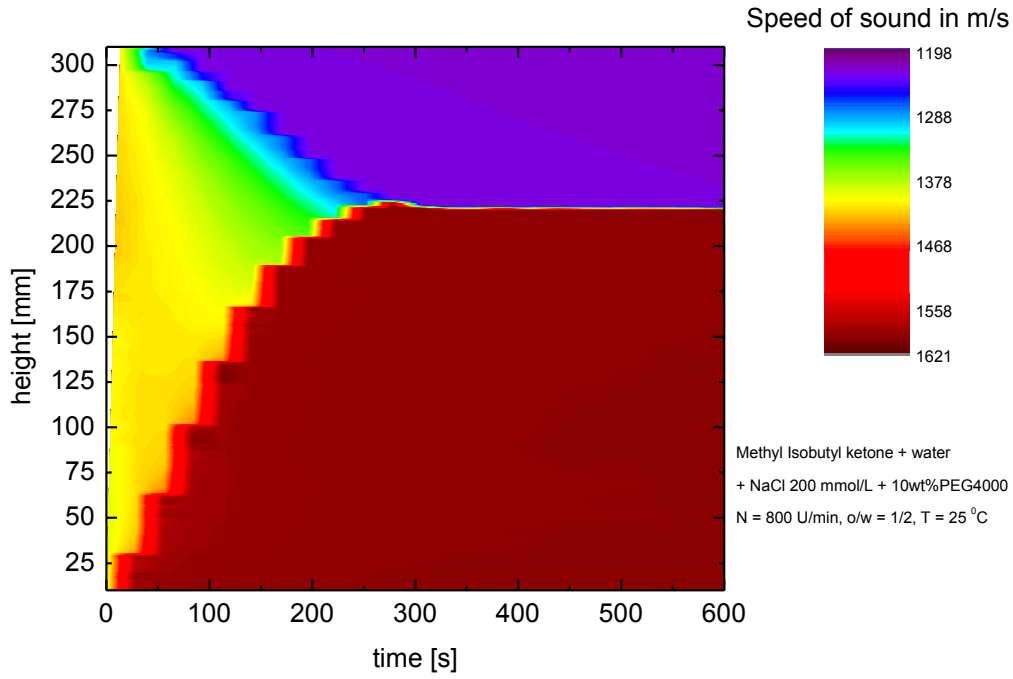

Fig. 8-12: Ultrasonic scanner result of MIBK and water with 10 wt%PEG4000 and NaCl concentration 200 mmol/L, o/a = 1/2

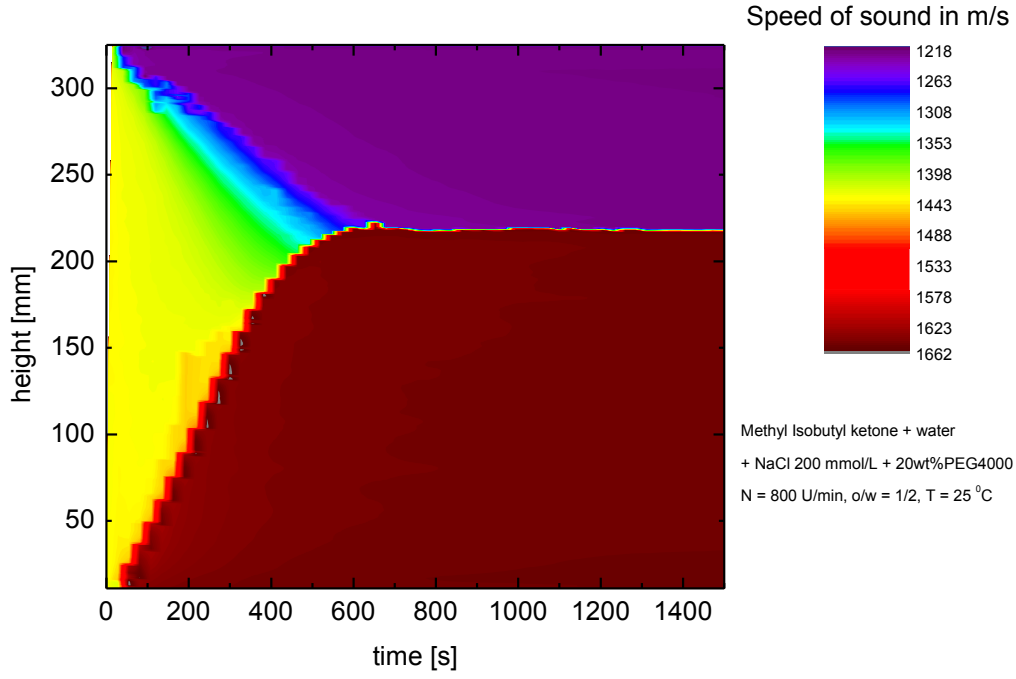

Fig. 8-13: Ultrasonic scanner result of MIBK and water with 20 wt% PEG4000 and NaCl concentration 200 mmol/L, o/a = 1/2

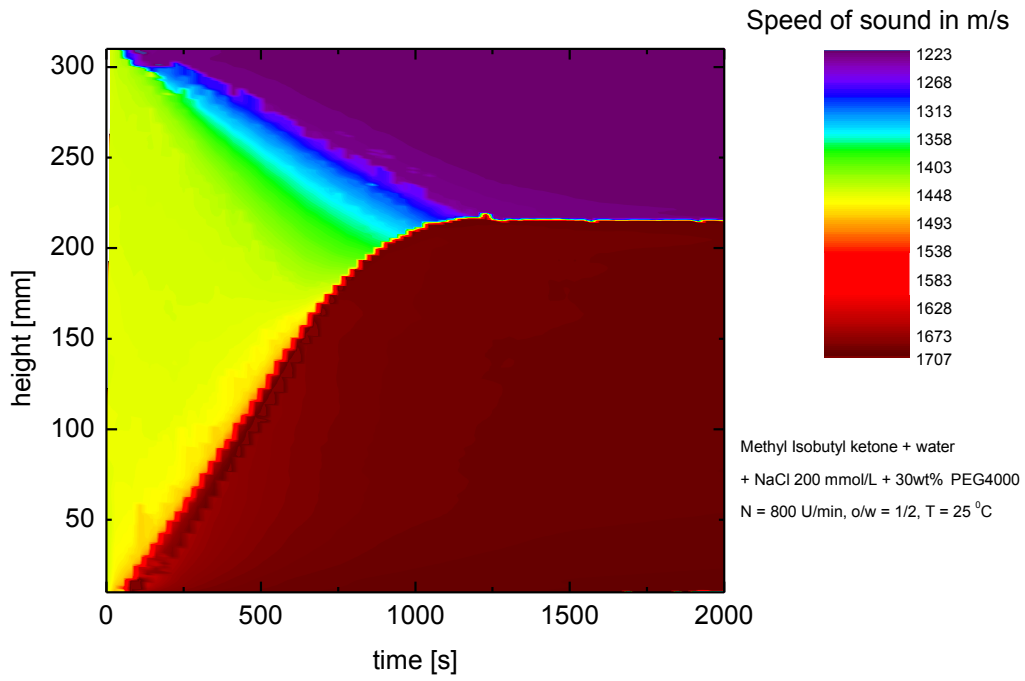

Fig. 8-14: Ultrasonic scanner result of MIBK and water with 30 wt% PEG4000 and NaCl concentration 200 mmol/L, o/a = 1/2

8.5 Comparison between Henschke model and experimental data

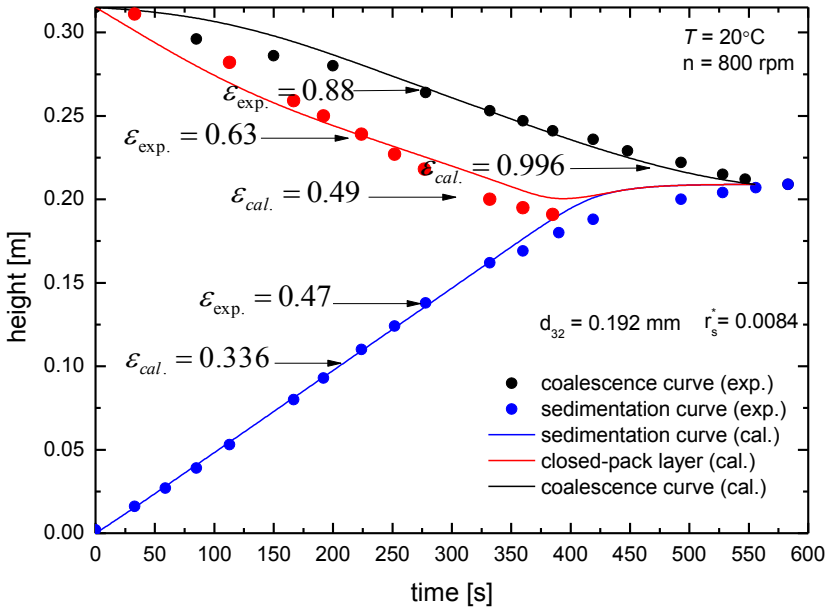

Fig. 8-15: System MIBK and water with 20 wt% PEG4000 and 200 mmol of NaCl.

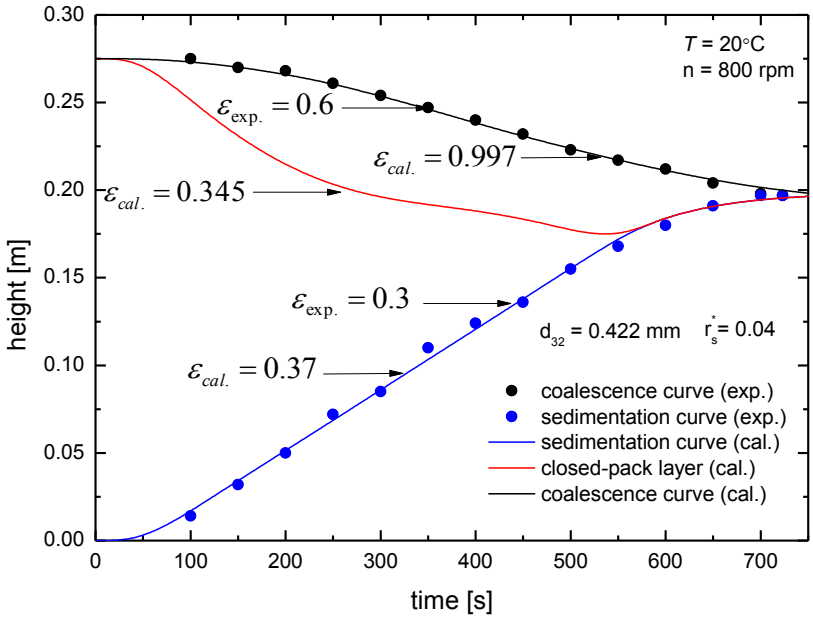

Fig. 8-16: System cyclohexanone and water with 20 wt% PEG4000 and 50 mmol of NaCl.

8.6 Experimental data: influence of electrolyte and viscosity

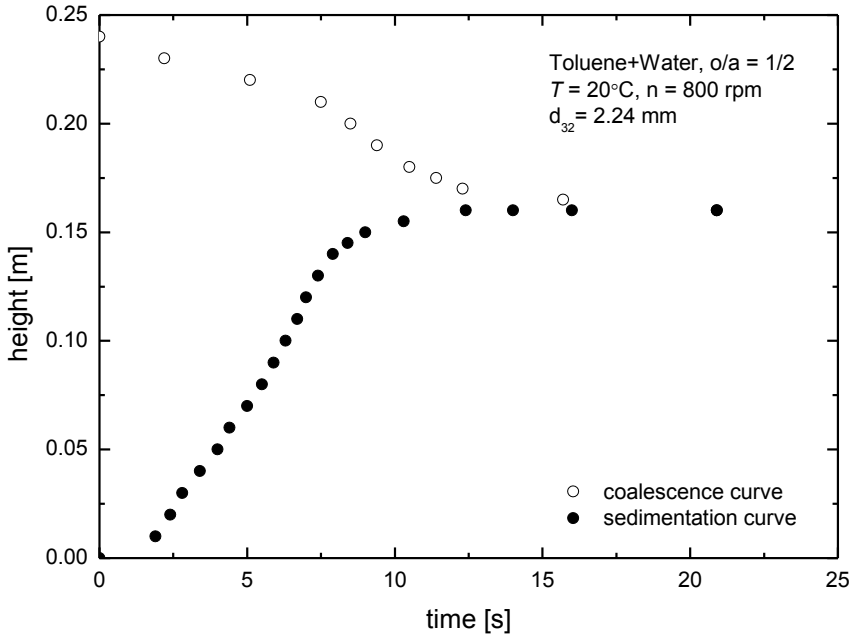

Fig. 8-17: System toluene + water o/a = 1/2

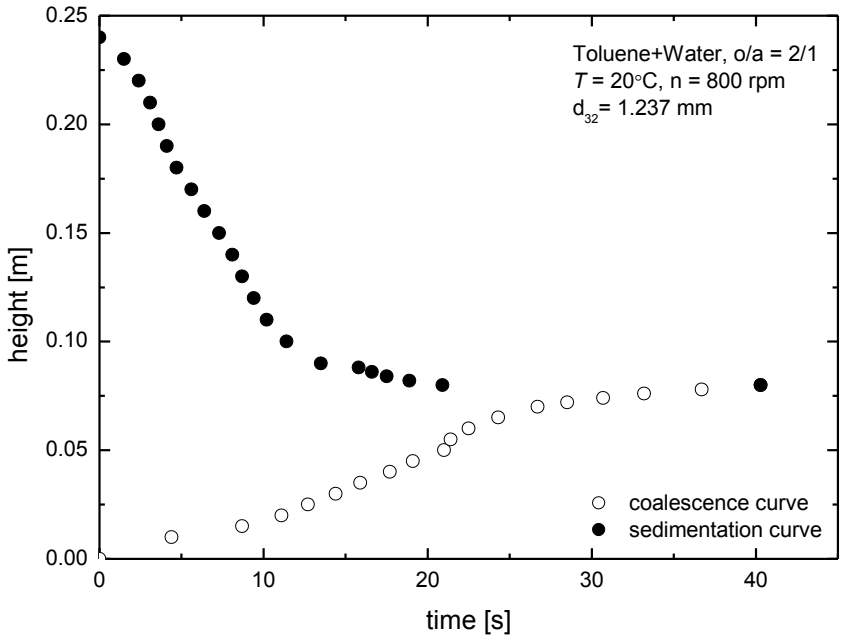

Fig. 8-18: System toluene + water o/a = 2/1

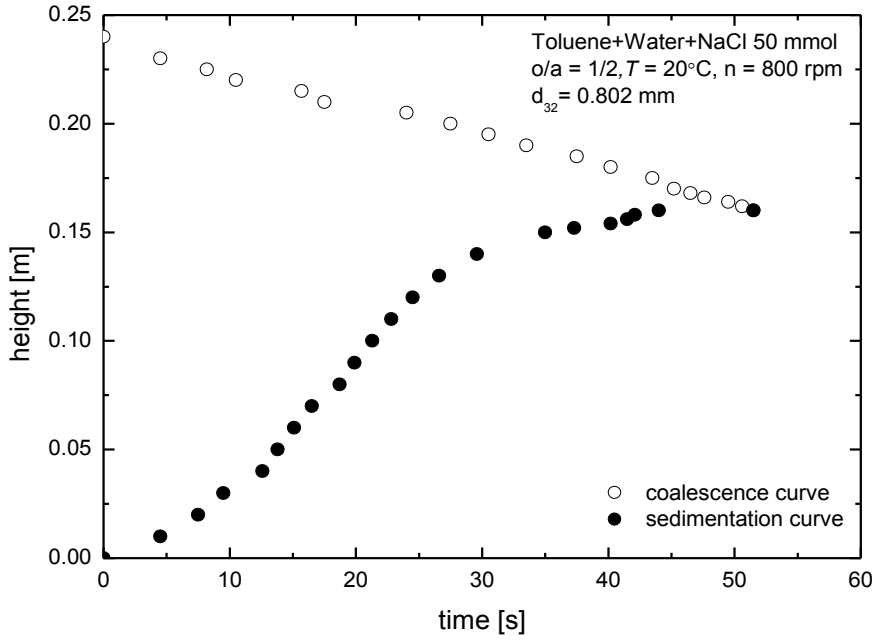

Fig. 8-19: System toluene + water + NaCl 50 mmol/L o/a = 1/2

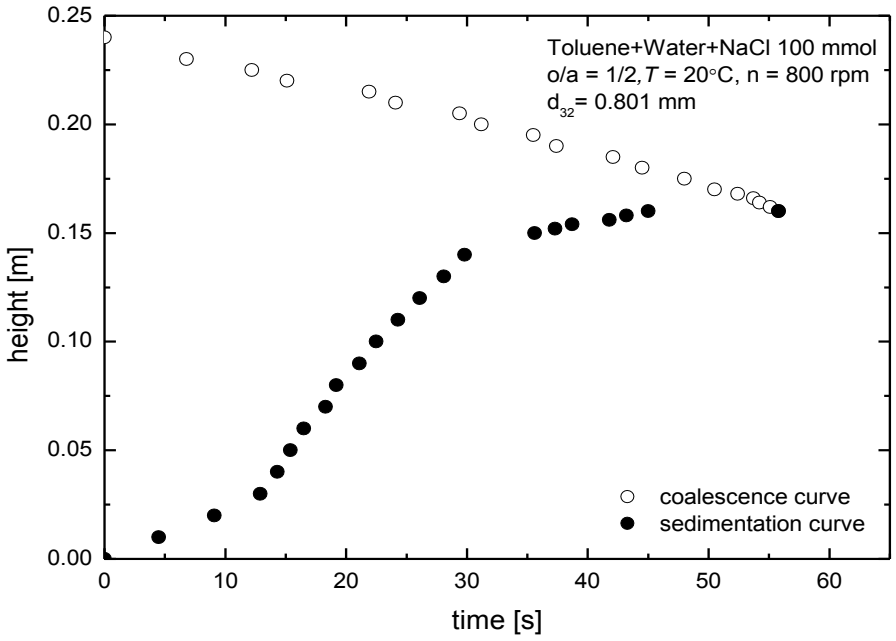

Fig. 8-20: System toluene + water + NaCl 100 mmol/L o/a = 1/2

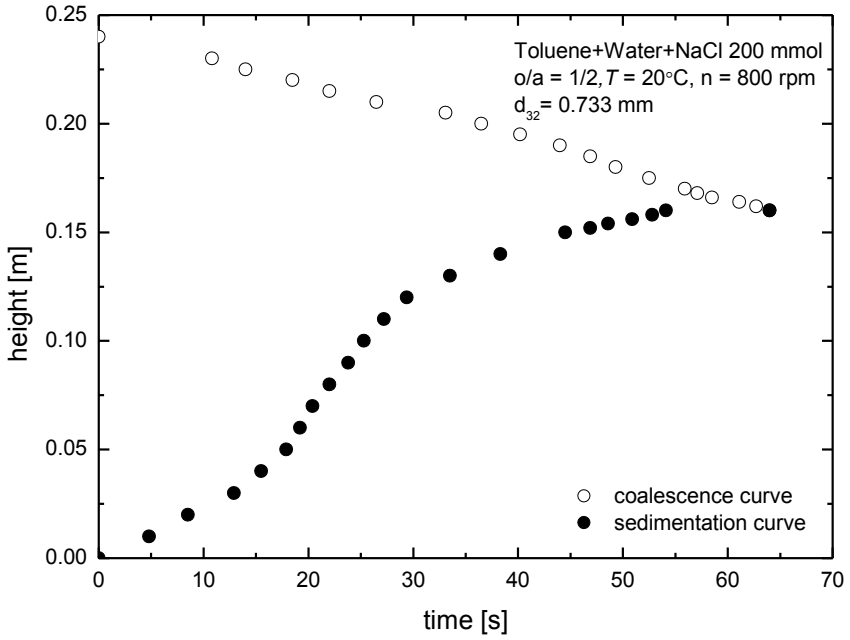

Fig. 8-21: System toluene + water + NaCl 200 mmol/L o/a = 1/2

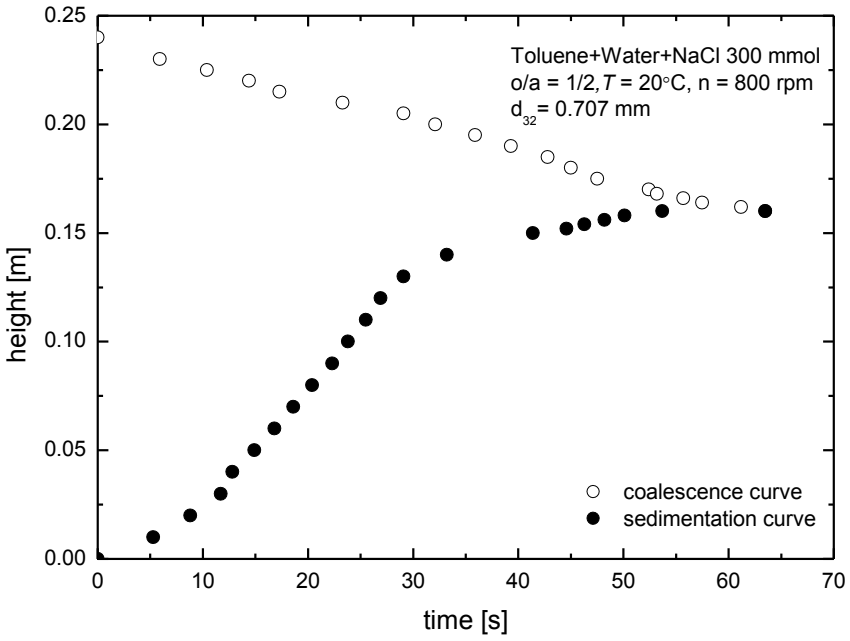

Fig. 8-22: System toluene + water + NaCl 300 mmol/L o/a = 1/2

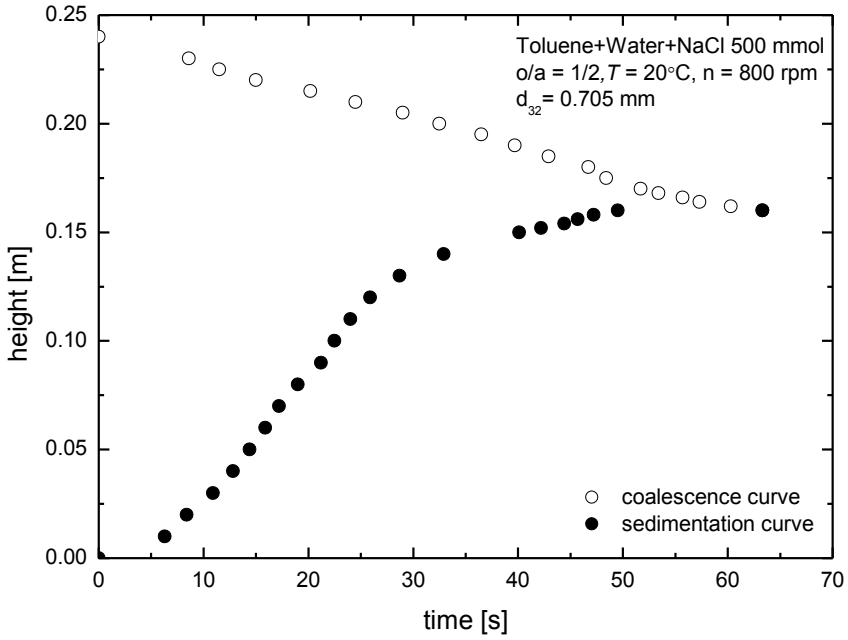

Fig. 8-23: System toluene + water + NaCl 500 mmol/L o/a = 1/2

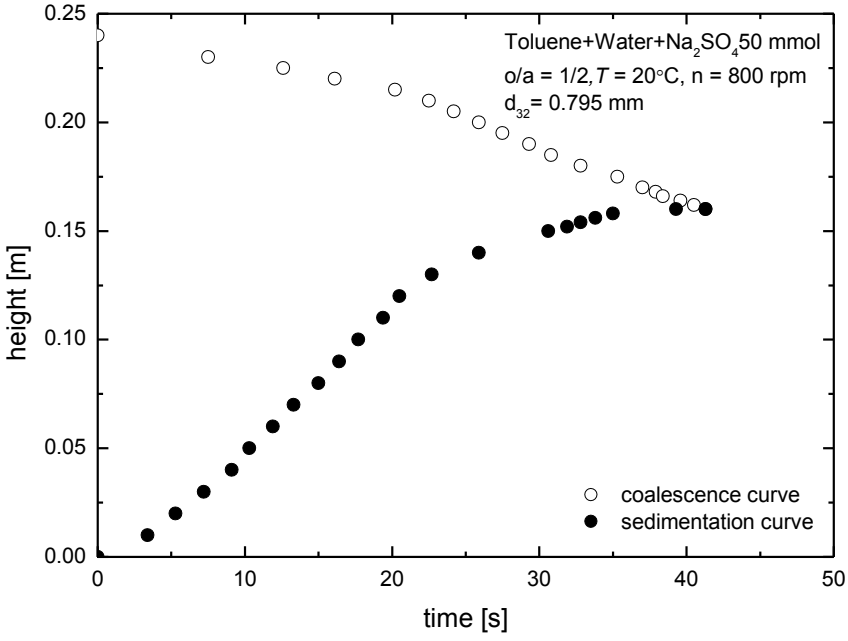

Fig. 8-24: System toluene + water + Na_2SO_4 50 mmol/L o/a = 1/2

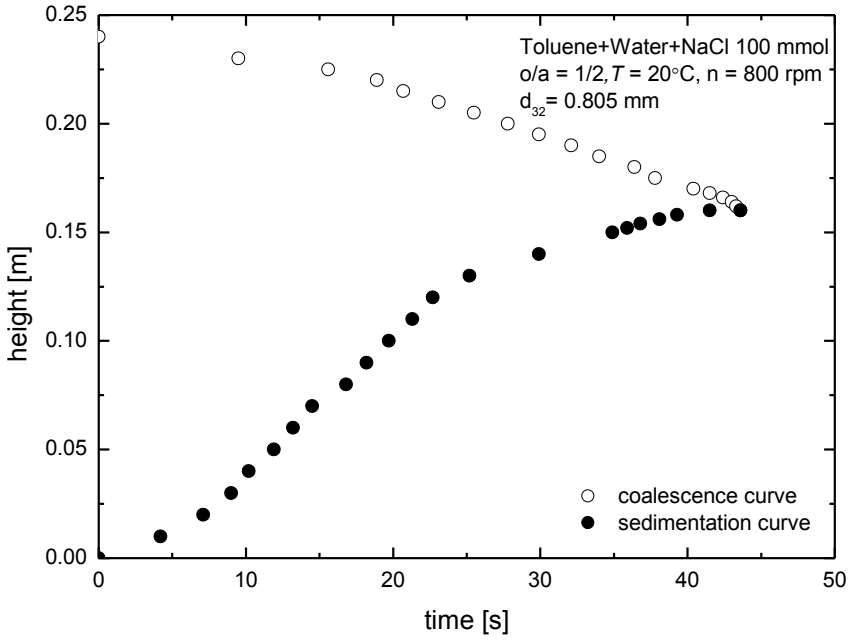

Fig. 8-25: System toluene + water + Na_2SO_4 100 mmol/L o/a = 1/2

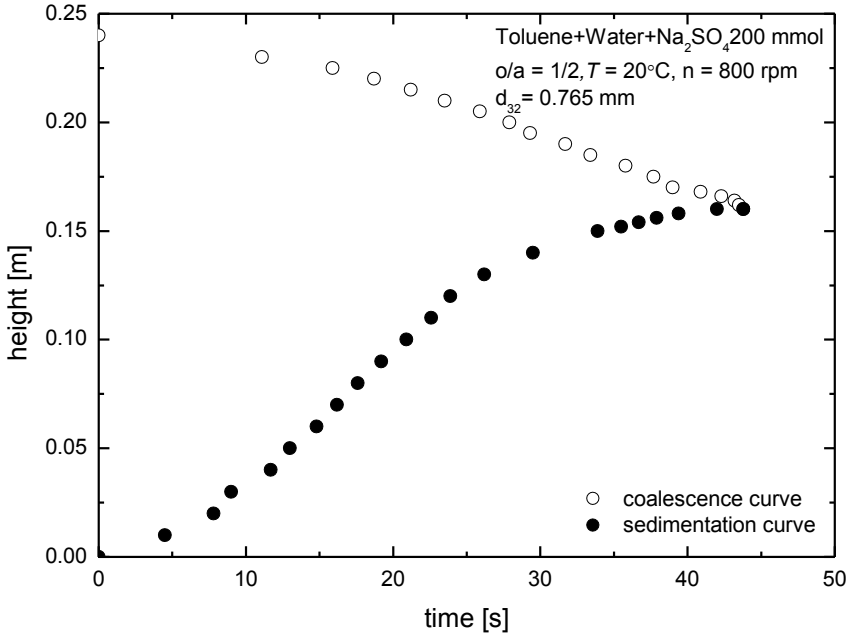

Fig. 8-26: System toluene + water + Na_2SO_4 200 mmol/L o/a = 1/2

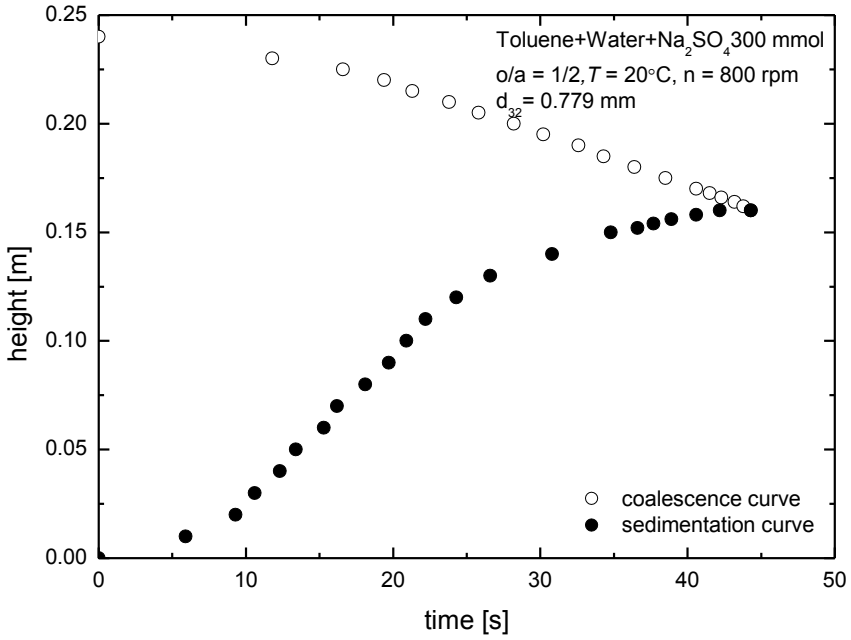

Fig. 8-27: System toluene + water + Na_2SO_4 300 mmol/L o/a = 1/2

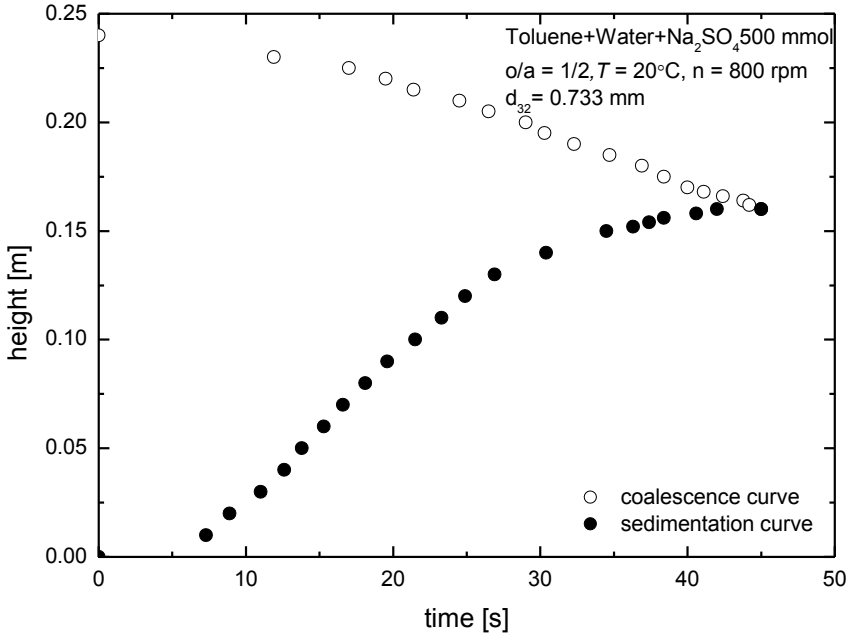

Fig. 8-28: System toluene + water + Na_2SO_4 500 mmol/L o/a = 1/2

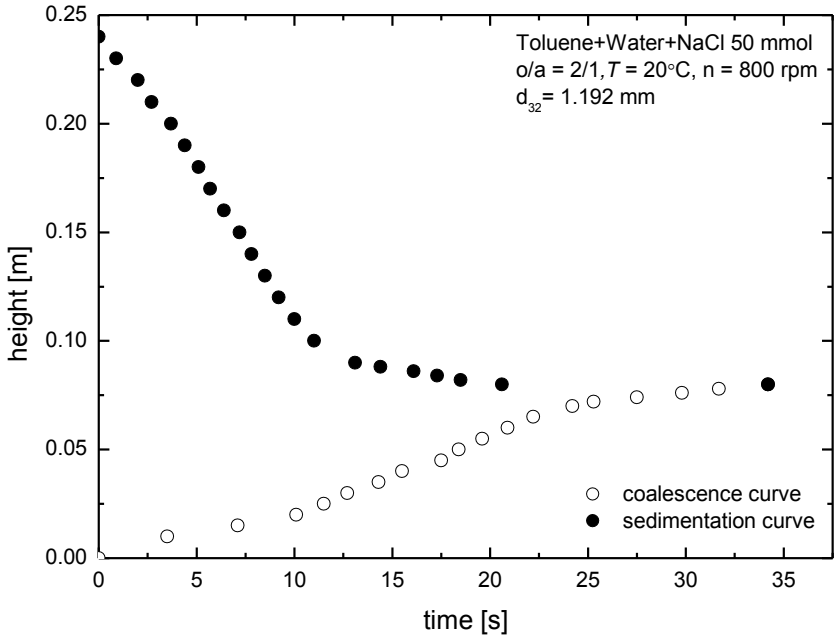

Fig. 8-29: System toluene + water + NaCl 50 mmol/L o/a = 2/1

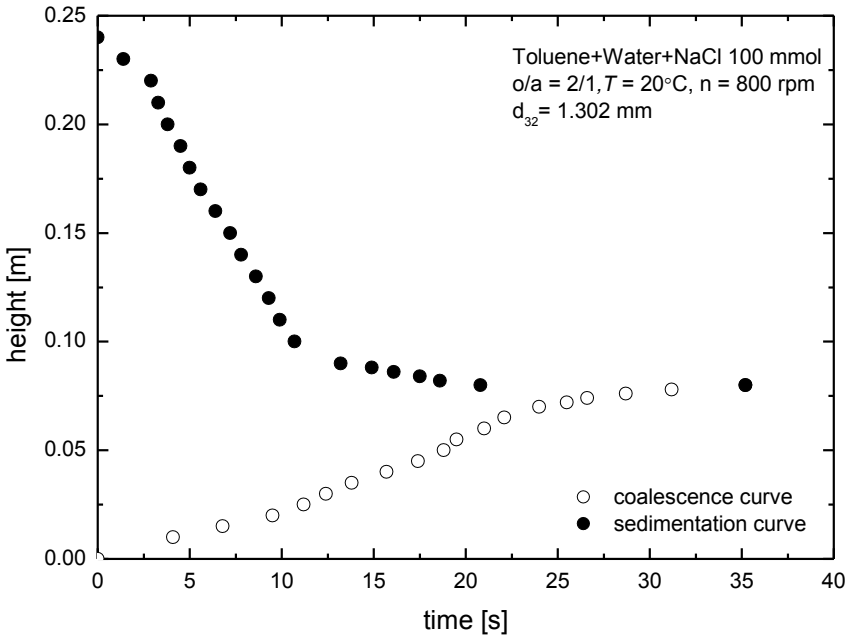

Fig. 8-30: System toluene + water + NaCl 100 mmol/L o/a = 2/1

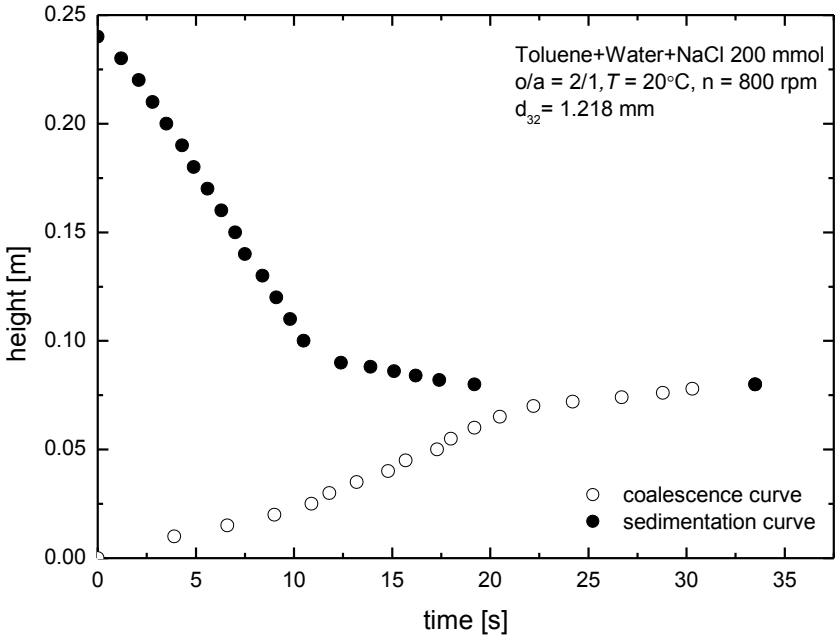

Fig. 8-31: System toluene + water + NaCl 200 mmol/L o/a = 2/1

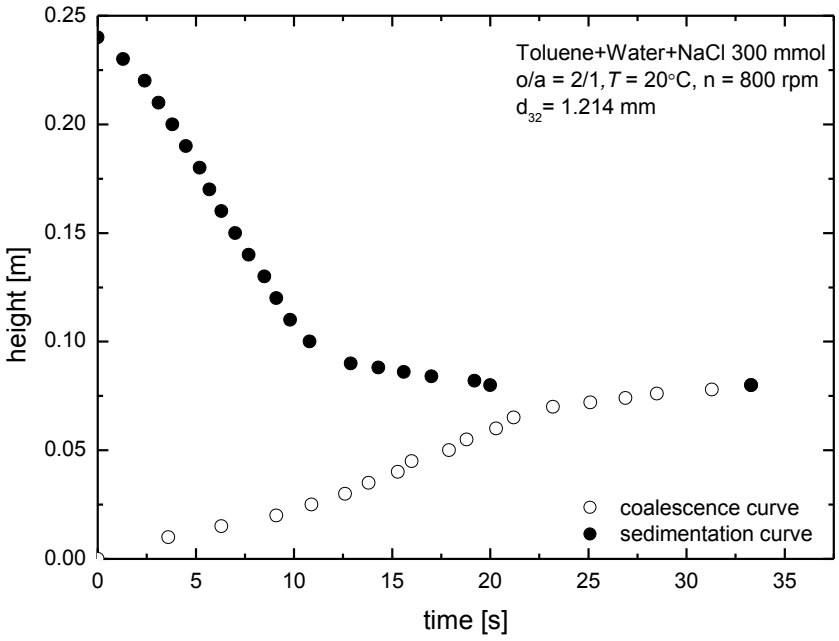

Fig. 8-32: System toluene + water + NaCl 300 mmol/L o/a = 2/1

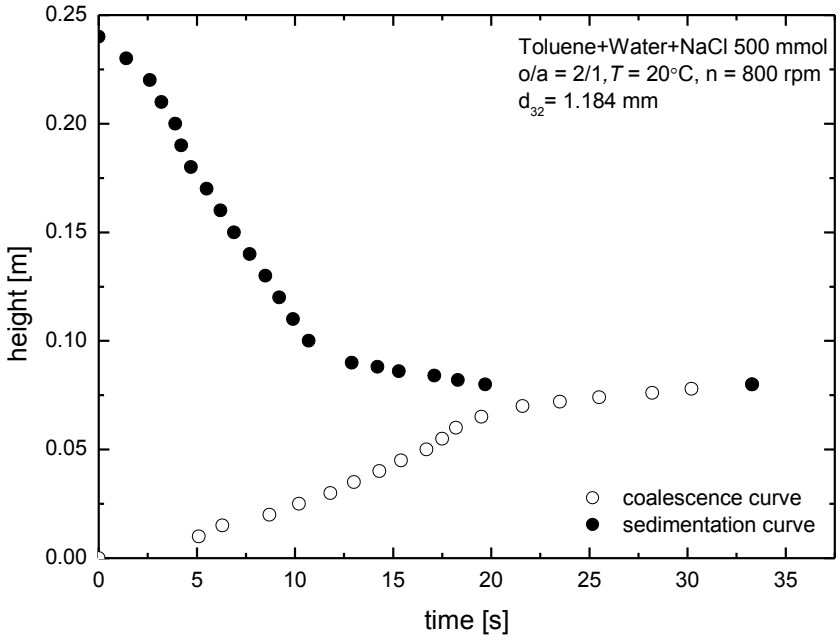

Fig. 8-33: System toluene + water + NaCl 500 mmol/L o/a = 2/1

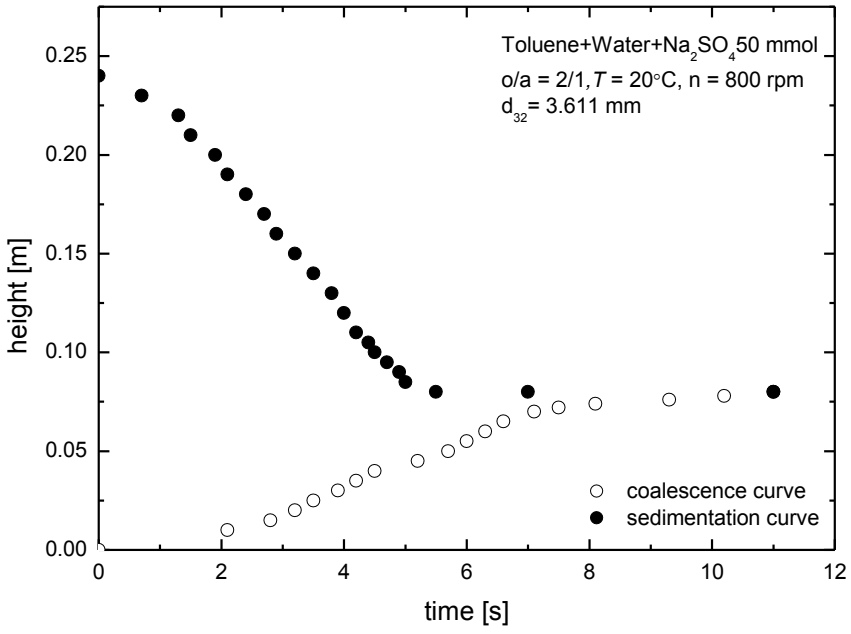

Fig. 8-34: System toluene + water + Na_2SO_4 50 mmol/L o/a = 2/1

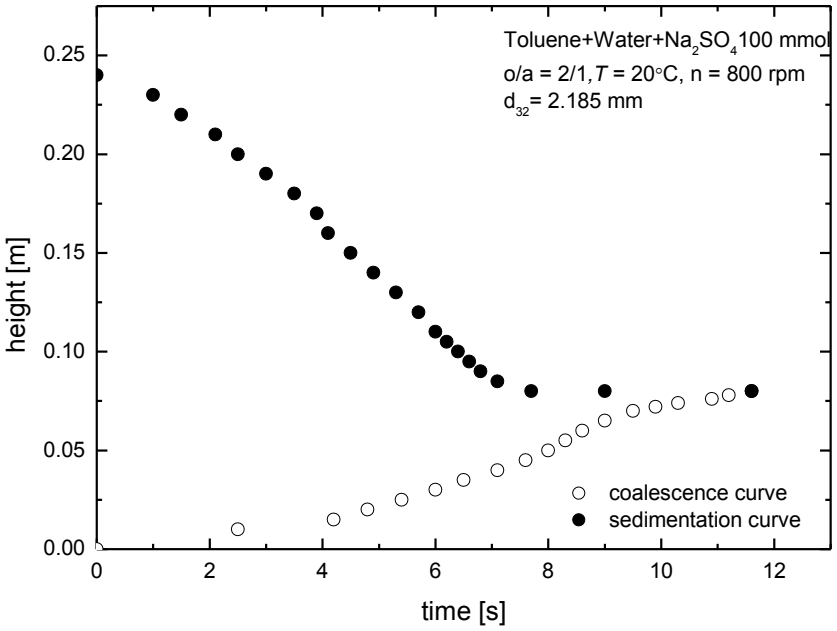

Fig. 8-35: System toluene + water + Na_2SO_4 100 mmol/L o/a = 2/1

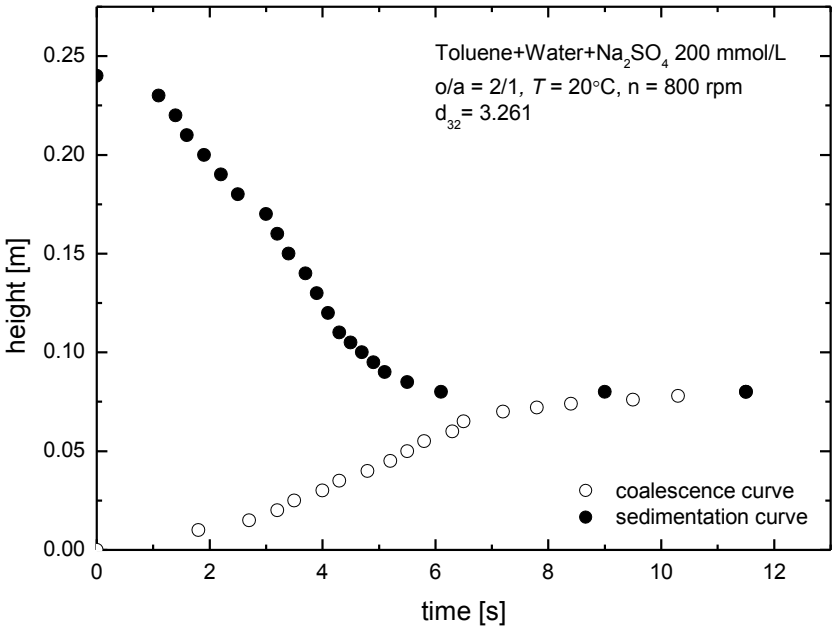

Fig. 8-36: System toluene + water + Na_2SO_4 200 mmol/L o/a = 2/1

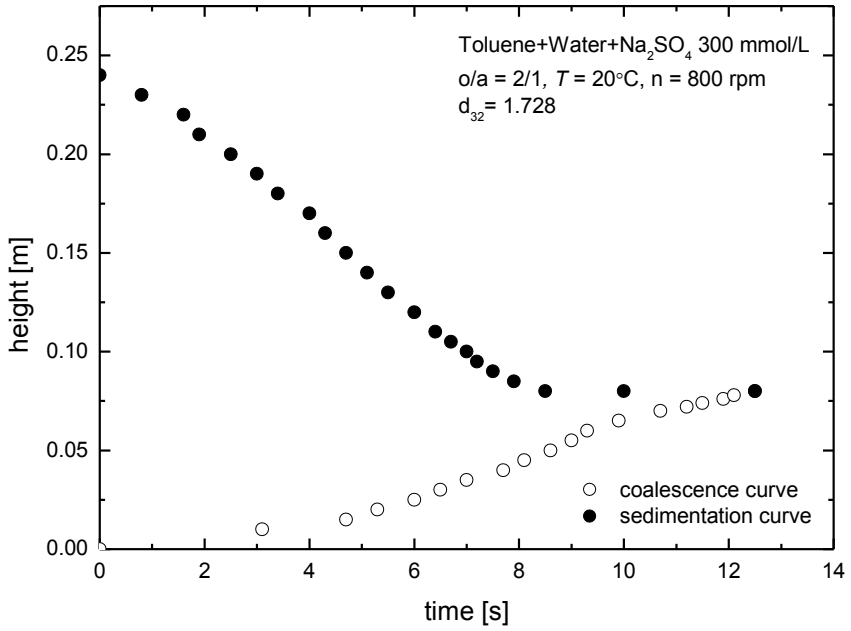

Fig. 8-37: System toluene + water + Na_2SO_4 300 mmol/L o/a = 2/1

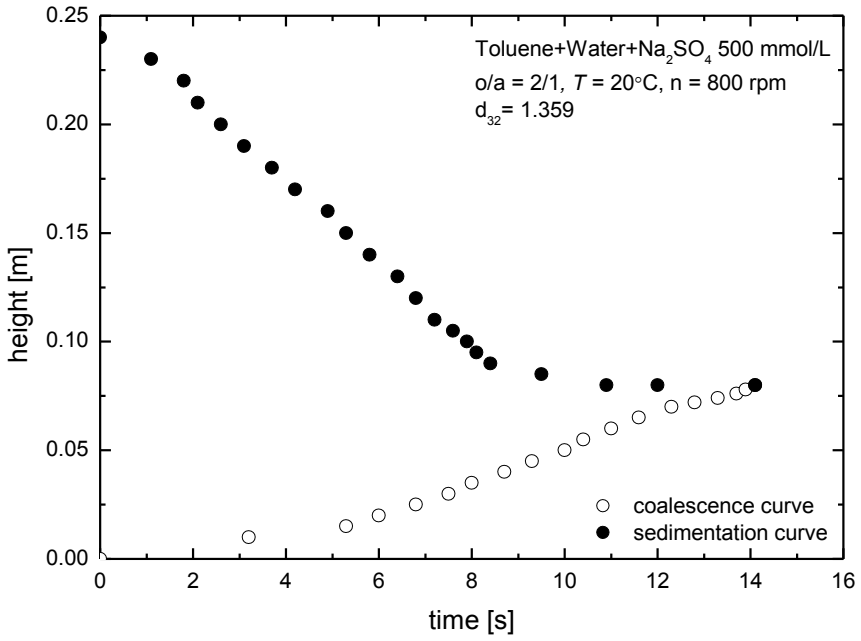

Fig. 8-38: System toluene + water + Na_2SO_4 500 mmol/L o/a = 2/1

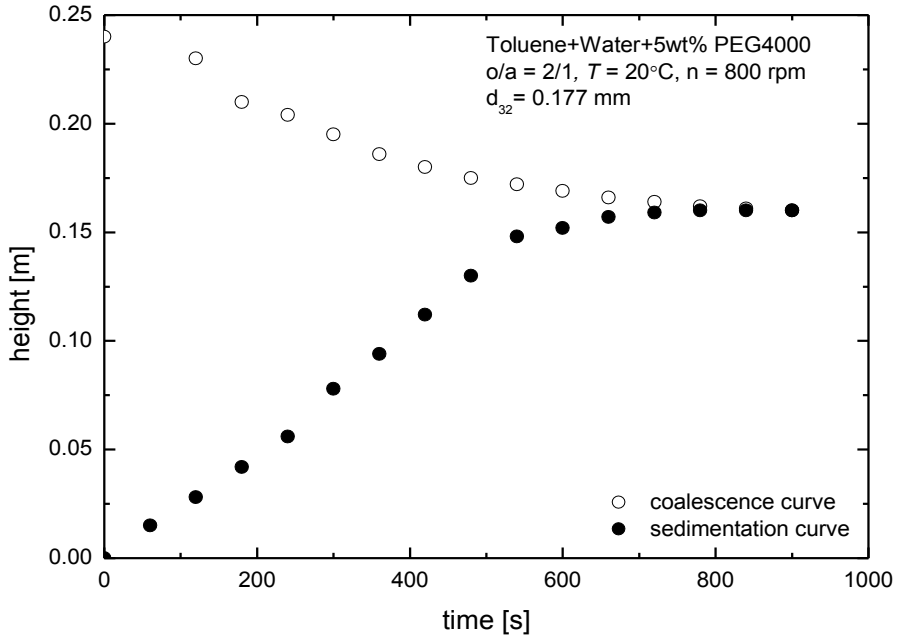

Fig. 8-39: System toluene + water + 5 wt% PEG4000 o/a = 1/2

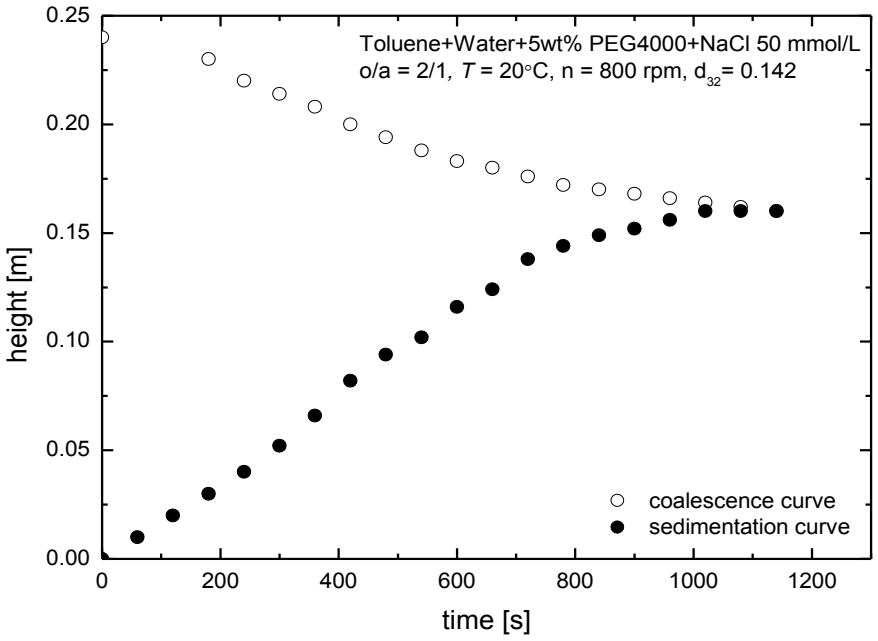

Fig. 8-40: System toluene + water + 5 wt% PEG4000+ NaCl 50 mmol/L o/a = 1/2

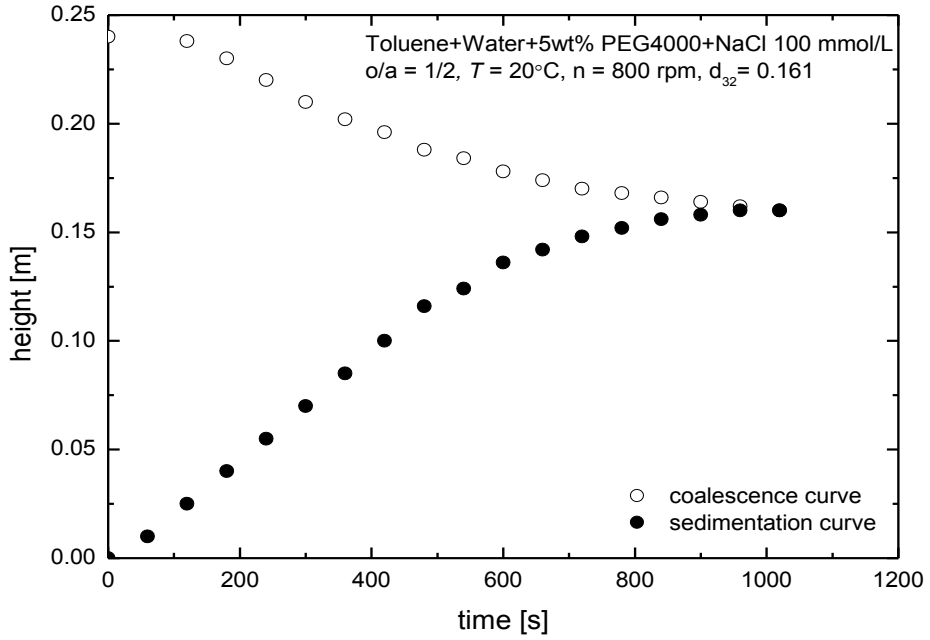

Fig. 8-41: System toluene + water + 5 wt% PEG4000+ NaCl 100 mmol/L o/a = 1/2

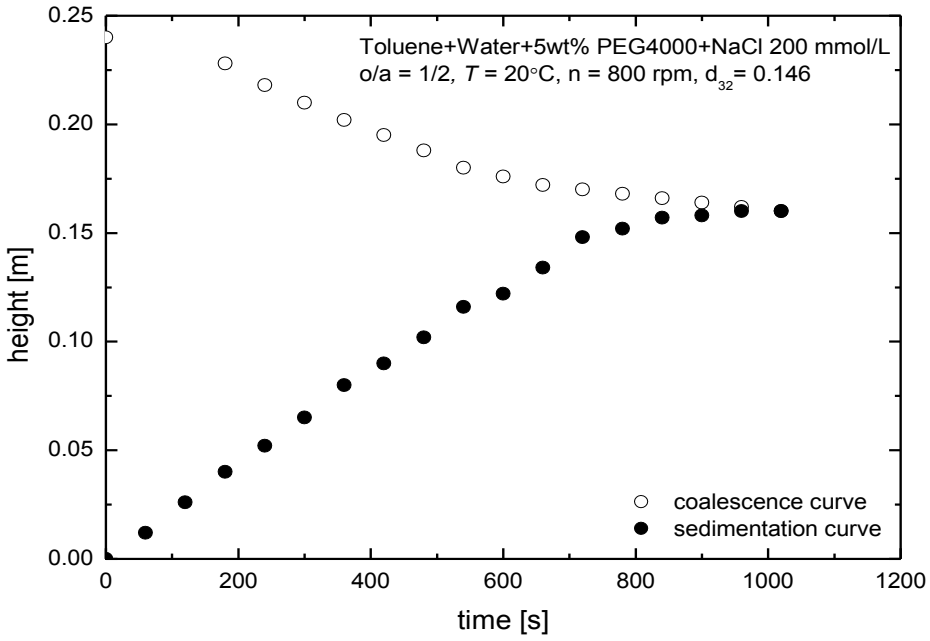

Fig. 8-42: System toluene + water + 5 wt% PEG4000+ NaCl 200 mmol/L o/a = 1/2

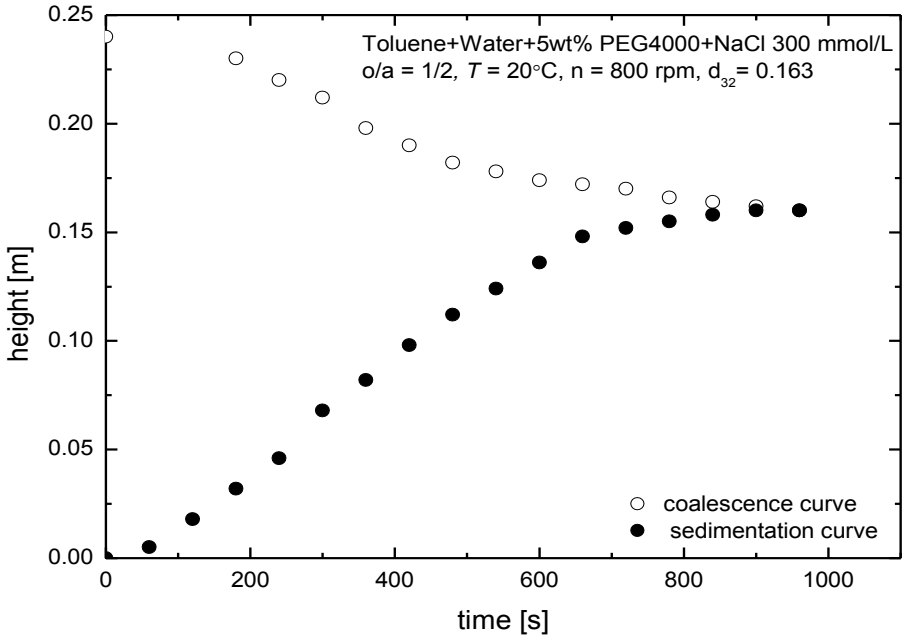

Fig. 8-43: System toluene + water + 5 wt% PEG4000+ NaCl 300 mmol/L o/a = 1/2

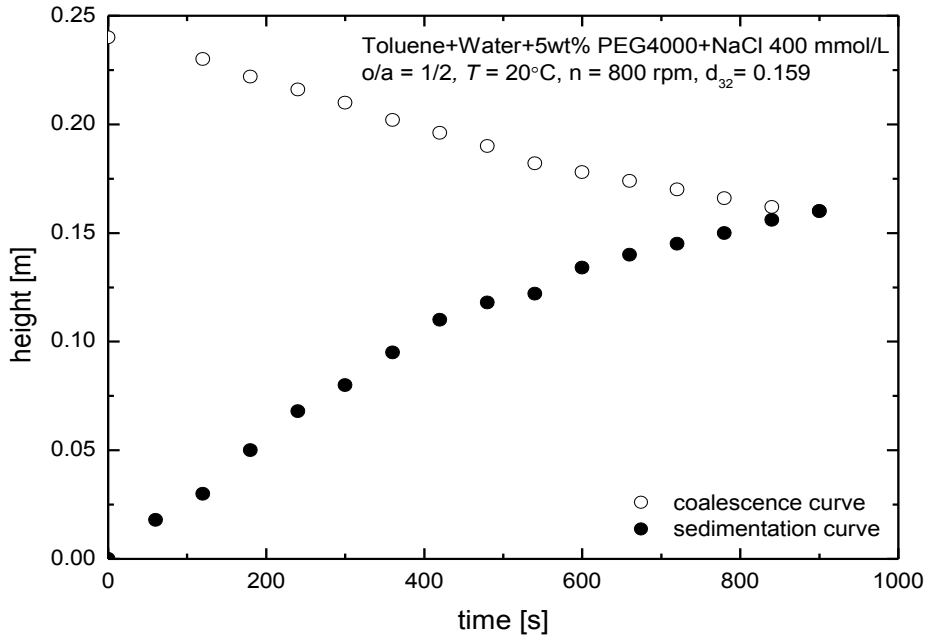

Fig. 8-44: System toluene + water + 5 wt% PEG4000+ NaCl 400 mmol/L o/a = 1/2

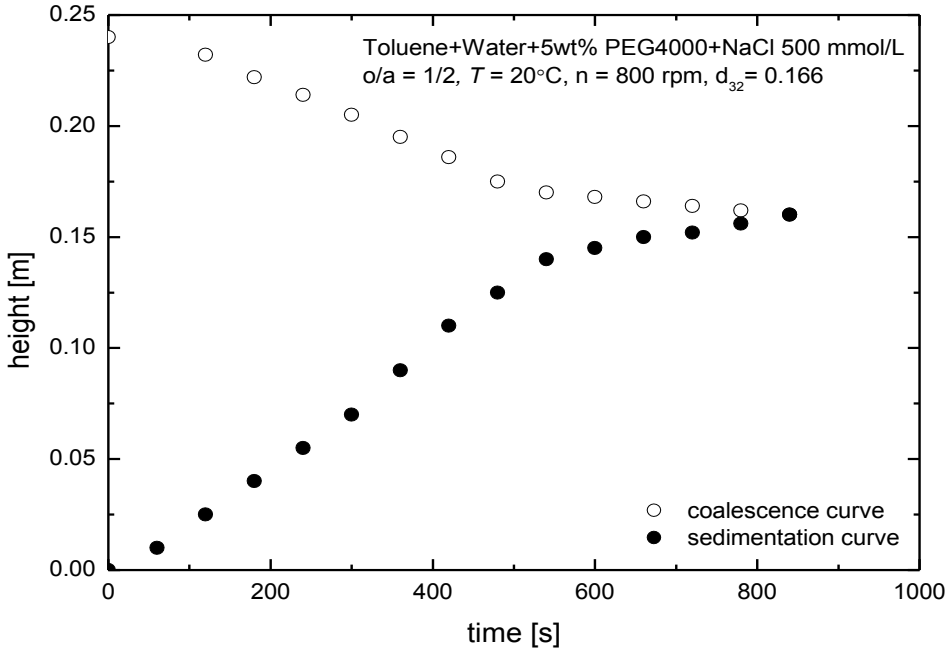

Fig. 8-45: System toluene + water + 5 wt% PEG4000+ NaCl 500 mmol/L o/a = 1/2

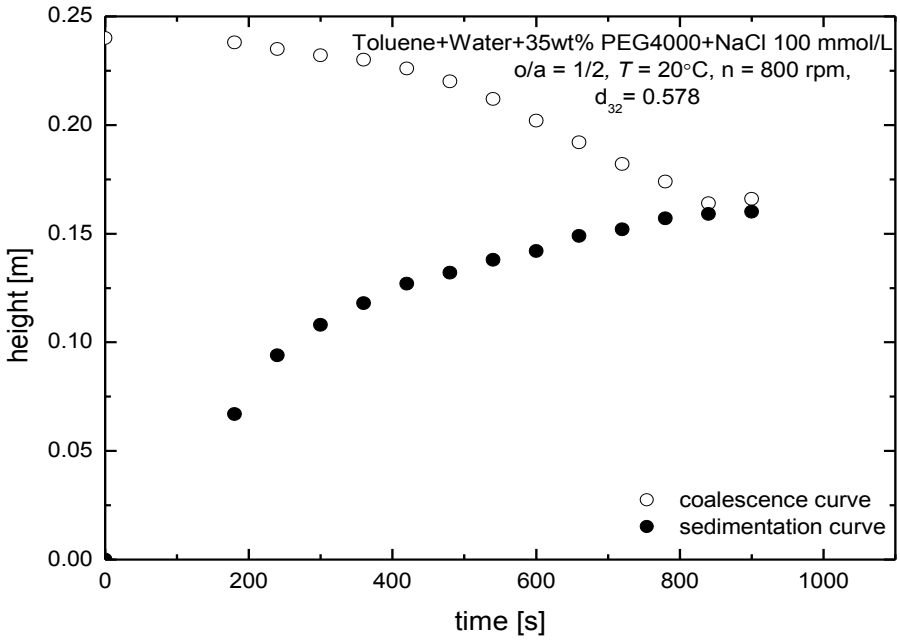

Fig. 8-46: System toluene + water + 35 wt% PEG4000+ NaCl 100 mmol/L o/a = 1/2

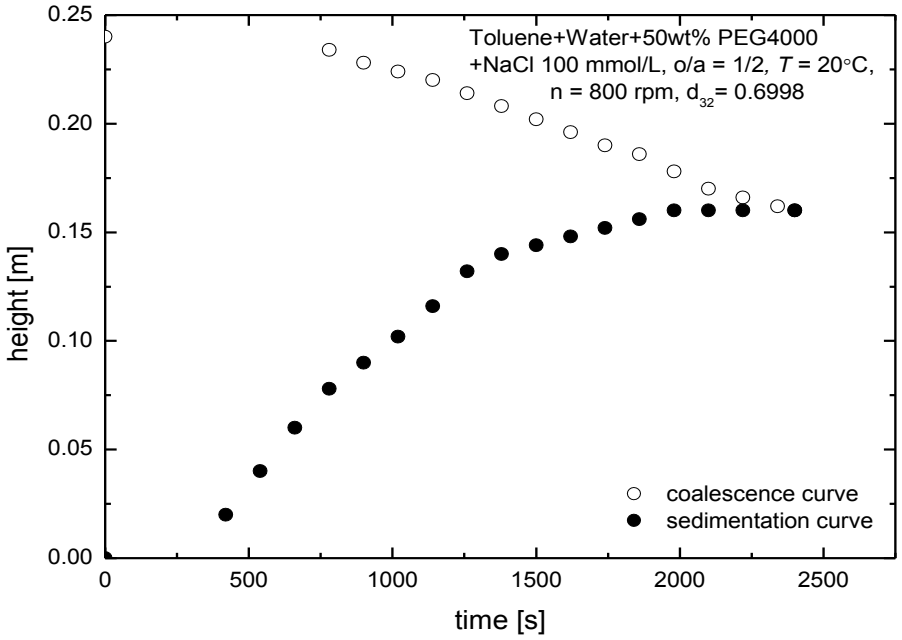

Fig. 8-47: System toluene + water + 50 wt% PEG4000+ NaCl 100 mmol/L o/a = 1/2

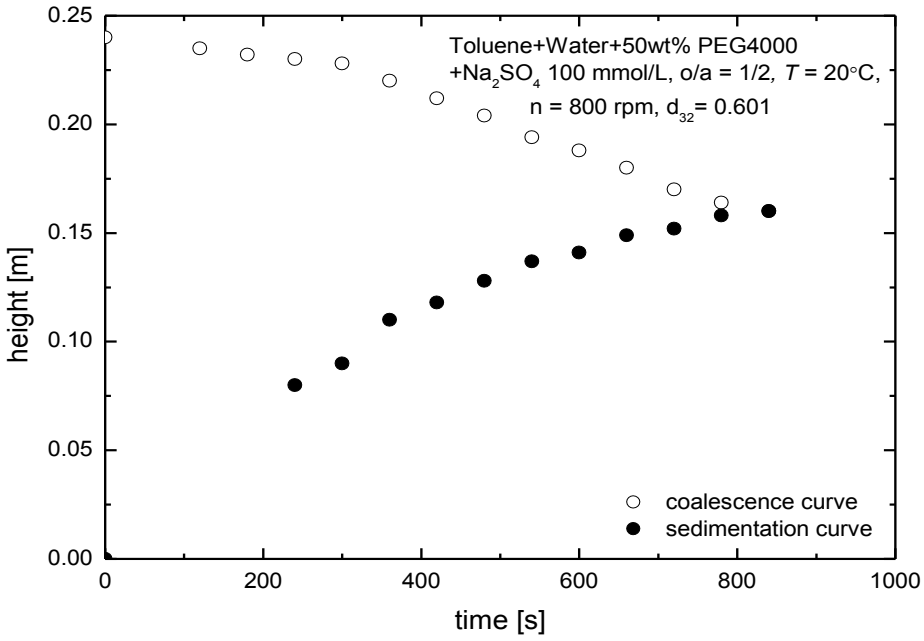

Fig. 8-48: System toluene + water + 35 wt% PEG4000+ Na_2SO_4 100 mmol/L o/a = 1/2

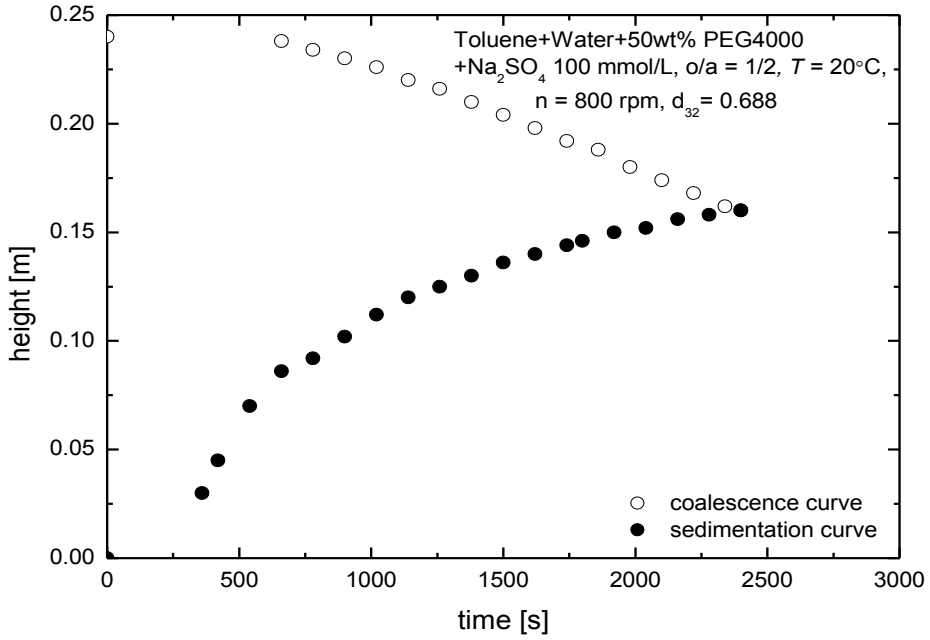

Fig. 8-49: System toluene + water + 50 wt% PEG4000+ Na_2SO_4 100 mmol/L o/a = 1/2

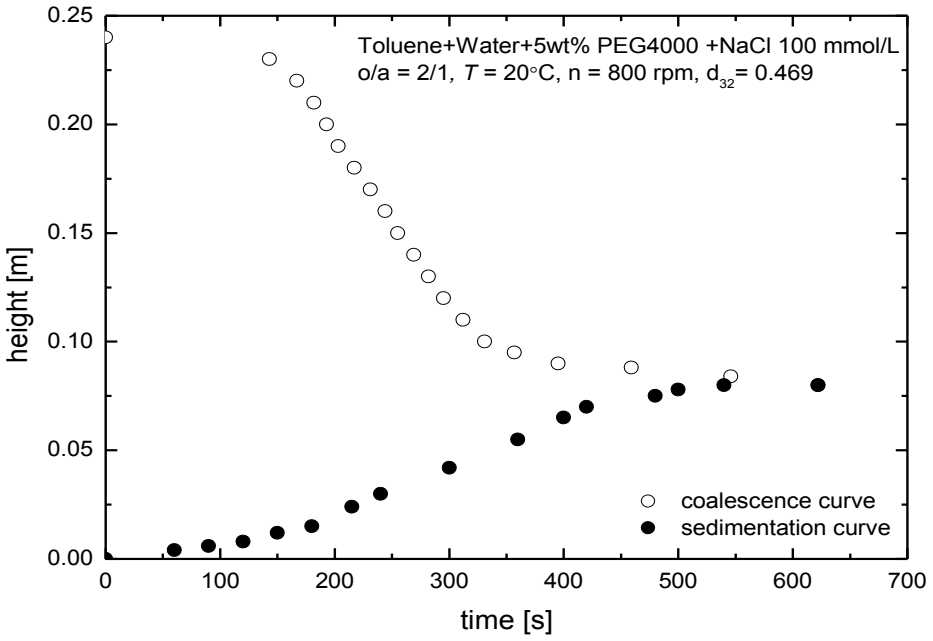

Fig. 8-50: System toluene + water + 5 wt% PEG4000+ NaCl 100 mmol/L o/a = 2/1

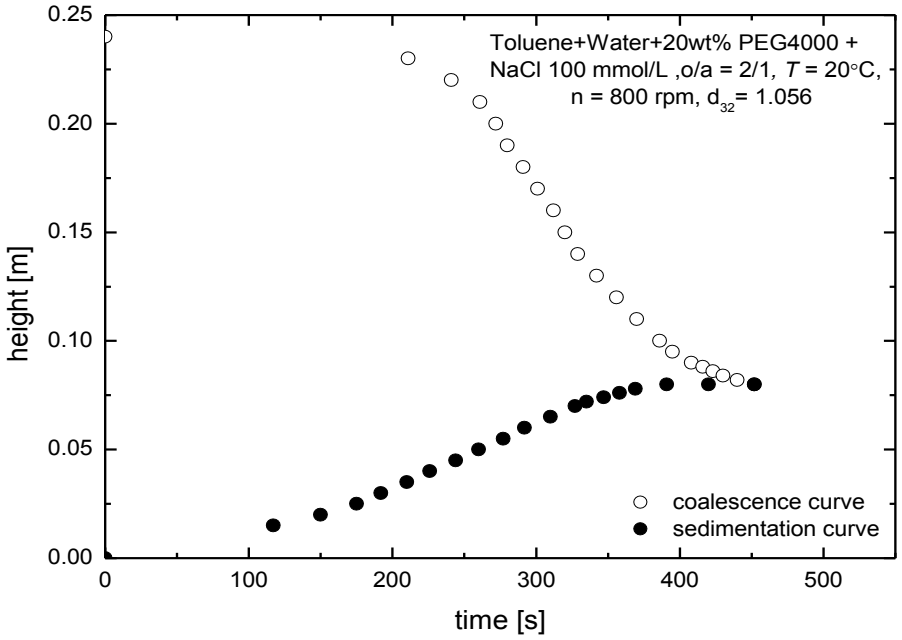

Fig. 8-51: System toluene + water + 20 wt% PEG4000+ NaCl 100 mmol/L o/a = 2/1

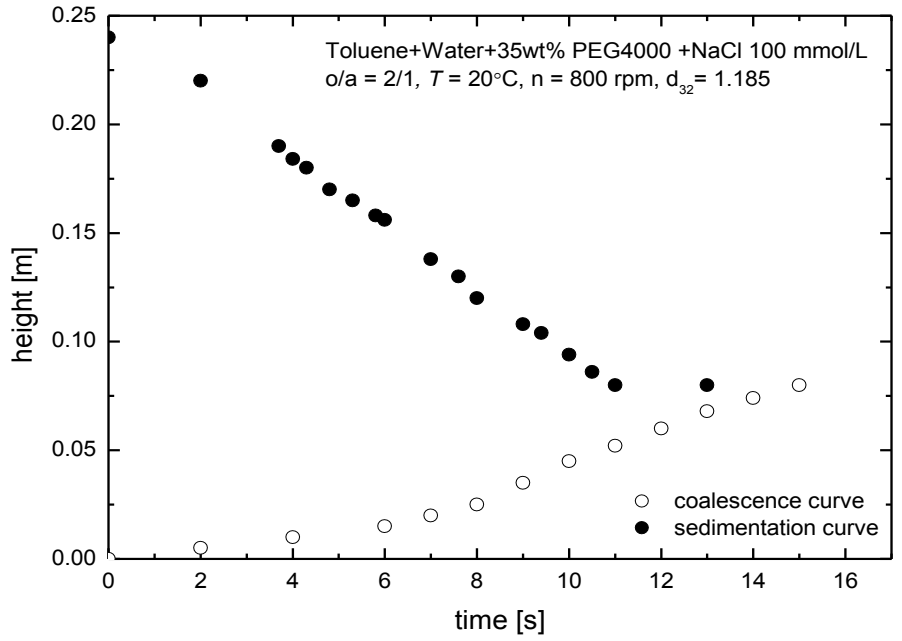

Fig. 8-52: System toluene + water + 35 wt% PEG4000+ NaCl 100 mmol/L o/a = 2/1

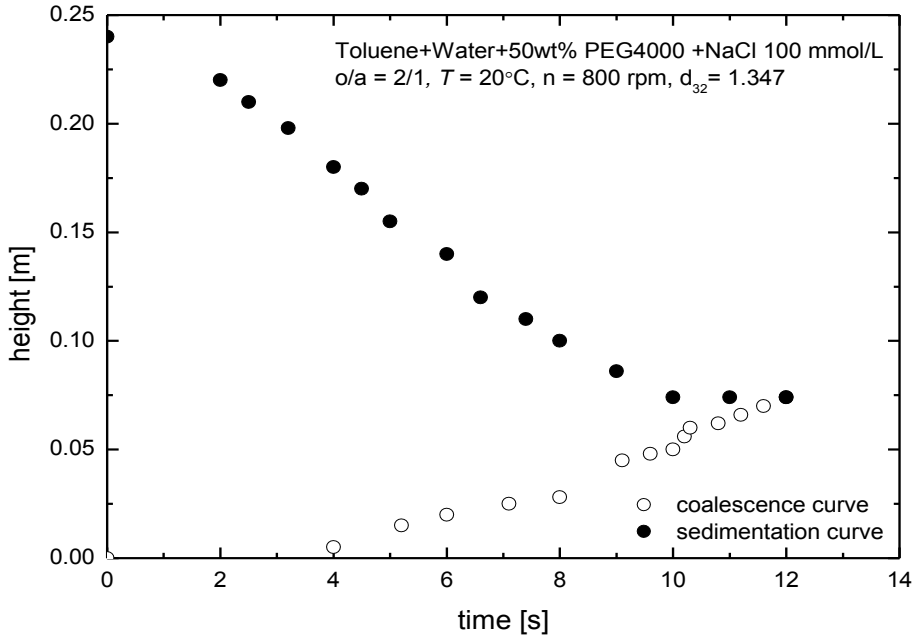

Fig. 8-53: System toluene + water + 50 wt% PEG4000+ NaCl 100 mmol/L o/a = 2/1

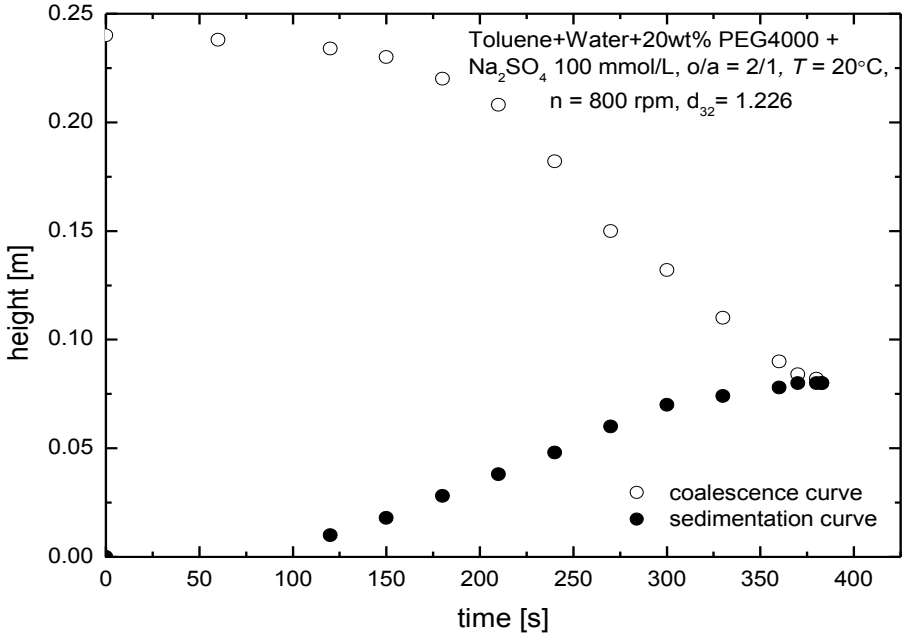

Fig. 8-54: System toluene + water + 20 wt% PEG4000+ Na_2SO_4 100 mmol/L o/a = 2/1

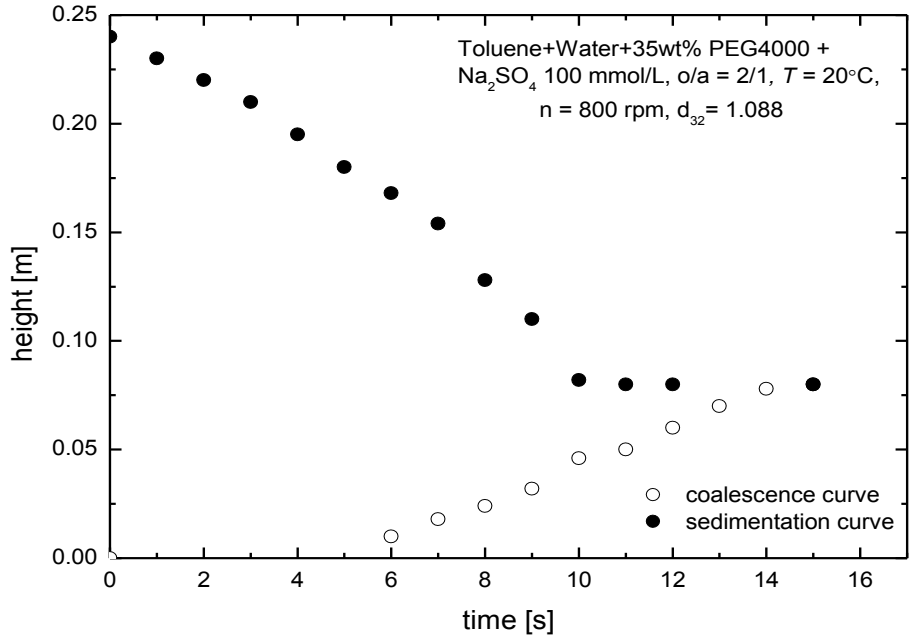

Fig. 8-55: System toluene + water + 35 wt% PEG4000+ Na_2SO_4 100 mmol/L o/a = 2/1

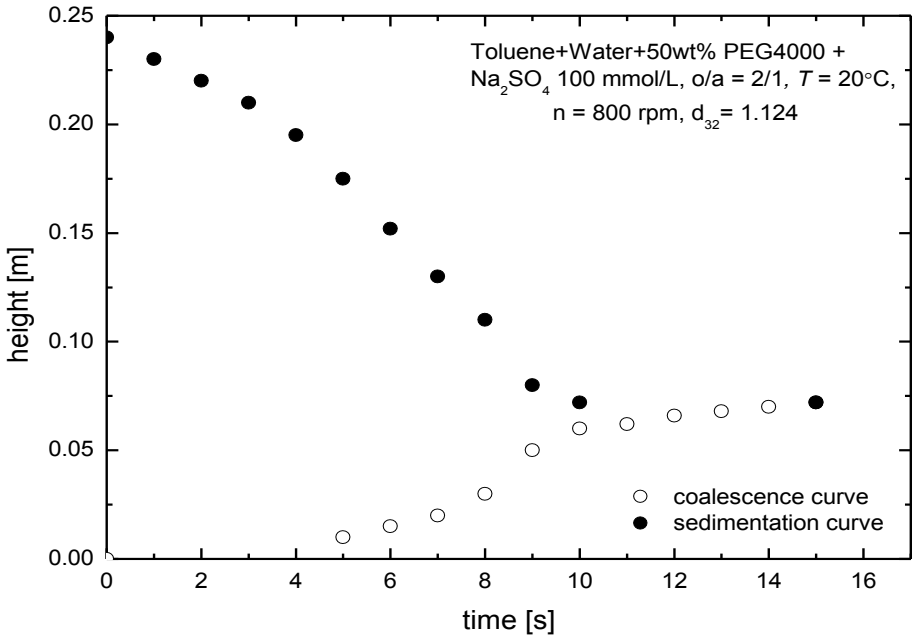

Fig. 8-56: System toluene + water + 50 wt% PEG4000+ Na_2SO_4 100 mmol/L o/a = 2/1

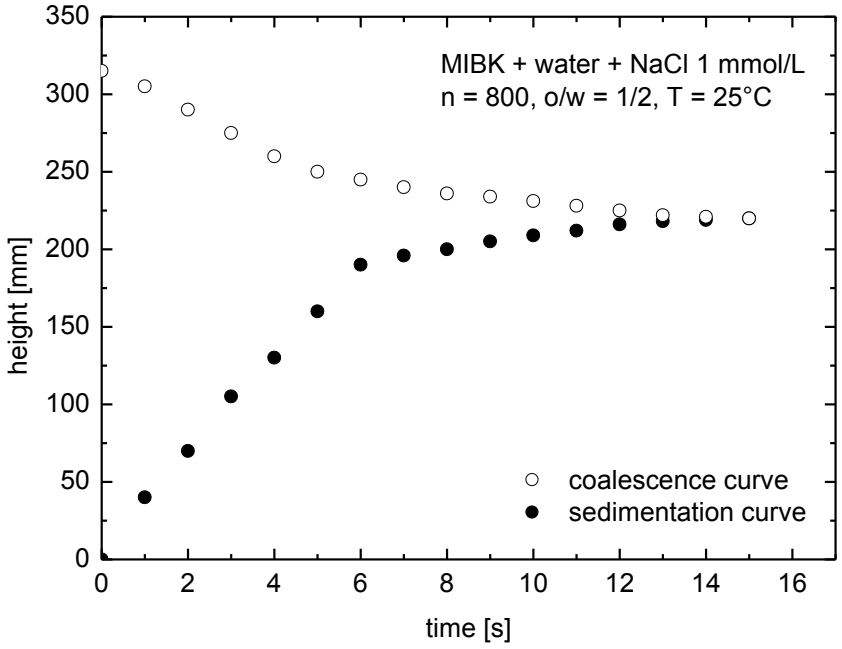

Fig. 8-57: System MIBK + water + NaCl 1 mmol/L o/a = 1/2

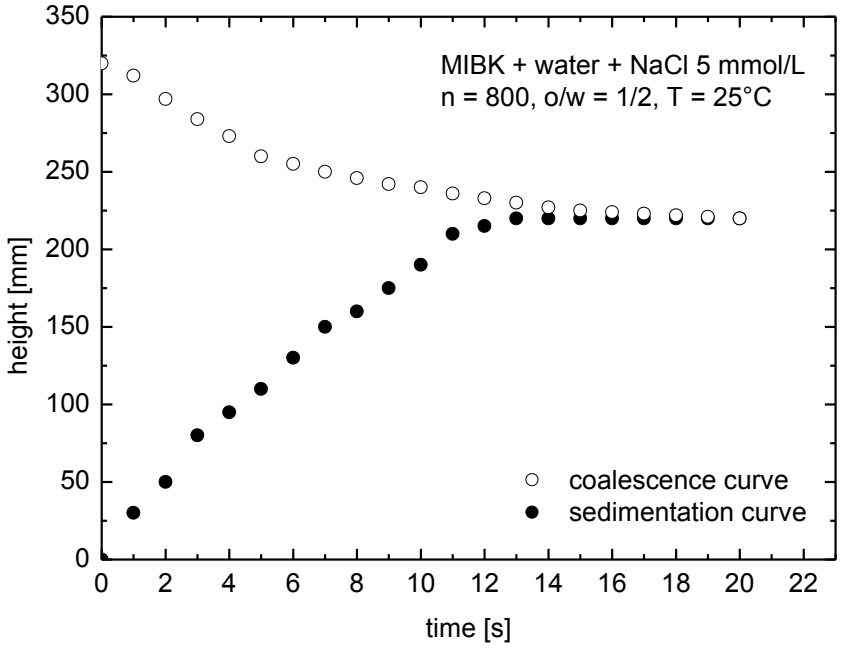

Fig. 8-58: System MIBK + water + NaCl 5 mmol/L o/a = 1/2

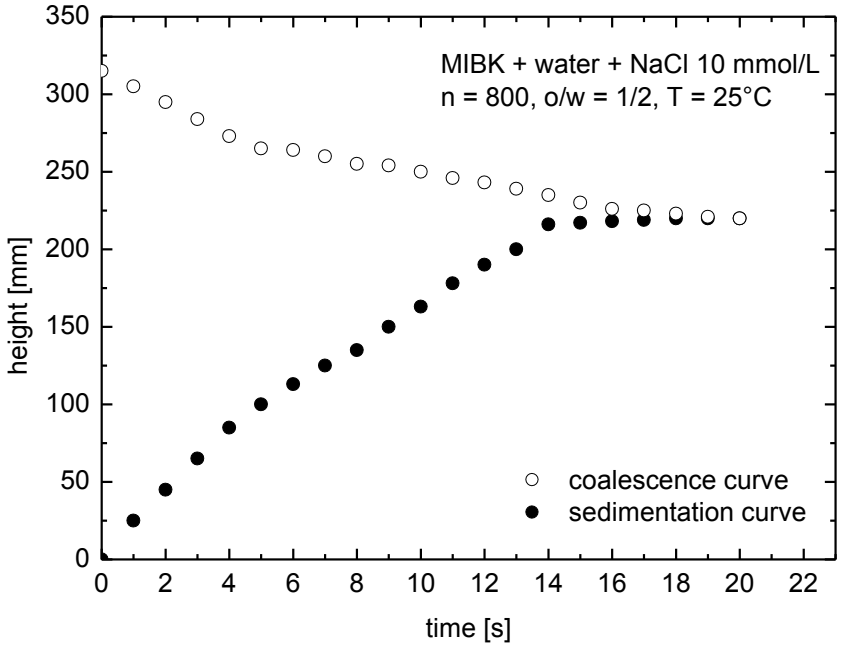

Fig. 8-59: System MIBK + water + NaCl 10 mmol/L o/a = 1/2

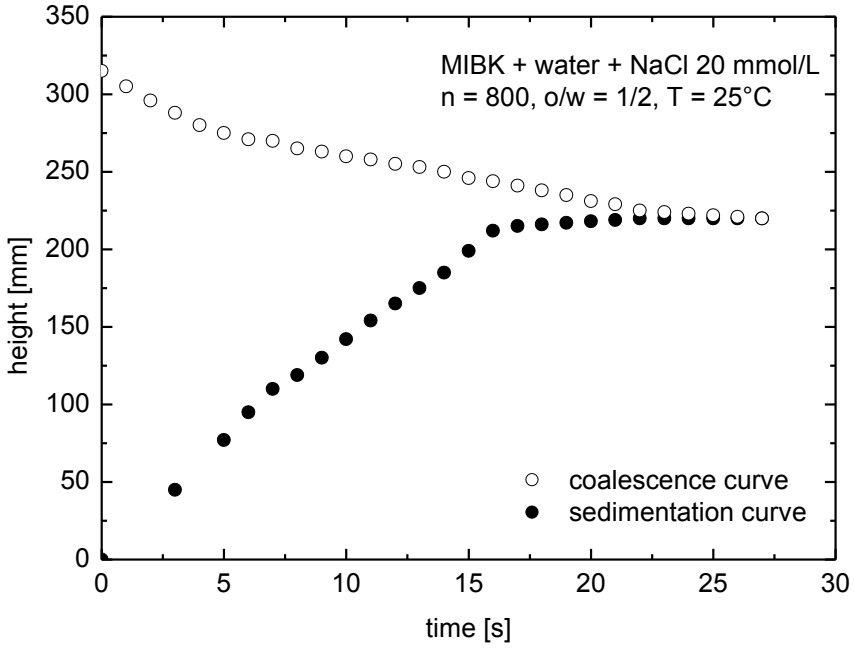

Fig. 8-60: System MIBK + water + NaCl 20 mmol/L o/a = 1/2

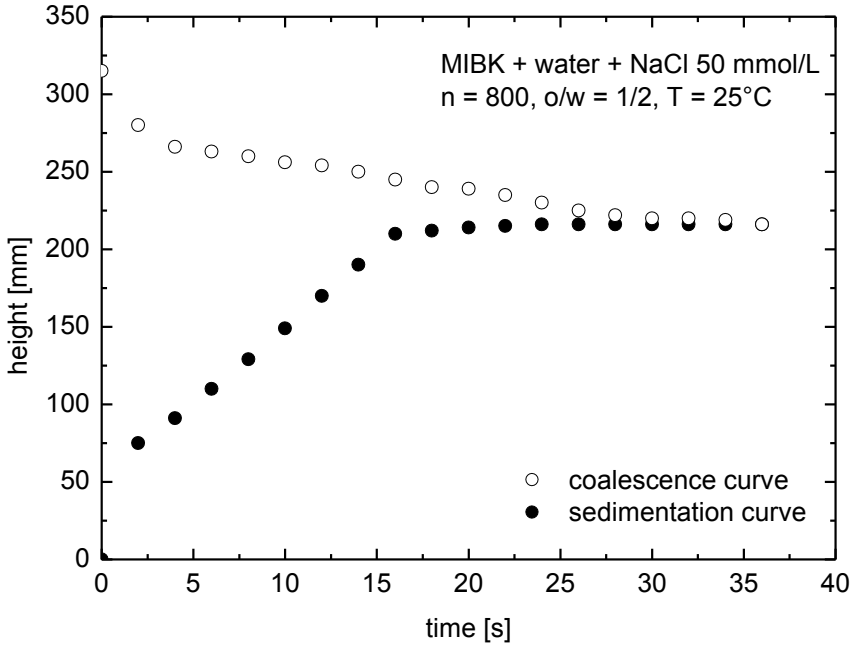

Fig. 8-61: System MIBK + water + NaCl 50 mmol/L o/a = 1/2

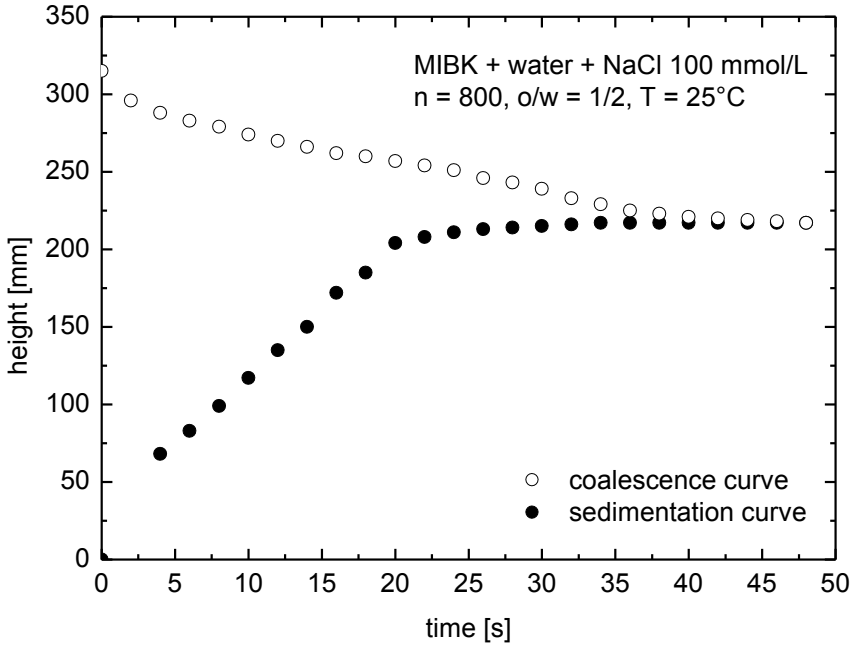

Fig. 8-62: System MIBK + water + NaCl 100 mmol/L o/a = 1/2

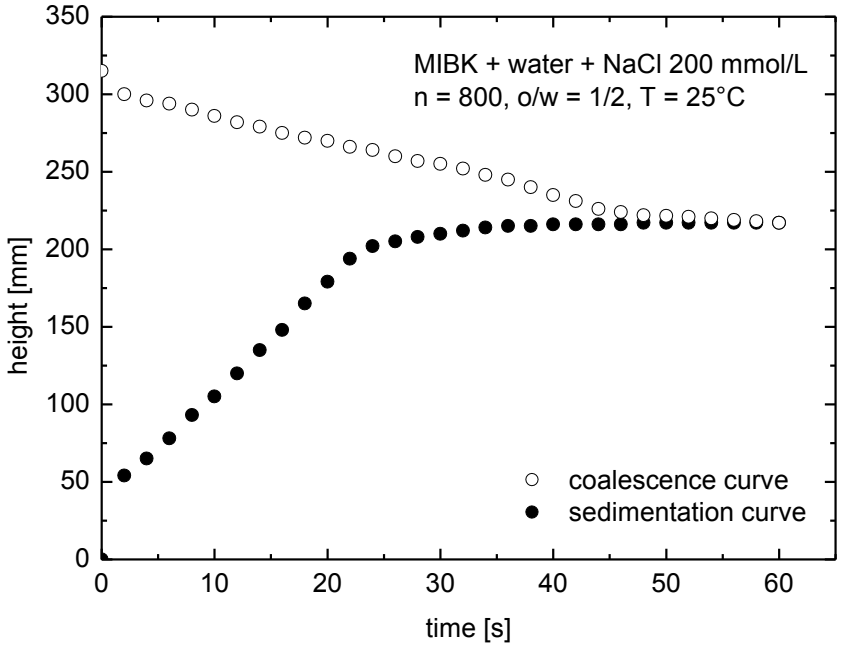

Fig. 8-63: System MIBK + water + NaCl 200 mmol/L o/a = 1/2

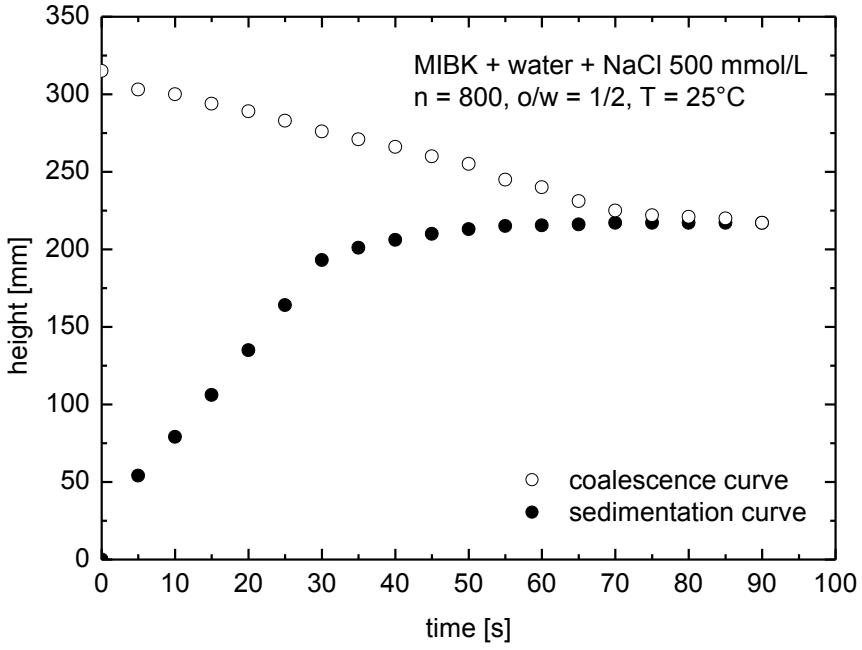

Fig. 8-64: System MIBK + water + NaCl 500 mmol/L o/a = 1/2

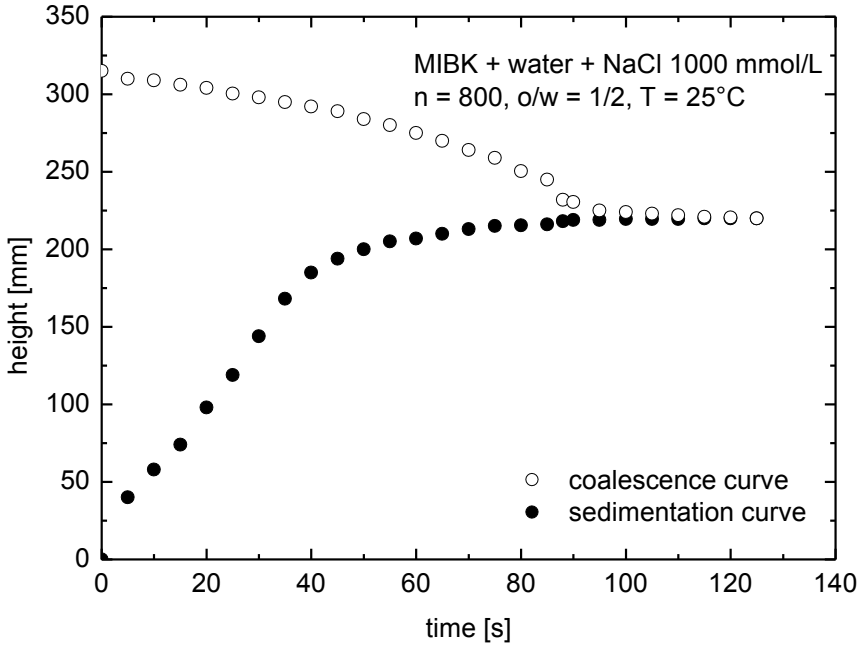

Fig. 8-65: System MIBK + water + NaCl 1000 mmol/L o/a = 1/2

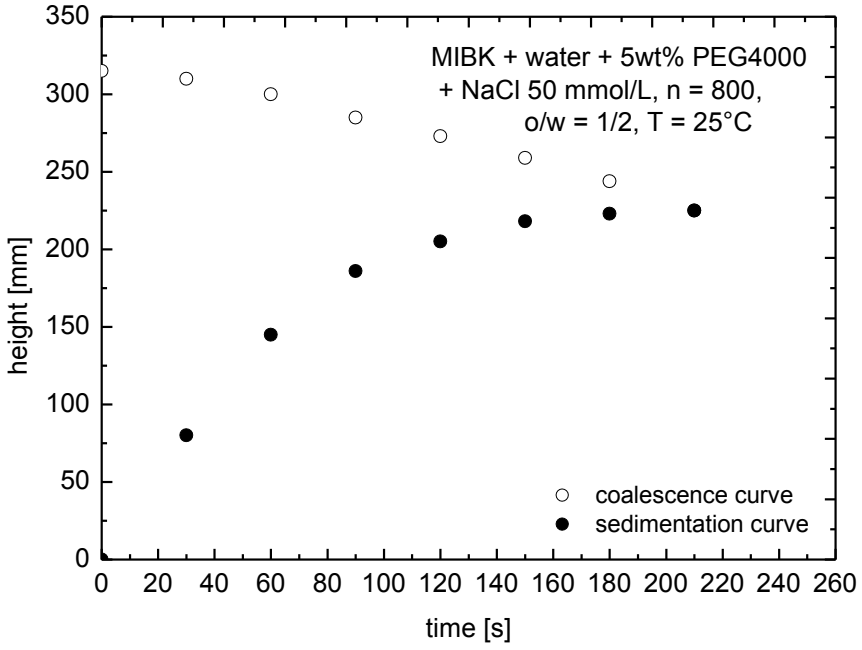

Fig. 8-66: System MIBK + water + 5 wt% PEG4000+ NaCl 50 mmol/L o/a = 1/2

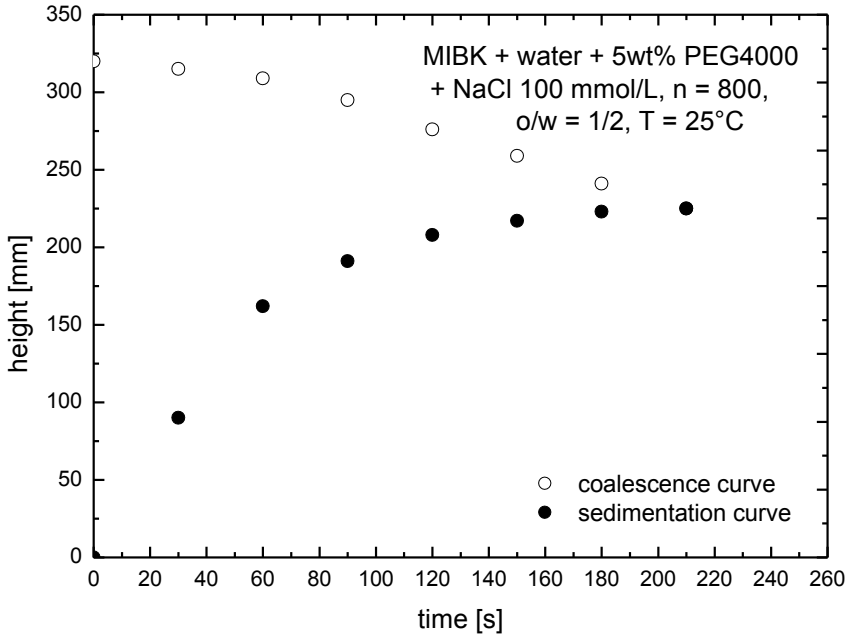

Fig. 8-67: System MIBK + water + 5 wt% PEG4000+ NaCl 100 mmol/L o/a = 1/2

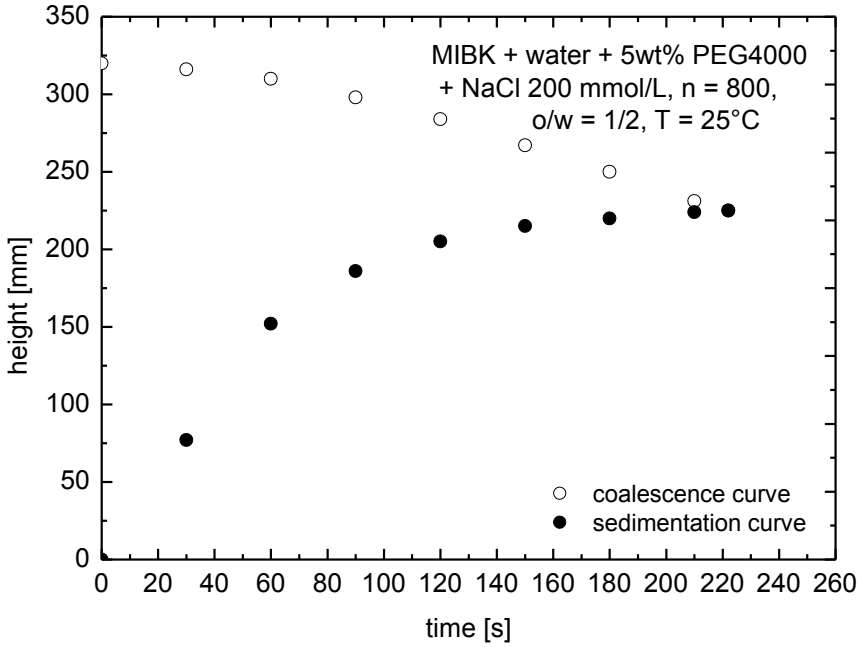

Fig. 8-68: System MIBK + water + 5 wt% PEG4000+ NaCl 200 mmol/L o/a = 1/2

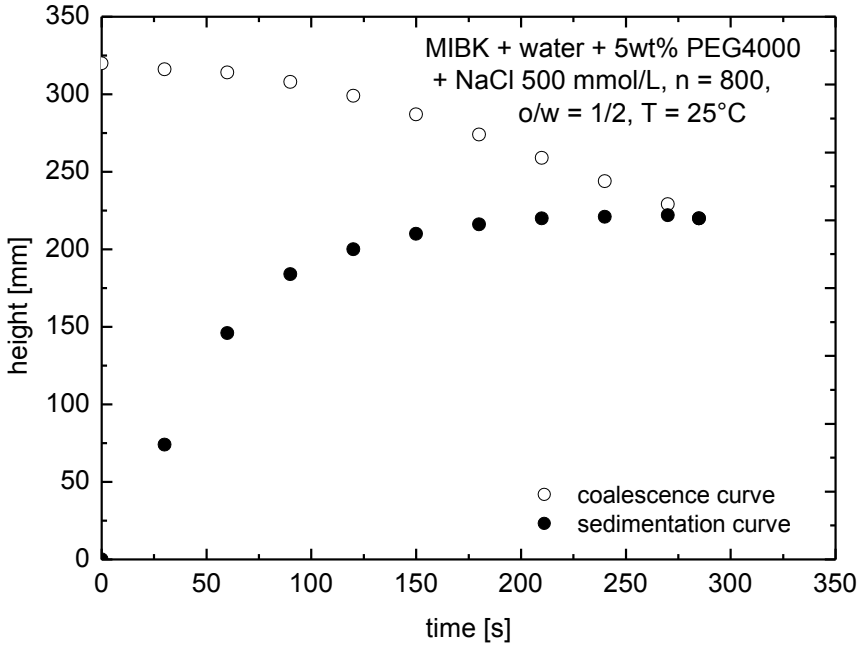

Fig. 8-69: System MIBK + water + 5 wt% PEG4000+ NaCl 500 mmol/L o/a = 1/2

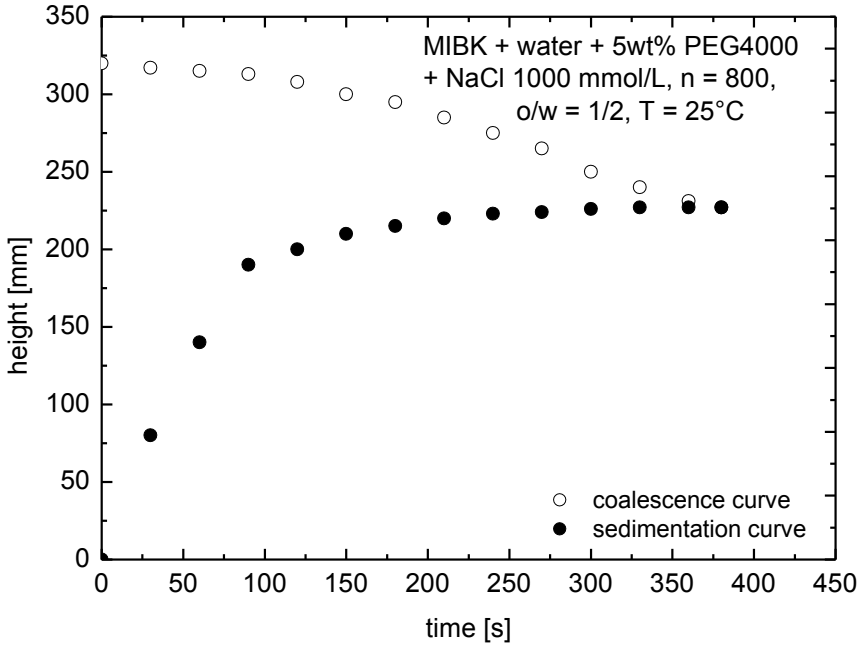

Fig. 8-70: System MIBK + water + 5 wt% PEG4000+ NaCl 1000 mmol/L o/a = 1/2

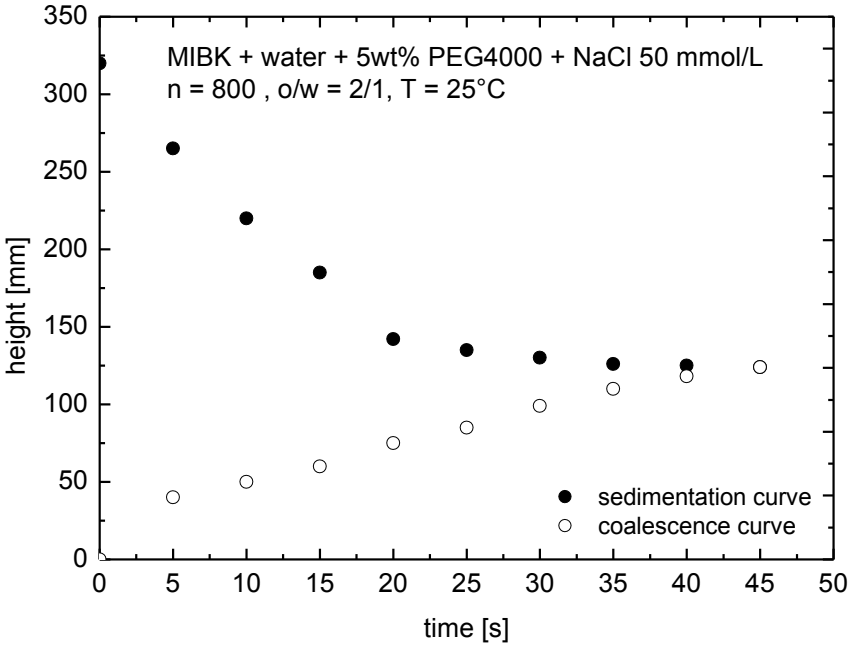

Fig. 8-71: System MIBK + water + 5 wt% PEG4000+ NaCl 50 mmol/L o/a = 2/1

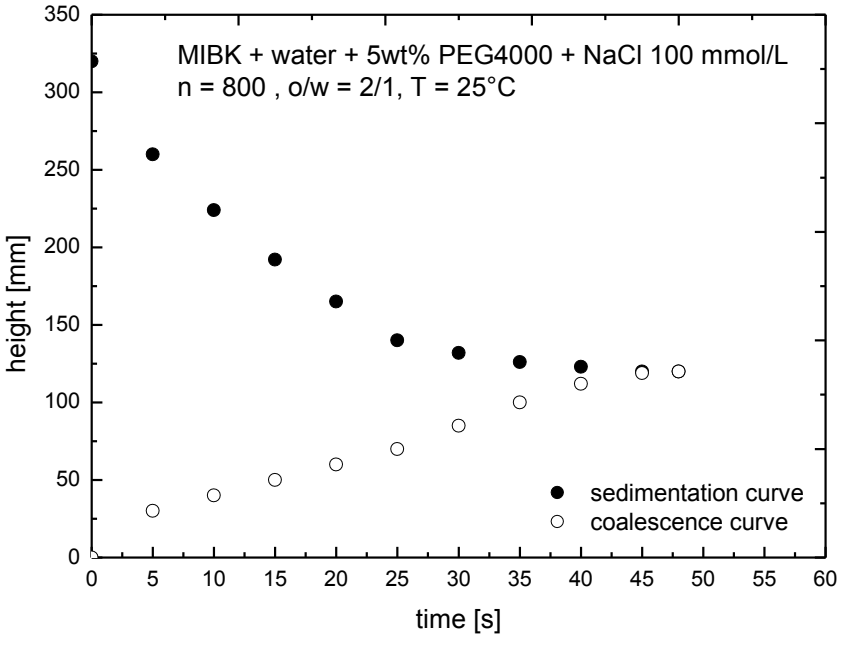

Fig. 8-72: System MIBK + water + 5 wt% PEG4000+ NaCl 100 mmol/L o/a = 2/1

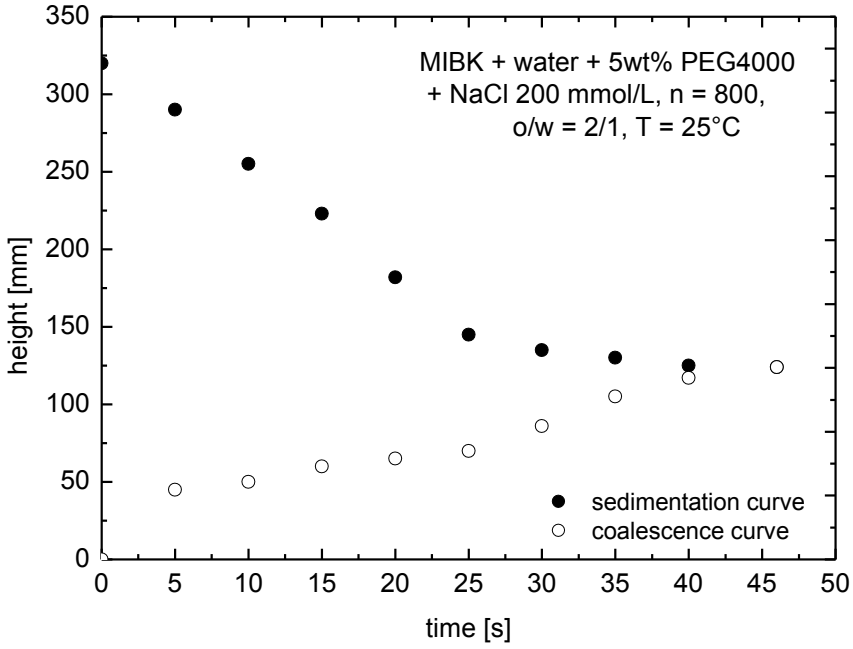

Fig. 8-73: System MIBK + water + 5 wt% PEG4000+ NaCl 200 mmol/L o/a = 2/1

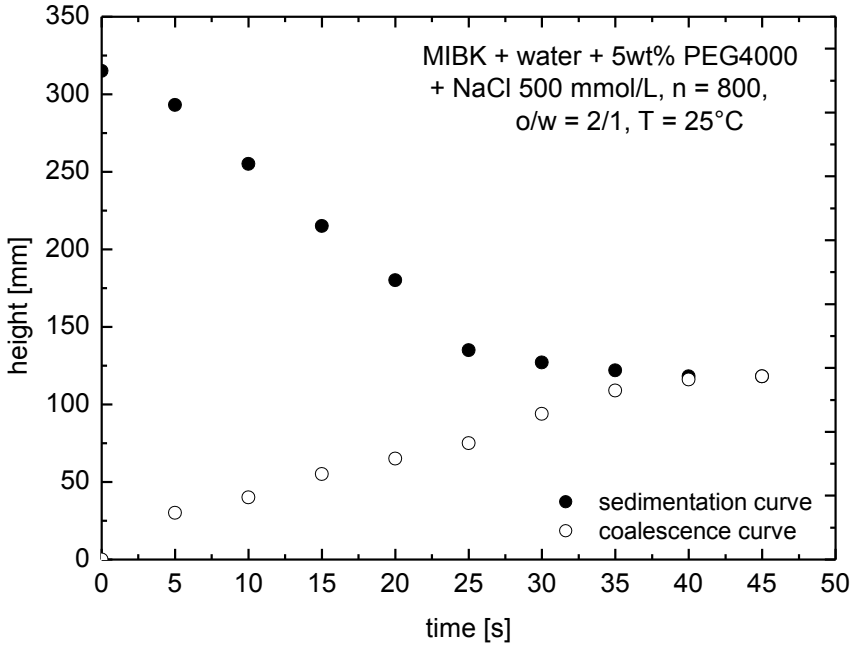

Fig. 8-74: System MIBK + water + 5 wt% PEG4000+ NaCl 500 mmol/L o/a = 2/1

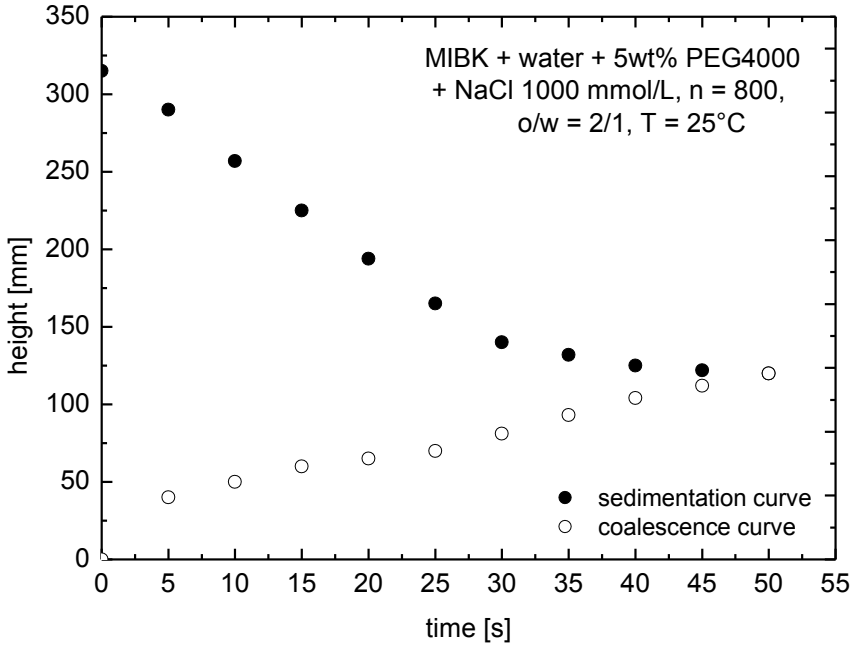

Fig. 8-75: System MIBK + water + 5 wt% PEG4000+ NaCl 1000 mmol/L o/a = 2/1

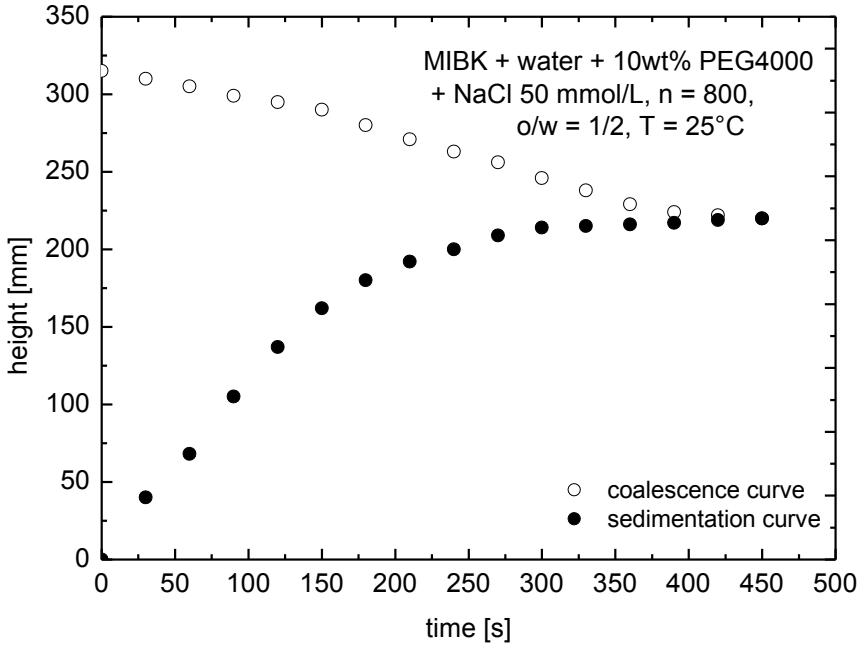

Fig. 8-76: System MIBK + water + 10 wt% PEG4000+ NaCl 50 mmol/L o/a = 1/2

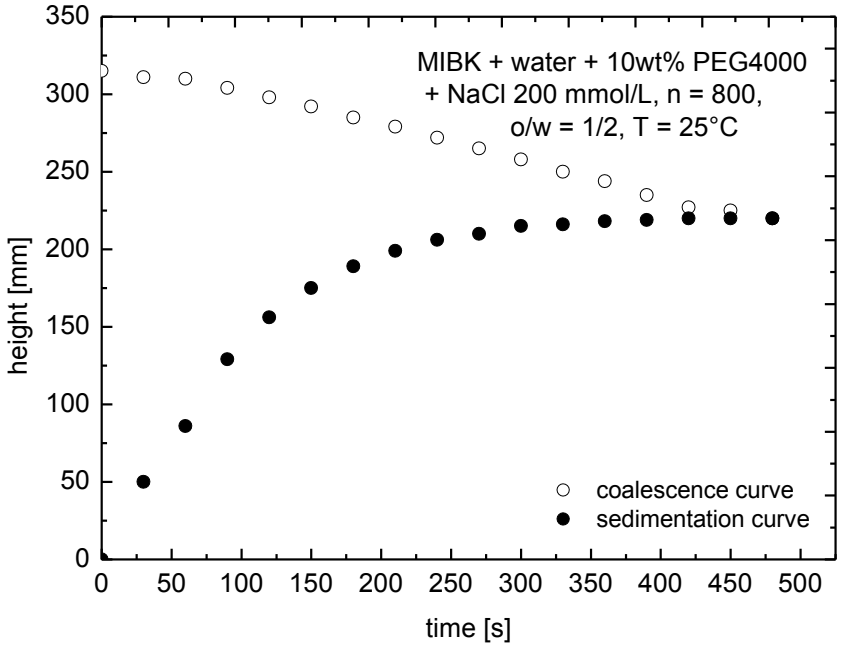

Fig. 8-77: System MIBK + water + 10 wt% PEG4000+ NaCl 200 mmol/L o/a = 1/2

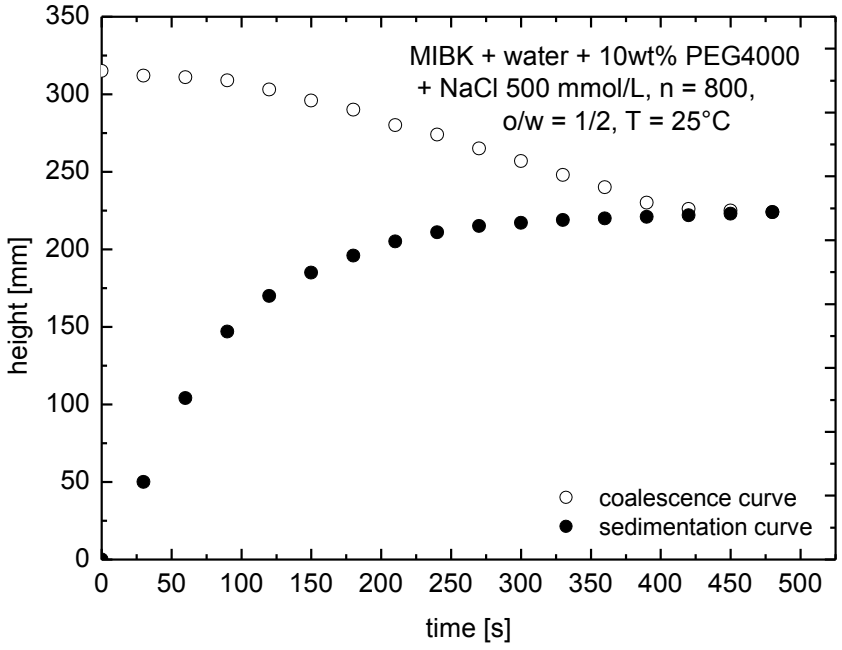

Fig. 8-78: System MIBK + water + 10 wt% PEG4000+ NaCl 500 mmol/L o/a = 1/2

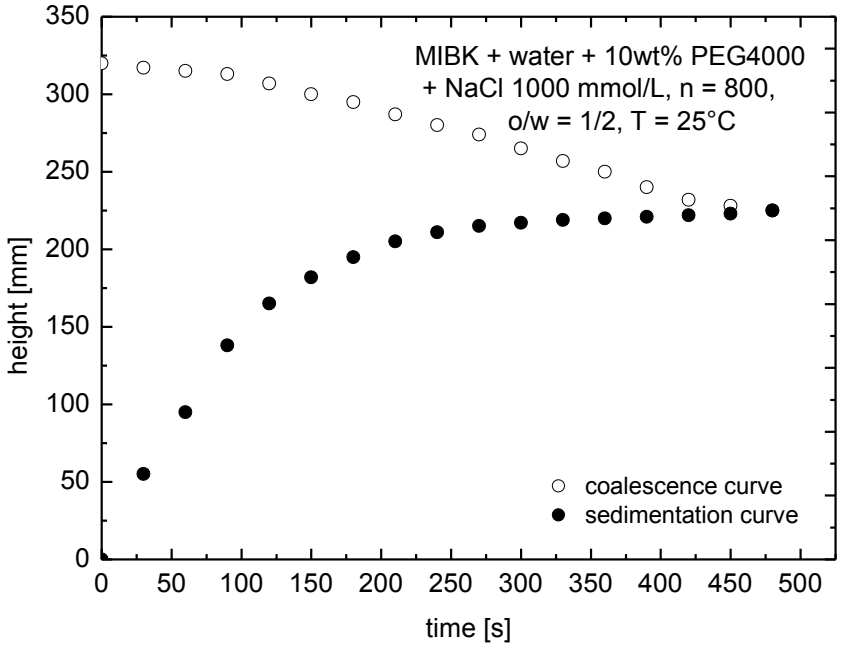

Fig. 8-79: System MIBK + water + 10 wt% PEG4000+ NaCl 1000 mmol/L o/a = 1/2

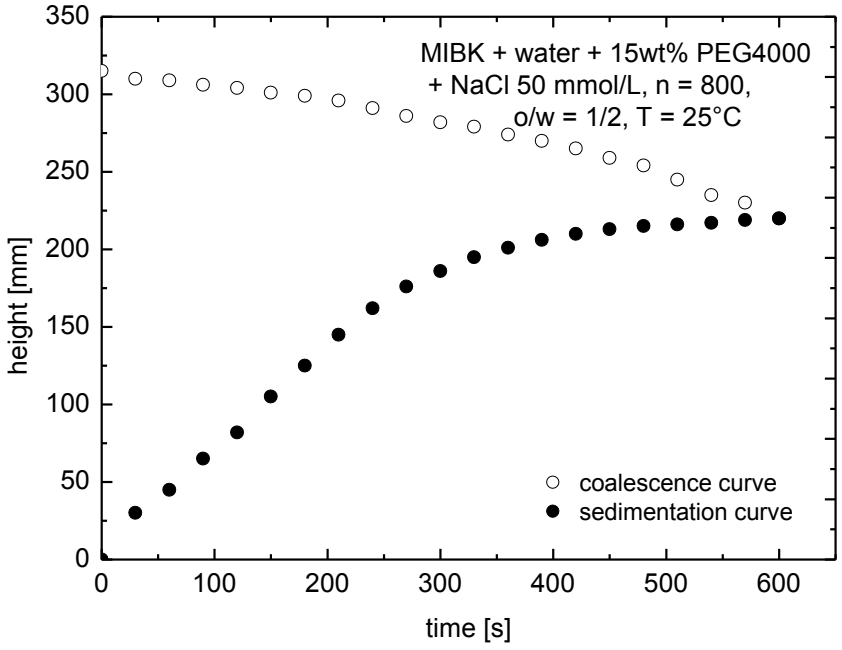

Fig. 8-80: System MIBK + water + 15 wt% PEG4000+ NaCl 50 mmol/L o/a = 1/2

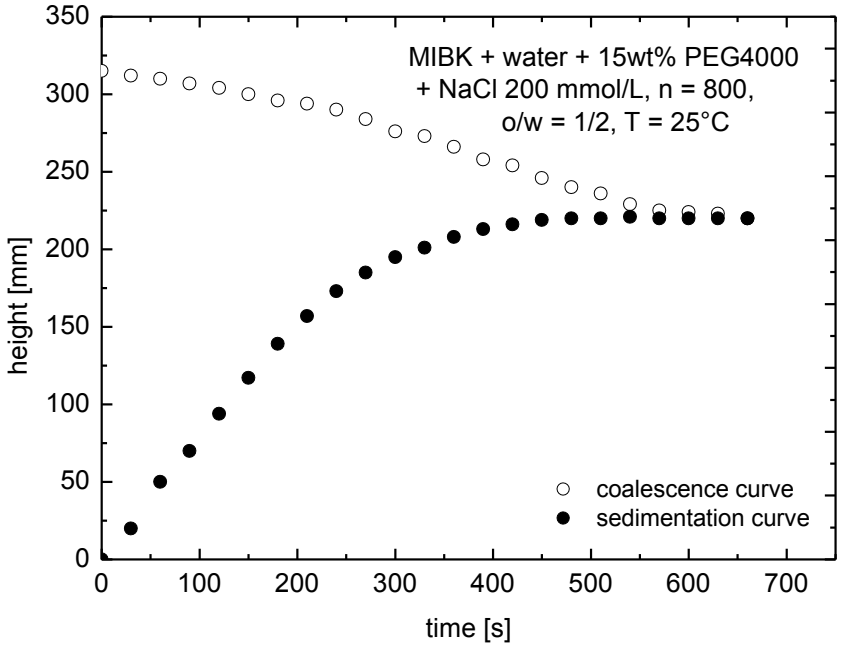

Fig. 8-81: System of MIBK + water + 15 wt% PEG4000+ NaCl 200 mmol/L o/a = 1/2

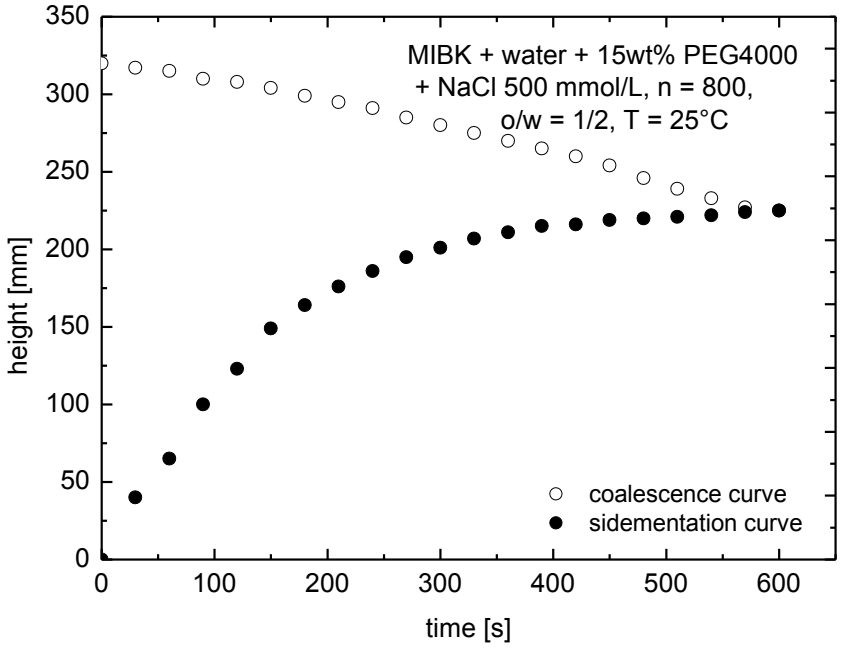

Fig. 8-82: System MIBK + water + 15 wt% PEG4000+ NaCl 500 mmol/L o/a = 1/2

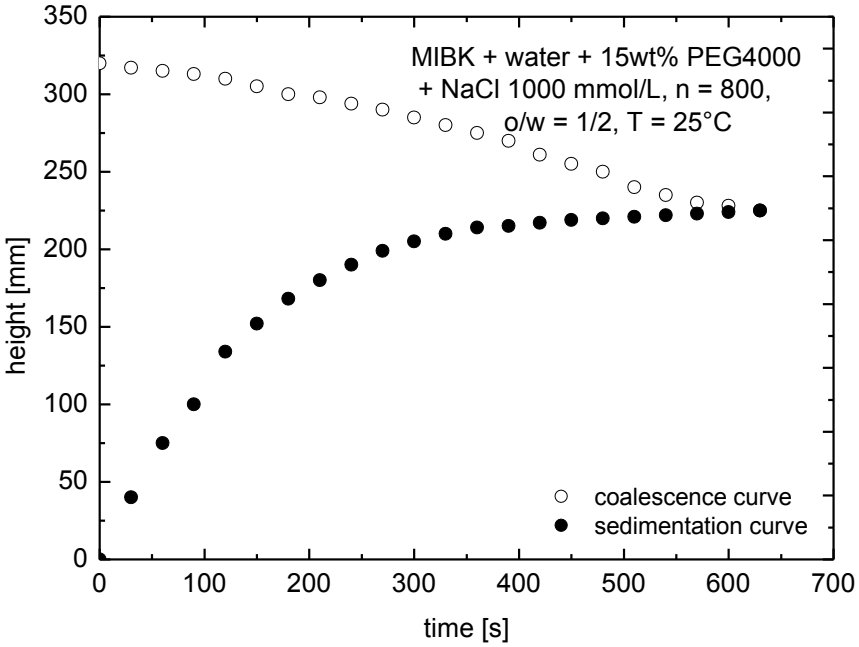

Fig. 8-83: System MIBK + water + 15 wt% PEG4000+ NaCl 1000 mmol/L o/a = 1/2

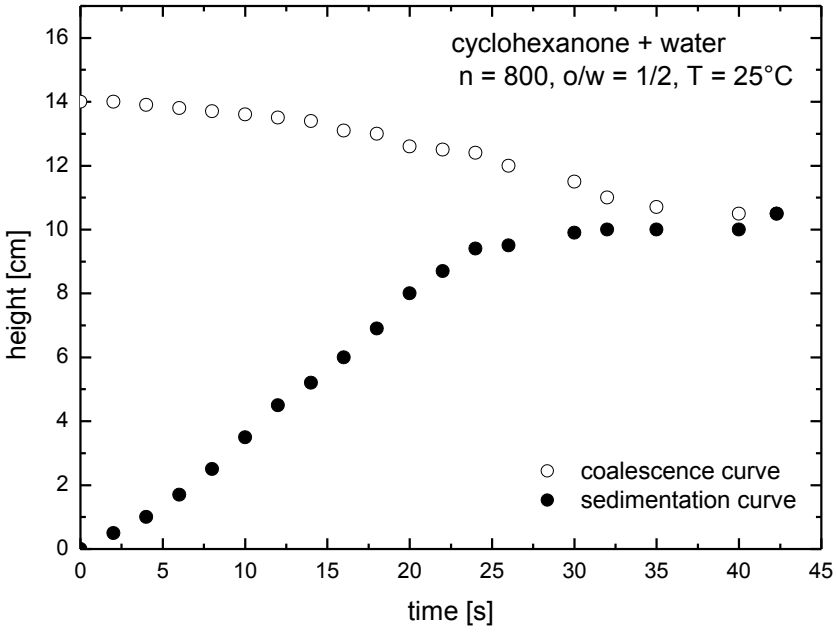

Fig. 8-84: System cyclohexanone + water o/a = 1/2

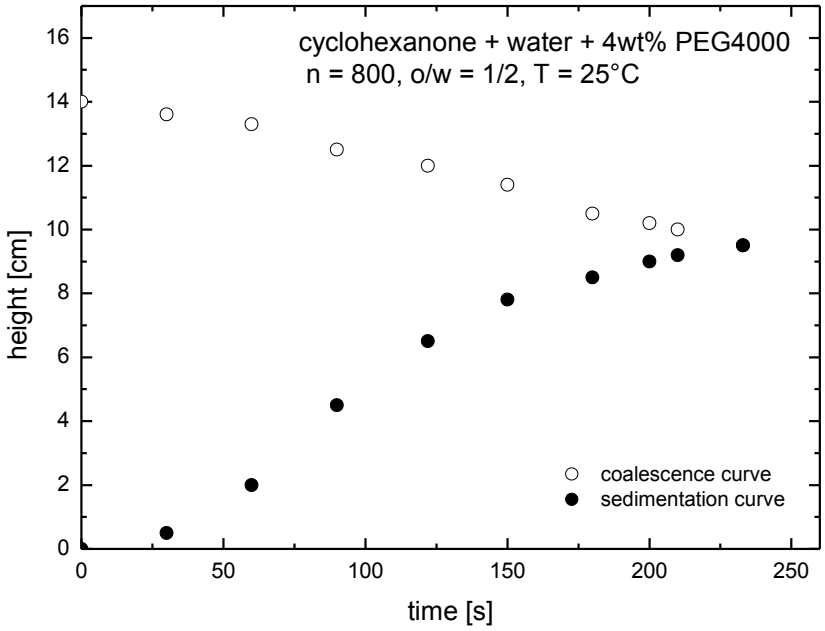

Fig. 8-85: System cyclohexanone + water+ 4 wt% PEG4000 o/a = 1/2

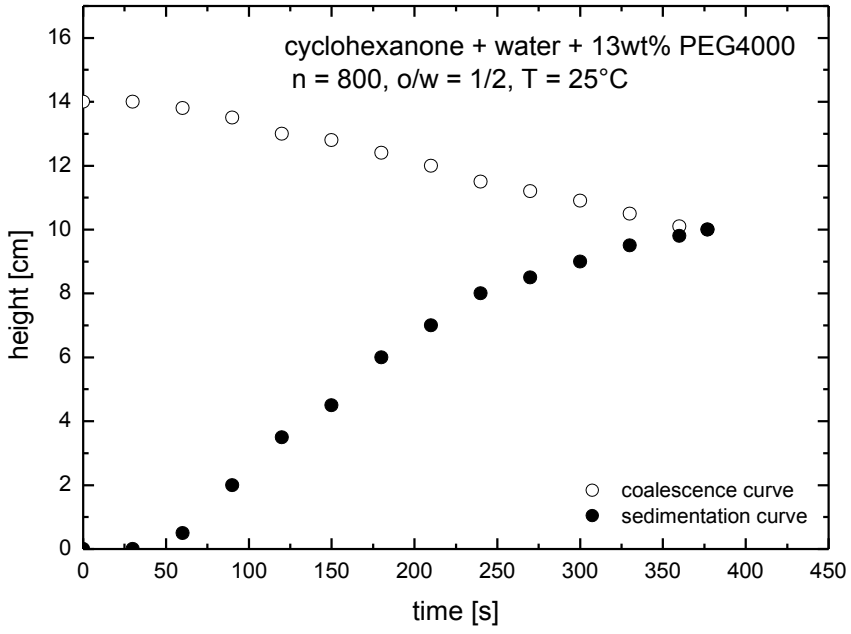

Fig. 8-86: System cyclohexanone + water+ 13 wt% PEG4000 o/a = 1/2

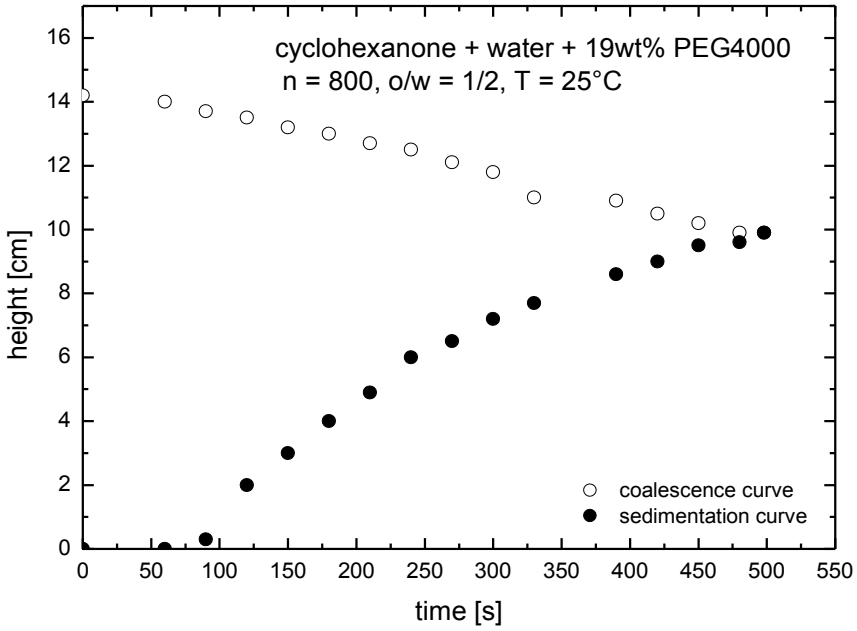

Fig. 8-87: System cyclohexanone + water+ 19 wt% PEG4000 o/a = 1/2

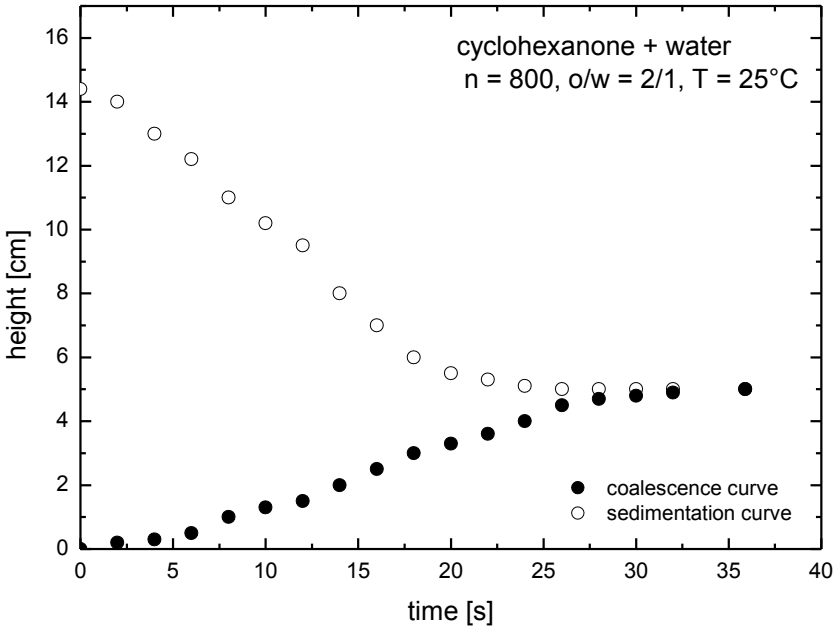

Fig. 8-88: System cyclohexanone + water o/a = 2/1

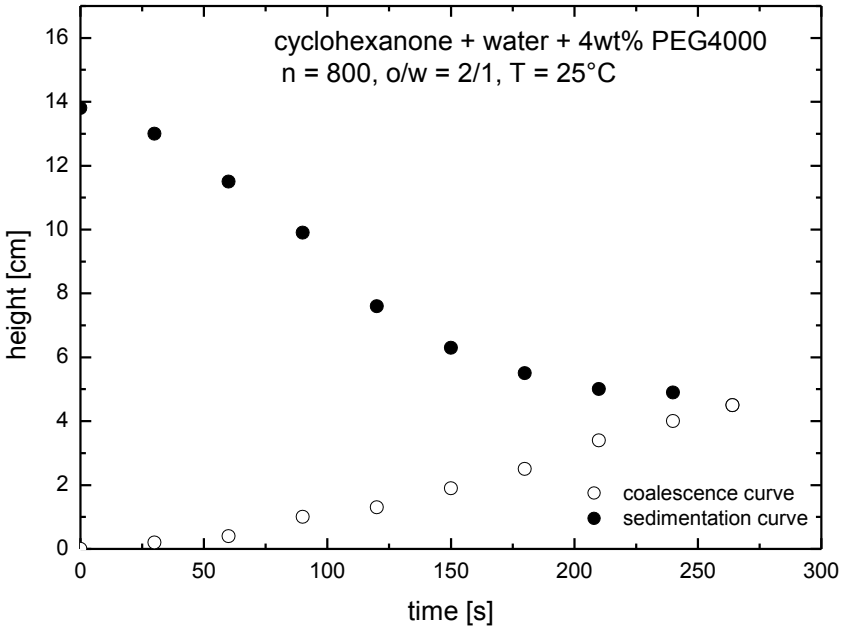

Fig. 8-89: System cyclohexanone + water+ 4 wt% PEG4000 o/a = 2/1

8.7 Experimental data: influence of inclined plate on phase separation

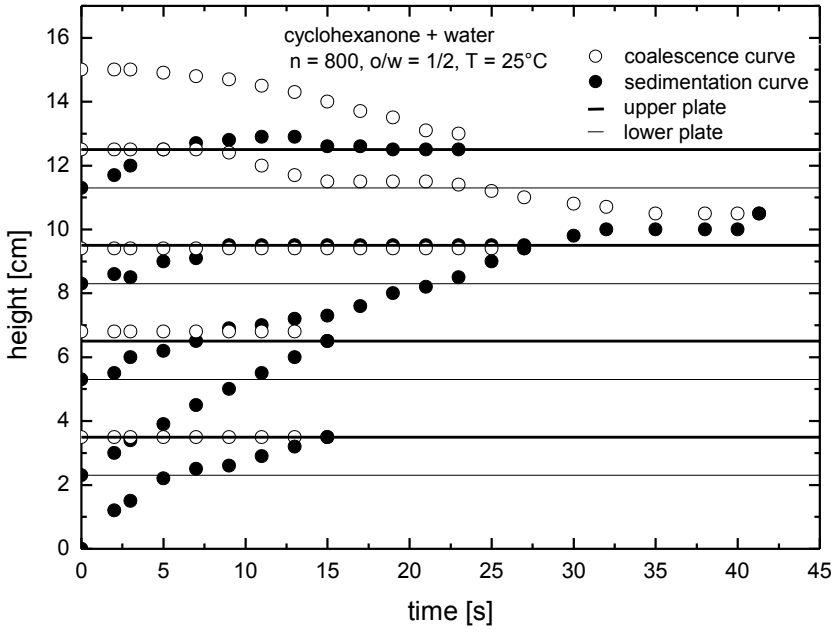

Fig. 8-90: Influence of inclined plate: system cyclohexanone + water o/a = 1/2

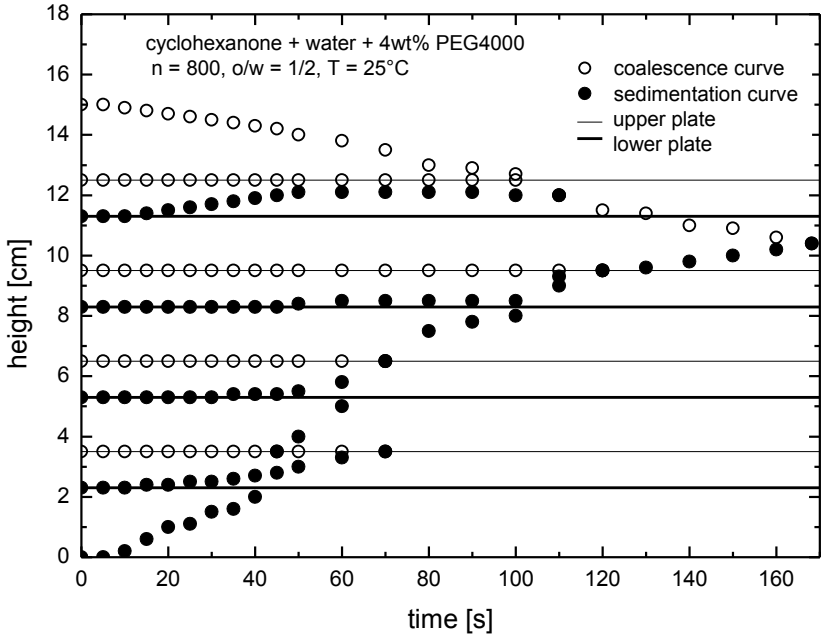

Fig. 8-91: Influence of inclined plate: system cyclohexanone + water+ 4 wt% PEG4000 o/a = 1/2

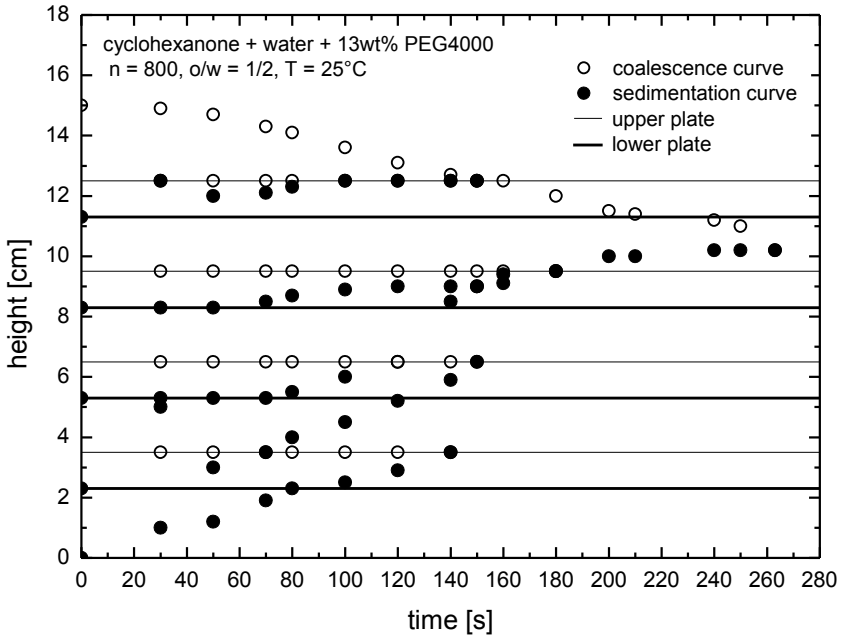

Fig. 8-92: Influence of inclined plate: system cyclohexanone + water+ 13 wt% PEG4000 o/a = 1/2

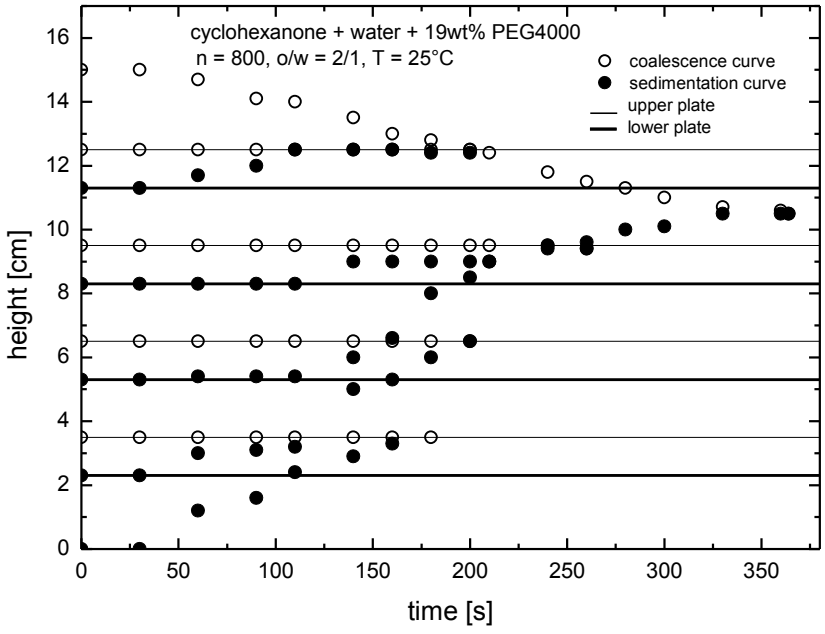

Fig. 8-93: Influence of inclined plate: system cyclohexanone + water+ 19 wt% PEG4000 o/a = 1/2

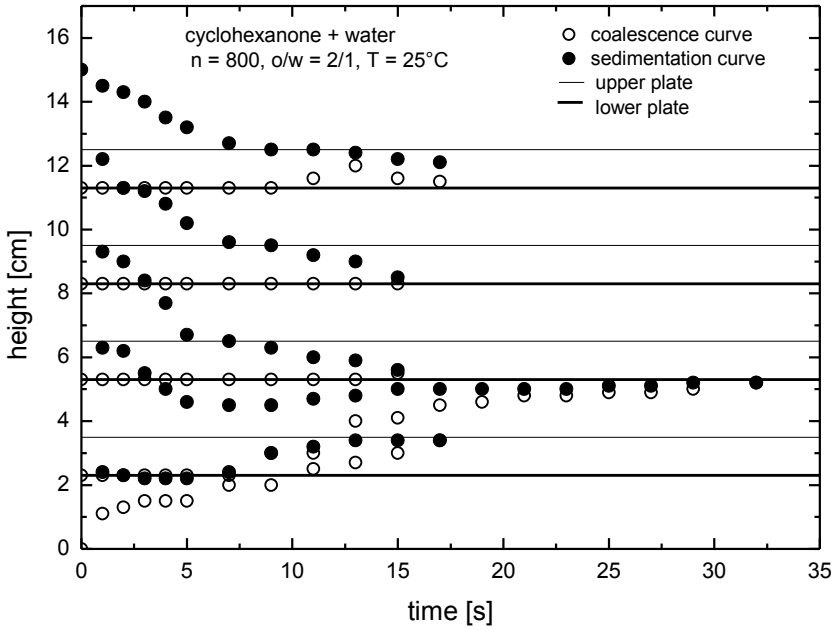

Fig. 8-94: Influence of inclined plate: system cyclohexanone + water o/a = 2/1

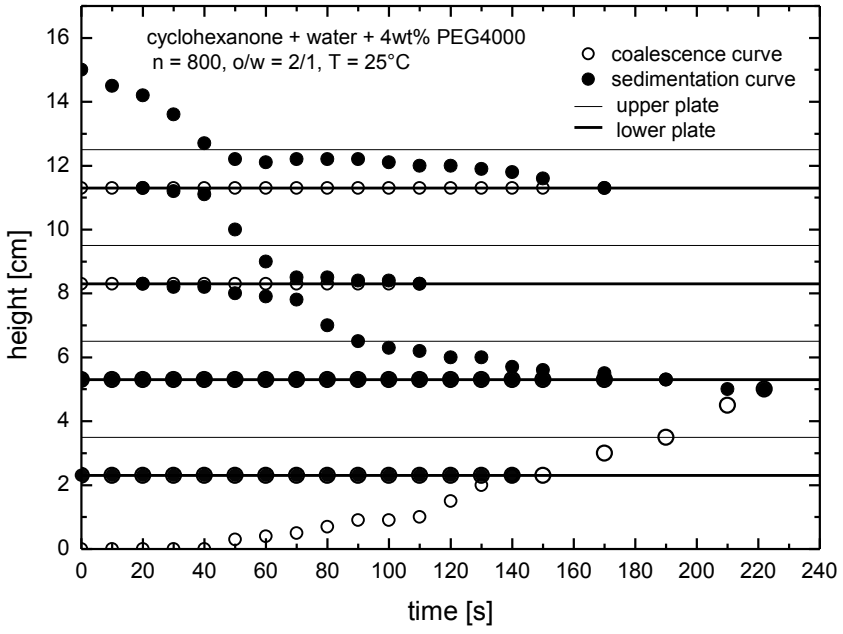

Fig. 8-95: Influence of inclined plate: system cyclohexanone + water+ 4 wt% PEG4000 o/a = 2/1

8.8 Publications

Article in a professional journal

Macher, R.; Bol, P.; Pfennig, A.: Charakterisierung und Abtrennung von Feinsttrübungen mithilfe von Zentrifugalabscheidern. - in: Chemie-Ingenieur-Technik 86 (2014) 9 , S. 1465 – 1465

Mungma, N.; Chuttrakul, P.; Pfennig, A.: Liquid-liquid Phase Separation in Batch Settling with Inclined Plate. - in: Jurnal Teknologi / Science and Engineering [Elektronische Ressource] 67 (2014) 4, S. 55 – 58

Pfennig, A.; Buchbender, F.; Chuttrakul, P.; Kopriwa, N. S.: Koaleszenz in Extraktionskolonnen und Abscheidern. - in: Chemie-Ingenieur-Technik 85 (2013) 9, S. 1359 – 1359

Chuttrakul, P.; Pfennig, A.; Kopriwa, N.; Anursan, K.: Einfluss von Elektrolyten und hoher Voskosität auf die Flüssig/Flüssig-Trennung. - in: Chemie-Ingenieur-Technik 84 (2012) 8, S. 1374 – 1374

Anusarn, K.; Chuttrakul, P.; Schmidt, M.; Kangsadan, T.; Pfennig, A.: Influence of Electrolytes and High Viscosity on Liquid-Liquid Separation. - in: World Academy of Science, Engineering and Technology 72 (2012) , S. 193 – 197

Contribution to conference (meeting, congress, workshop) proceedings

Bol, P.; Pfennig, A.: Analyzing the sedimentation and coalescence behavior of polydisperse droplets in opaque systems using ultrasonic technique. - in: ISEC 2014 International Solvent Extraction Conference (2014), S. 178 - 178

Chuttrakul, P.; Pfennig, A.: Sedimentation of polydisperse droplets in liquid-liquid separation processes. - in: 10. Minisymposium Verfahrenstechnik Proceedings (2014), S. 64 – 67

Aunyindee, I.; Cano Castro, A.; Chuttrakul, P.; Pfennig, A.: Application of Ultrasonic Spectroscopy to Quantify Sedimentation of Polydisperse Emulsions. - in: Book of Abstracts (2013), S. 86 – 91

Poster

Chuttrakul, P.; Pfennig, A.: Sedimentation and coalescence behavior of polydisperse droplets in viscous systems. - in: Jahrestreffen der Fachgruppe Extraktion und Fluidverfahrenstechnik. Fulda, Deutschland am: 27.03.2014

Chuttrakul, P.; Tantichumnan, C.; Kangsadan, T.; Pfennig, A.: Influence of viscosity on sedimentation and coalescence in horizontal settler. - in: Jahrestreffen der Fachgruppe Extraktion und Fluidverfahrenstechnik. Fulda, Deutschland am: 27.03.2014

Pungsang, P.; Chuttrakul, P.; Scherübel, P.; Kangsadan, T.; Pfennig, A.: Modeling of coalescence behavior in high-viscosity systems. - in: Jahrestreffen der Fachgruppe Extraktion und Fluidverfahrenstechnik. Fulda, Deutschland am: 27.03.2014

Macher, R.; Bol, P.; Pfennig, A.: Charakterisierung und Abtrennung von Feinsttrübungen mithilfe von Zentrifugalabscheidern. - in: ProcessNet-Jahrestagung und 31. DECHEMA-Jahrestagung der Biotechnologen 2014. Aachen am: 29.09.2014

Aunyindee, I.; Cano Castro, A.; Chuttrakul, P.; Pfennig, A.: Application of Ultrasonic Spectroscopy to Quantify Sedimentation of Polydisperse Emulsions. - in: 9. Minisymposium der Verfahrenstechnik. Leoben am: 17.04.2013

Chuttrakul, P.; Pfennig, A.; Kopriwa, N.; Anursan, K.: Effect of electrolytes on liquid-liquid separation. - in: ProcessNet-Jahrestagung und 30. DECHEMA-Jahrestagung der Biotechnologen. Karlsruhe am: 10.09.2012

Lectures or presentations

Bol, P.; Pfennig, A.: Analyzing the sedimentation and coalescence behavior of polydisperse droplets in opaque systems using ultrasonic technique. - in: ISEC 2014 International Solvent Extraction Conference. Würzburg am: 07.09.2014

Chuttrakul, P.; Pfennig, A.: Sedimentation of polydisperse droplets in liquid-liquid separation processes. - in: 10. Minisymposium Verfahrenstechnik. am: 17.06.2014

Mungma, N.; Chuttrakul, P.; Pfennig, A.: Liquid-liquid phase separation in batch settling with inclined plates. - in: International Conference on Separation Technology ICoST 2013. Johor Bahru am: 19.09.2013

Pfennig, A.; Buchbender, F.; Chuttrakul, P.; Kopriwa, N. S.: Koaleszenz in Extraktionskolonnen und Abscheidern. - in: Jahrestreffen der Fachgemeinschaft Fluiddynamik und Trenntechnik. Würzburg am: 25.09.2013

Chuttrakul, P.; Kopriwa, N.; Ruckes, S.; Rüngeler, B.; Pfennig, A.: Influence of electrolytes on liquid-liquid separation. - in: AIChE Annual Meeting. Minneapolis am: 16.10.2011

9 Bibliography

Aarts, D.G.A.L., Lekkerkerker, H.N.W., 2008: Droplet coalescence: drainage, film rupture and neck growth in ultralow interfacial tension systems. J. Fluid Mech. 606, 275-294.

Abid S., Chester A.K., 1994: The drainage and rupture of partially-mobile films between colliding drops at constant approach velocity., Int. J. Multiphase flow 20, 613-629.

Al-Zuhair, S., 2004: Using liquid–liquid deep settling model in determining the design parameters of crude palm oil settler. Sep. Purif. Technol. 35, 133–140.

Andersson, K. E. B., 1961: Pressure drop in ideal fluidization, Chem. Eng.Sci., 15, 276–297.

Anusarn, K., Chuttrakul, P., Schmidt, M., and Pfennig, A., 2012: Influence of Electrolytes and High Viscosity on Liquid-Liquid Separation. WASET.72: 1116-1120.

Anusarn, K., 2012: A study on the influence of ions on the settling behavior in high-viscosity systems. Master thesis, AVT.TVT, RWTH Aachen University, Germany.

Aunyindee, I., 2013: Experimental studies of the sedimentation behavior of polydisperse droplets in high-viscosity systems. Master thesis, CEET, TU Graz, Austria.

Aunyindee, I.; Cano Castro, A.; Chuttrakul, P.; Pfennig, A.: Application of Ultrasonic Spectroscopy to Quantify Sedimentation of Polydisperse Emulsions. - in: Book of Abstracts (2013), S. 86 – 91

Bazhlekov, I.B., Chesters, A.K., van der Vosse, F.N., 2000: The effect of the dispersed to continuous-phase viscosity ratio on film drainage between interacting drop., Int. J. Multiphase flow 26, 445-466.

Bol, P.; Pfennig, A.: Analyzing the sedimentation and coalescence behavior of polydisperse droplets in opaque systems using ultrasonic technique. - in: ISEC 2014 International Solvent Extraction Conference. Würzburg am: 07.09.2014

Bonnet, J. C. and Tavlarides, L. L., 1987: Ultrasonic Technique for Dispersed-Phase Holdup. Ind. Eng. Chem. Res., 26, 811-815.

Carlucci, G., 2010: Drop size distribution in stirred liquid/liquid systems: Influence of the dispersed phase. Master thesis, Institut für Prozess- und Verfahrenstechnik, Tu Berlin, Germany.

Castro, A. C., 2013: Determination of the settling behavior of organic/aqueous systems using new approaches. Master thesis, CEET, TU Graz, Austria.

Cents, A. H. G., Brilman, D. W. F., Versteeg., 2004: Measuring Bubble, Drop and Particle Sizes in Multiphase Systems with Ultrasound. AIChE J. 50 (11), 2750-2762.

Chen, C. T., Maa, J. R.,Yang, Y. M., Chang, C. H., 1998: Effects of electrolytes and polarity of organic liquids on the coalescence of droplets at aqueous-organic interfaces. Surf. Sci. 406 (1998) 167–177.

Chesters, A.K., 1991: The modeling of coalescence process in fluid-liquid dispersions: a review of current understanding. Chem. Eng. Res. Des. 69, 259-270.

Chevaillier, J.P., Klaseboer, E., Masbernat, O. and Gourdon, C., 2006: Effect of mass transfer on the film drainage between colliding drops. J. Colloid Interf Sci. 299, 472-485.

Chuttrakul, P., Pfennig, A., 2014: Sedimentation of polydisperse droplets in liquid-liquid separation processes. 10. Minisymposium Verfahrenstechnik, Wien.

Chuttrakul, P., Tantichumnan, C., Kangsadan, T., Pfennig, A., 2014: Influence of viscosity on sedimentation and coalescence in horizontal settler. Jahrestreffen der Fachgruppe Extraktion und Fluidverfahrenstechnik,. Fulda.

Carlucci, G., 2010: Drop size distributions in stirred liquid/liquid systems Influence of the dispersed phase. Master thesis, PVT, TU Berlin, Germany.

Davis, R. H., Birdsell, K. H., 1988: Hindered settling of semidilute monodisperse and polydisperse suspensions. AIChE J. Vol. 34, No. 1, 123-129.

Dullien F.A.L., 1992: Porous media, Fluid transport and Pore structure. 2nd edition, Academic Press Inc.

Effertz, M., 2011: Experimentelle Untersuchung des Einflusses von Salzen auf das Phasentrennverhalten von MiBK + Wasser. Studienarbeit, AVT.TVT, RWTH Aachen University, Germany.

EL-Hamouz, A., 2009: Drop Size Distribution in a Standard Twin-Impeller Batch Mixer at High Dispersed-Phase Volume Fraction. Chem. Eng. Technol. 32, No. 8, 1203-1210.

Findlay, J. A. P., 2013: Sedimentation of large polydisperse particles. Master thesis, CEET, TU Graz, Austria.

Frankforter, G.B., Cohen L., 1994: Equilibria in the Systems, Water, Acetone and Inorganic Salts. J. Am. Chem. Soc. 36, p.1103–1134.

Frising, T., NoÏk, C., Dalmazzone, C., 2006: The Liquid/Liquid Sedimentation Process: From Droplet Coalescence to Technologically Enhanced Water/Oil Emulsion Gravity Separatiors: A Review. J. Dispersion Sci. Technol. 27, 1035-1057.

Hartland, S., Vohra, D. K., 1978: Koaleszenz in vertikalen dichtgepackten Dispersionen. Chem. Ing. Tech. 50, Nr. 9, 673-682.

Hartland, S., 1981: Coalescence in dense-packed gas/liquid and liquid/liquid dispersions. Tenside Det. 18 (4), 178-189.

Hartland, S., Jeelani, S. A. K., 1987: Choice of model for predicting the dispersion height in liquid/liquid gravity settlers from batch settling data. Chem. Eng. Sci. Vol. 42, No. 8, 1927-1938.

Hartland, S., Jeelani, S. A. K., 1988: Prediction of Sedimentation and Coalescence Profiles in a Decaying Batch Dispersion. Chem. Eng. Sci. Vol. 43, No. 9, 2421-2429.

Hartland, S., Vohra, D. K., 1978: Shape of a vertical column of drops approaching an interface. AIChE J. 24 (5), 811-817.

Henschke, M ., 1994: Dimensionierung liegender Flüssig-flüssig-Abscheider anhand diskontinuierlicher. Absetzversuche. Germany. RWTH Aachen.

Henschke, M., Schlieper, L., and Pfennig, A., 2002: Determination of a coalescence parameter from batch settling experiments. Chem. Eng. J. 85:369–378.

Hülswitt, N., 2004: Dimensionierung liegender Flüssig-Flüssig-Abscheider mit Einbauten auf der Basis von Laborversuchen. Germany. RWTH Aachen.

Ishii, M., Zuber, N., 1979: Drag coefficient and relative velocity in bubbly, droplet or particulate flows, AIChE J. 25 (5), 843–855.

Israelachvili J.N., 1991: Intermolecular and Surface Forces. 2nd edn, Academic, New York.

Jeelani, S. A. K., Hartland, S., 1985: Prediction of Steady State Height from Batch Settling Dispersion Data. AIChE J. Vol. 31, No. 5, 711-720.

Jeelani, S. A. K., Hartland, S., 1998: Effect of Dispersion Properties on the Separation of Batch Liquid-Liquid Dispersions. Ind. Eng. Chem. Res. 37, 547-554.

Jeelani, S. A. K., Pandit, A. and Hartland, S., 1990: Factors affecting the decay of batch liquid-liquid dispersions, Can. J. Chem. Eng., 68: 924–931.

Jurado, E., Bravo, V., Camacho, F., Vicaria, J.M., Fernandez-Arteaga, A., 2007 Estimation of the distribution of droplet size, interfacial area and volume in emulsions. Colloids Surf., A: Physicochem. Eng., 295, 91-98.

Khatchikian, P., and Rieble, U., 1999: Phase Velocity of Ultrasonnd in Suspensions of Large Particles. Acta Acustica, 85, 800-808.

Leite, F. L., Bueno, C. C., Roz, A. L. D., Ziemath, E. C., Oliveira Jr., O. N., 2012: Theoretical Models for Surface Forces and Adhesion and Their Measurement Using Atomic Force Microscopy. Int. J. Mol. Sci.,13,12773-12856

Manodumrongthum, S., 2012: Experimental studies on settling behavior of different high-viscous systems. Bachelor thesis, AVT.TVT, RWTH Aachen University, Germany.

Mersmann, A., 1980: Zum Flutpunkt in Flüssig/Flüssig-Gegenstromkolonnen, Chemie-Ingenieur-Technik, 52: 933–942.

Mungma, N., 2013: Influence of internal to phase separation in high-viscosity system. Master thesis, CEET, TU Graz, Austria.

Mungma, N., Chuttrakul, P., Pfennig, A., 2014: Liquid-liquid Phase Separation in Batch Settling with Inclined Plate. Teknologi. 67:4, 55-58.

Nadiv, C., Semiat, R., 1995: Batch Settling of Liquid-Liquid Dispersion. Ind. Eng. Chem. Res., 34, 2427-2435.

Nevers N. and Wu J. L., 1971. Bubble Coalescence in Viscous Fluids. AIChE J. 17, No. 1, p. 182-186.

Ngan K. H., Ioannou K., Rhyne L. D., Wang W., Angeli P., 2009: A methodology for predicting phase inversion duringliquid–liquid dispersed pipeline flow. Chem. Eng. Res. Des. 87, p. 318–324.

Pattarawut, J., 2010: Experimental comparison of the coalescence behavior in two cells. Germany. RWTH Aachen.

Pfennig, A., Schwerin, A., 1998: Influence of Electrolytes on Liquid-Liquid Extraction. Ind. Eng. Chem. Res., 37, 3180-3188

Pilhofer, T., Mewes, D., 1979: Siebboden Extraktionskolonnen, Verlag Chemie, Weinheim, Germany.

Punsang, P., 2014: Modeling and experiment studies of coalescence behavior in high-viscosity systems. Master thesis, CEET, TU Graz, Austria.

Pungsang, P.; Chuttrakul, P.; Scherübel, P.; Kangsadan, T.; Pfennig, A.: Modeling of coalescence behavior in high-viscosity systems. - in: Jahrestreffen der Fachgruppe Extraktion und Fluidverfahrenstechnik. Fulda, Deutschland am: 27.03.2014

Reddy, S. R. and Fogler, H. S., 1981: Emulsion stability: delineation of different particle loss mechanisms, J. Colloid Interface Sci., 79(1): 105–113.

Rhodes, M., ed., 2008: Introduction to Particle Technology. 2nd ed, John Wiley &Son, Ltd.

Rhosonics., 2012: Ultrasonic Suspension Analyzer MANUAL Rhosonics SUSS-2008.

Richardson, J.F., Zaki, W.N., 1954: Sedimentation and Fluidization: Part I. Trans. Instn Chem. Engrs., 32.

Ruckes, S., Pfennig, A., 2011: Schlussbericht: Untersuchungen zum Einfluss von Mulm auf das Abscheideverhalten organisch- wässriger Stoffsysteme. AiF, IGF 14997 N.

Saboni, A., Gourdon, C. and Chesters, A.K., 1995: Drainage and rupture of partially mobile films during coalescence in liquid-liquid systems under a constant interaction force. J. Colloid Interf Sci. 175, 27-35.

Schlieper, L., Chatterjee, M., M. Henschke, and Pfennig, A., 2004: Liquid-Liquid Phase Separation in Gravity Settler with Inclined Plates. AIChE J. 50: 802-811.

Schoolenberg.G and During.F., 1998. Coalescence and interfacial tension measurements for polymer melts: A technique using the spinning drop apparatus. Polym. J. Vol. 39 No. 4, p. 757-763.

Smallwood, I. M., 1996: Handbook of organic solvent properties. John Wiley &Son, Ltd.

Siebenhofer M., 2014: Privatissimum, Graz University of Technology, December 2014

Singh, K.K., Mahajani, S.M., Shenoy, K.T., Ghosh S.K., 2008: Representative drop sizes and drop size distributions in A/O dispersions in continuous flow stirred tank, Hydrometallurgy 90, 121–136.

Soika, M., Pfennig, A., 2005: Extraktion Eine Frage des Wassers. Chem. Ing.Tech. 77 No.7, 905-911.

Stevens, G. W., Pratt, H. R. C., Tai, D. R., 1989: Droplet coalescence in aqueous electrolyte solutions. J. Colloid Interface Sci., Vol. 136, No. 2.

Supardan, M. D., Masuda, Y., Maezawa, A., Uchida, S., 2006: Use of Ultrasonic Technique for Measuring Interfacial Area in a Two-Dimensional Bubble Column. J. Chem. Eng. Jpn. 39 (7), 687-692.

Tantichumnan, C., 2014: Influence of Viscosity on Sedimentation and Coalescence Behavior. Master thesis, CEET, TU Graz, Austria.

Wang W., Gong J., Ngan K. H. and Angeli P., 2009: Effect of glycerol on the binary coalescence of water drops in stagnant oil phase. Chem. Eng. Res. Des. 87, 1640-1648.